FEASIBILITY OF BLUE ENERGY PRODUCTION USING REVERSE ELECTRODIALYSIS IN KWAZULU NATAL COASTAL REGION: MODELLING STUDY USING COMSOL MULTIPHYSICS

By

Lungisani Ngcobo

BTech in Chemical Engineering

Date: January 2024

Supervisor: Dr P.T Ngema

Co-Supervisors: Prof. Armel Tumba Kaniki, Dr Nkululeko Nkosi

Submitted in fulfillment of the requirements for the degree of Master of Engineering in the Department of Chemical Engineering, Faculty of Engineering, and the Built Environment at Durban University of Technology

PREFACE

The study was conducted under the supervision of Dr. P.T Ngema and co-supervision of Prof. Armel Tumba Kaniki, and Dr Nkululeko Nkosi at Durban University of Technology (DUT), Department of Chemical Engineering in collaboration with Mangosuthu University of Technology (MUT).

Student: Lungisani Ngcobo

Signature Date:01/25/2024

As the candidate's supervisor, I agree to the submission of this dissertation/thesis.

Supervisor: Dr. P.T Ngema.

Signature Date: 23/03/24

Co-Supervisor: Prof. KA Tumba

Signature Date: 23/03/24

Co-Supervisor: Dr N Nkosi.

Signature… Date: 23/03/24

DECLARATION

I, Lungisani Ngcobo, the undersigned student, declare that.

(i) The research reported in this dissertation, except where otherwise indicated, is my original work.

(ii) This dissertation has not been submitted for any degree or examination at any other university.

(iii) This dissertation does not contain other persons' data, pictures, graphs, or other information, unless specifically acknowledged as being sourced from other persons.

(iv) This dissertation does not contain other persons' writing, unless specifically acknowledged as being sourced from other researchers. Where other written sources have been quoted, then:

(a) Their words have been re-written, but the general information attributed to them has been referenced,

(b) Where their exact words have been used, their writing has been placed inside quotation marks, and referenced.

(v) Where I have reproduced a publication of which I am an author, co-author, or editor, I have indicated in detail which part of the publication was written by myself alone and have fully referenced such publications.

(vi) This dissertation does not contain text, graphics or tables copied and pasted from the internet, unless specifically acknowledged, and the source being detailed in the dissertation and in the References sections.

_01/25/2024_____

Lungisani Ngcobo Date

DEDICATION

This work is dedicated to my mother and father who made it possible for me to reach this far in pursuing my dreams. Their hard work and support were the strength I needed to reach this far. I would also like to dedicate this work to my fiancée for the support she gave me through the process of this work I would also like to dedicate this work to my late grandmother Nomusa Eunice Mbatha. Finally, I dedicate this work to my son, Lwandle Ndlovu.

ACKNOWLEDGEMENTS

First and foremost, all prayers and gratitude go to the Almighty Shembe uNYAZILWEZULU and to my ancestors for providing me with a strength to complete this master's degree. Also, I want to thank my fiancée Nompilo Penelope Ndlovu and my mother, father, and brother, Mrs. Khanyisile Mlele, Mr. Samson Mlele, and Lungile Mlele for their prayers.

I would also like to express my utmost gratitude and appreciation to the following people for the support and contribution towards the completion of this thesis:

- To my supervisor Dr P.T Ngema for the advice, support, encouragement, and guidance towards finishing this degree, I sincerely appreciate and grateful for your help.

- My co-supervisor Prof Kaniki Tumba, thank you for believing in me and thank you for your help, advice, and guidance.

- Dr Nkululeko Nkosi thank you for mentoring and grooming me, as well as encouraging and inspiring me to produce the best of me and to train me to think outside the box. God bless you in abundantly.

- My family for not giving up on me and supporting me.

- To Ayanda Mbele, thank you for giving me your laptop when I didn't have my own laptop so that I can finish this work.

- Zinhle Innocentia Mkhize whenever I got stuck or have a problem regarding my dissertation you helped me with a smile never complained, thank you very much.

- Lereko Letuka, Refiloe Molao, Zininzi Mpafa, Bonginhlanhla Buthelezi, Sibusiso Madonsela, Nkosenhle Madonsela, Zamani Ngubo whenever I don't feel like doing my thesis you guys gave me encouragement thank you very much.

ABSTRACT

Renewable energies have gained an increasing focus in recent years, due to the climate crisis contributed or associated with the current energy generation sources in South Africa. Thus, in this thesis, a renewable energy source called salinity gradient energy or blue energy will be presented and studied.

The main objectives outlined in this dissertation were to evaluate the theoretical potential of electric energy production from the KwaZulu Natal rivers which are uThukela, uMvoti, uMkhomazi, Amanzimtoti, Umgeni, and uMfolozi. Finally, to optimize and simulate RED membrane and design reverse electrodialysis membranes and feeding pumps.

In terms of the theoretical potential for producing electricity in the studied estuaries, it was concluded that the uThukela estuary has a considerably higher potential than the others. So, by this information, the possibility of designing the pilot plant in this estuary was studied, noting that the location of the pilot plant where the energy produced is greater and the capital cost are lower is at the mouth of the uThukela river.

As for the pilot plant of RED, it was concluded that it is economically viable since the profit/loss found was R0 which is a break-even point, the plant is not generating a profit, but it's also not generating a loss and since the focus for now is to try generating power. It's economically viable in the sense that it covers its costs, but it is not profitable in terms of generating surplus revenue. It was concluded that using cheap and very thin membranes with high fluxes can increase the performance of the reverse electrodialysis. Also, the performance can be increased by using more than two reverse electrodialysis stacks instead of one.

RESEARCH OUTPUTS

ARTICLE

1. **Lungisani Ngcobo.,** Peterson T. Ngema., Tumba A. Kaniki, and Nkululeko Nkosi. 2023. Reverse Electrodialysis Technology installation in KwaZulu-Natal coastal region: A modelling study using COMSOL Multiphysics. Available: https://www.iicbe.org/proceedingspdf.php?id=44

CONFERENCE

1. **Lungisani Ngcobo.,** Peterson T. Ngema., Tumba A. Kaniki, and Nkululeko Nkosi. 2023. Reverse Electrodialysis technology installation. 39th Johannesburg International Conference on Chemical, Biological and Environmental Engineering. November 16-17, 2023, Johannesburg (South Africa).

TABLE OF CONTENT

LIST OF FIGURES

LIST OF TABLES

NOMENCLATURE

Symbol	Description and units
A_m	Membrane area (m^2)
F	Faraday constant
N_m	Number of cells in a stack
P_{gross}	Gross power (W)
R_{stack}	Stack resistance (Ω)
R_{ele}	Electrode resistance (Ω)
R_{AEM}	Anion exchange membrane (Ω)
R_{CEM}	Cation exchange membrane (Ω)
R_{sw}	Sea water compartment resistance (Ω)
R_{rw}	River water compartment resistance (Ω)
P_d	Power density (W/m^2)
R_{load}	External resistance (Ω)
T	Temperature (K)
I_{PP}	Current density (A/m^2)
R_{cell}	Cell resistance (Ω)
r	Activity coefficient
E_T	Electrical potential (V)
R_e	Reynolds number
C	Concentration (mol/m^3)
D_{water}	Diffusion constant of water (m^2/s)
D_{NaCl}	Diffusion constant of sodium chloride(m^2/s)
J_{dl}	Diffusion of ions
J_{ml}	Migration of ions
δ_m	Membrane thickness (m)
J'_{water}	Volumetric water flux (m/s)
M_{water}	Molecular mass of water (g/mol)
ρ_{water}	Density of water (kg/m^3)
J_{NaCl}	Ionic flux across the membrane (mol/m^2s)
E_{uc}	Actual unit cell potential (V)
U	Terminal voltage (V)
P_{max}	Maximum external power (W)
Δp_{sw}	Pressure drops over seawater channel (Pa)
Δp_{rw}	Pressure drops over river water channel (Pa)
μ	Dynamic viscosity $(Pa.s)$
L	Length of membrane(m)
Q	Volumetric flow rate of water (m^3/s)
δ_{sw}	Sea water compartment thickness (m)
δ_{rw}	River water compartment thickness (m)
b	Width of membrane (m)

ABBREVIATION

Symbol	Description and units
AEM	Anion Exchange Membrane
CEM	Cation Exchange Membrane
RED	Reverse Electrodialysis
IEM	Ion Exchange Membrane
EMF	Electromotive Force
SGP	Salinity Gradient Power
PRO	Pressure retarded Osmosis
$CAPMIX$	Capacitive mixing

SUBSCRIPT

Symbol	Description and units
c	Concentrated solution
d	Diluted solution
rw	River water
sw	Seawater

CHAPTER 1-INTRODUCTION

1.1 Renewable energy generation

The need for energy to support social and economic development has been growing steadily till this day. The increase in population and rising standards of living are the main cause of this increase in the world's energy consumption. Energy provides services to support both productive processes as well as essential human necessities including electricity, water, cooking, heating, cooling, and education. In many nations around the world, including South Africa, the use of fossil fuels (coal, oil, and gas) as a source of energy has grown dramatically since the 1850's and remains the most prevalent source to this day (Tshibangu 2017). The use of fossil fuel as a source of energy has led to significant emissions of greenhouse gases which contribute to climate change (Mitigation 2011).

Emissions of greenhouse gases by fossil fuels have contributed to the increasing global average temperature of the earth, by trapping heat energy in the earth atmosphere (Mitigation 2011). Carbon dioxide (CO_2) emissions as well as those of other greenhouse gases including methane (CH_4), nitrous oxide (NO_X) and fluorinated gases are mostly to blame for this temperature increase (Kweku *et al.* 2018). Human health, the environment, and the atmosphere are all impacted by greenhouse gases. The impact on human health may lead to food shortages and the development of illnesses like cholera and malaria (Kweku *et al.* 2018).

Fossil fuels already supply more than 80% of the world's primary energy, and this is likely to be the case for some time, according to study conducted by the international energy agency, the global concentration of greenhouse gases can grow higher (Holloway *et al.* 2007). Unless considerable adjustments are made to energy regulations and practices or new means of generating energy that will be environmentally friendly and satisfy the rising needs of power. Due to the reason mentioned above, environmentally friendly strategies and technologies are being developed to ensure sustainable energy and alternative energy sources. Utilizing renewable energy sources is one approach to the problem. Salinity gradient energy (blue energy) which is a new member of renewable energies may hold the solution to the problem among them.

World net energy consumption in 2020 was approximately 25300 TW (Malanima 2022). Renewable energy sources are reported to provide for 28.7% (2021) of the total energy consumption (Ibrahim *et al.* 2021). Most of this renewable energy comes from hydropower stations (Kuleszo 2008). Hydropower is followed by solar and wind energy, with a share of 13% and 24%, respectively. The fact that these energy sources are not steady or continuous is a serious problem. They either depend on wind or the sun, this result in a fluctuation in electrical energy production (Simões 2023).

Hydropower is not, however the only source of renewable energy that water can provide. Energy from water is a renewable source of energy that can be harvested in multiple ways. In rivers and oceans there is a lot of energy potential to be utilized. A huge potential to electricity or power supply lies in the oceans. Power derived from the sea can be divided into three categories: thermal, chemical, and mechanical. First includes temperature gradient and the second includes salinity gradients, biomass and the third includes wave and tidal power as well as currents (Isaacs and Schmitt 1980).

Mechanical power so far has received most attention, and a few tidal and wave power plants are in operation (Goldemberg 2001). The thermal gradient has been also given some consideration. Chemical potential of the oceans has not been utilized until now even though it has been realized in the 1950's, and the concept was being developed further in the 70's. The reasons were mainly costs and unavailability of appropriate technologies. Now, with the advancement of membrane technologies and increased need for diverse and carbon-neutral power sources, salinity-gradient power has come back into focus.

1.2 Salinity gradient energy

Salinity gradients are caused by evaporation of water, which in turn is caused by energy from solar radiation (Kuleszo 2008). The evaporated water condenses and precipitates feeding the streams that flow into seas and oceans (Kuleszo 2008). According to Gibbs free energy of mixing, when fresh water and salty water mixes energy is released. Salinity gradients energy could be utilized for power generation as shown in Figure 1.1.

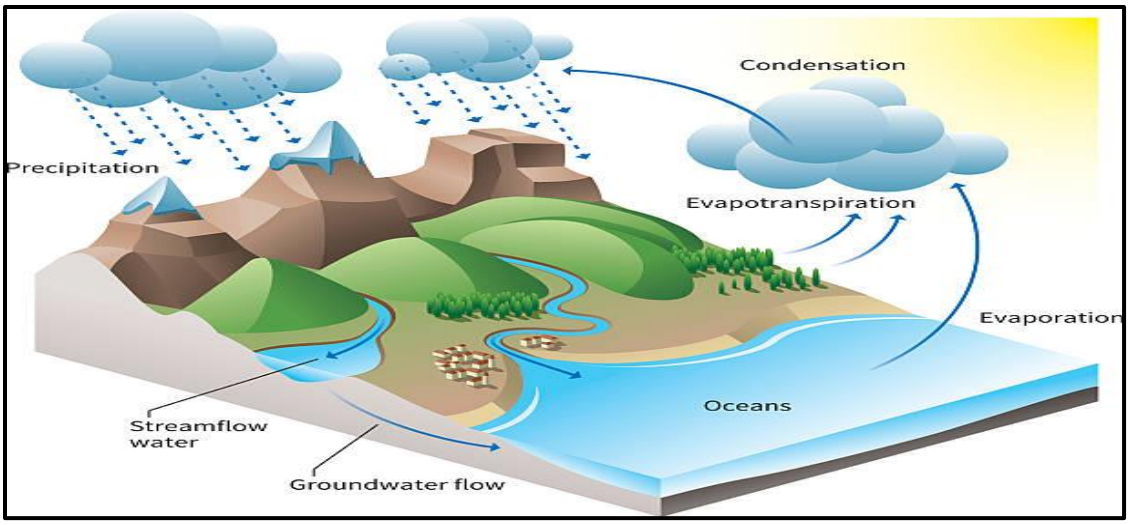

Figure 1.1: Simplified schematic of the hydrological cycle, showing the integration of salinity gradient (Duke 2016).

When sea water and river water with different concentrations come in to contact at the river mouth there is energy that's being released, and the amount of energy released at the river mouths depends on the properties and amounts of water and is governed by Gibb's equation (Equation 1.1). The free energy released during mixing two solutions of different volumes and concentration can be determined from the difference in chemical potential before and after mixing (Post *et al.* 2007). The Gibbs free energy released during mixing depends on several variables: volume, salinity and temperature of both sea water and river water (Ghiorso *et al.* 1983):

$$\mathbf{E} = \sum_{\mathbf{i}}\left(\mathbf{C_{i,C}V_C RT\ln\left(x_{i,C}\right) + C_{i,D}V_D RT\ln\left(x_{i,D}\right) - C_{i,B}V_B RT\ln\left(x_{i,B}\right)}\right) \qquad \textbf{Equation 1.1}$$

Where $E = energy\ (kJ)$, $V = volume\ (m^3)$, $T = temperature\ (K)$, $C = concentration\ (mol/m^3)$, $x = molar\ fraction$, $R = universal\ gas\ constant$, and subscripts $i = salt\ component$, $C = concentrated\ solution$, $D = diluted\ solution$, $B = brackish\ solution$.

Forgacs derived a simplified Equation 1.2 from Equation 1.1 (Forgacs 1982):

$$\mathbf{E = 2RT\left[C_D V_D \ln\frac{C_D(V_C+V_D)}{C_D V_D + C_C V_C} + C_C V_C \ln\frac{C_C(V_C+V_D)}{C_D V_D + C_C V_C}\right]} \qquad \textbf{Equation 1.2}$$

According to (Isaacs and Schmitt 1980) the salinity differences in the open ocean are too low and too remote to be utilized effectively, but the river mouths provide much higher gradients.

Mixing of fresh and sea water of average salinity at the river mouth releases energy equivalent to that of a waterfall over 200m high (Pattle 1954a).

Based on (Kuleszo 2008) the total amount of energy dissipated at the river mouths is expected to be quite high, although it is obvious that not all of the energy can be used, whether for technological, environmental, economic, or political reasons. Therefore, it is wise to define how these affect the amount of potential available power. The types of potential available power can be categorized using the division below, which are based on (Price and Probert 1997):

- Theoretical – defined as the annual energy that is potentially available if all energy being dissipated at the river mouths was produced without any energy losses.
- Technical – defined as the share of the theoretical energy that can be recovered under current technology, regardless of other constrictions.
- Economic – defined as the part of the technical potential that can be developed at costs competitive with other energy sources.
- Exploitable – defined as the fraction of the economic potential that can be used if the environment, political and other special constraints are accounted for.

Due to time limitations, this research focuses on quantification of theoretical potential only. Salinity Gradient Energy (SGE) can be captured by a variety of techniques when a controlled mixing device is used. The most well-known SGE capture techniques are reverse electrodialysis (RED), capacitive mixing (CAPMIX), and pressure retarded osmosis (PRO) (Simões 2023). The osmotic pressure difference across a semipermeable membrane is what propels PRO (Simões 2023). The adsorption and desorption of ions in capacitive layers is what drives CAPMIX (Simões 2023). The salinity gradient, which generates a potential differential across ion exchange membranes, is the driving force of RED (Simões 2023).

CAPMIX operates in a charge-discharge cycle since the feedwater must be swapped frequently, which makes it less desirable than the other two processes (Simões 2023). (Post *et al.* 2007) researched and compared the applicability of PRO and RED. The conclusion was that RED shows more potential for the concentration gradient existing between seawater and river water since higher power density and energy efficiency are retrieved (Simões 2023).

This thesis investigates RED process, using the salinity gradient between seawater and river water to retrieve energy.

1.3 Reverse Electrodialysis

Reverse electrodialysis is a membrane process that uses a RED stack to capture energy as shown in Figure 1.2. Pattle first proposed the idea in 1954. Since then, pilot facilities across the world in Netherlands, Italy, Japan, and South Korea have all received the technology.

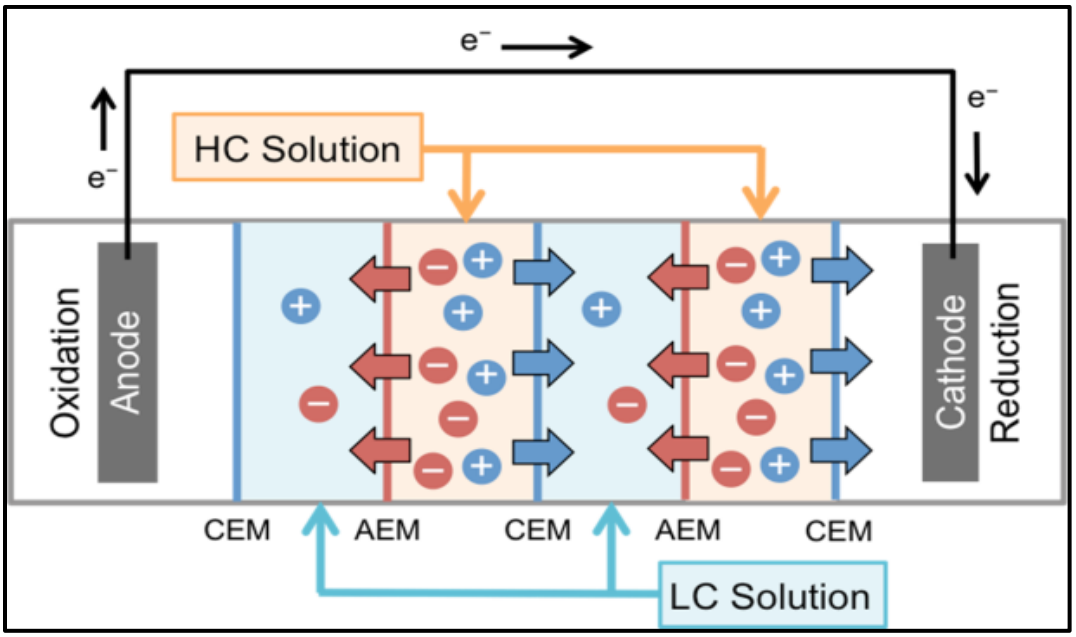

Figure 1.2: Schematic of the reverse electrodialysis process (Zhu, He and Logan 2015).

The stack consists of ion exchange membranes (IEMs), these membranes are anions exchange membranes (AEMs) and cation exchange membranes (CEMs), layered alternatively in the stack as it shown in Figure 1.2. Freshwater (river water) and saltwater (sea water) alternately pass through the compartments between the membranes (Simões 2023). Spacers or membrane profiling can be used to create the compartments. Cell pairs consist of one AEM, one CEM, one sea water compartment, and one river water compartment. There may be hundreds to thousands of cell pairs in a RED stack (Simões 2023). According to their charge and membrane selectivity, the ions would be transferred from the concentrated solution to the less concentrated solution. Cations would cross the CEMs while anions would cross the AEMs.

Potential difference over each membrane results from the feeding of two solutions with different salt concentrations between the compartments (Guimarães 2020). As a result, there is an increased potential differential throughout the membrane pile. An additional shielding membrane and two electrode (anode and cathodes) compartments, one at each end are required to enclose the membrane pile, where the ionic current is transformed into electrical current by electrodes and a redox pair (electrolytes) as it is shown in Figure 1.2 (Simões 2023). Anion passes through the anion exchange membrane, flowing towards the anode and the cation passes through the cation exchange membrane towards the cathode. In the last compartment, to maintain charge neutrality, a reduction reaction was occurred in this compartment because of the cations that pass through the final cation exchange membrane from the concentrated solution to the electrolyte solution in contact with the cathode (Guimarães 2020).

On the anode side, an oxidation reaction was occurred in the anode compartment to make up for the lost positive charges as cations move from the electrolyte solution to a less concentrated solution (Guimarães 2020). Therefore, the presence of an electric current in this circuit will be confirmed by connecting the cathode to the anode via an external circuit and keeping the battery (RED cell) supplied with both concentrated and less concentrated solutions continuously.

1.4 Description of study areas

1.4.1 Thukela River

The Thukela River is the largest river in the KwaZulu-Natal (KZN) Province, South Africa as shown in Figure 1.3 (Tenza 2018). This catchment originates from the Drakensburg escarpment, and it meanders 520 km through the central KZN until it reaches the Indian Ocean at approximately 85 km north of Durban (Tenza 2018). Ingangani River, Sundays River, Buffalo River, uMzinyathi, Mooi River, Klip River, Blood River and Bushmans River, all these rivers are the tributaries of this catchment (Tenza 2018) and (Gazette 23/08/2023).

The catchment area of this river is estimated to be approximately 29000 km^2 with the mean annual runoff (MAR) of $3865 \times 10^6\ m^3/a$ and $0.814\ mol/m^3$ of salt content (Tenza 2018) and (Gazette 23/08/2023). When observing the MAR alone, the uThukela catchment is the second largest river in South Africa, following the orange river which is in first position (Tenza 2018). Summers are

warm and temperature often reach more than 35℃, with rainfall exceeding 1000 mm/a along the escarpment and dropping down to less than 600 mm/a east of Weenen.

Figure 1.3 Picture of uThukela River discharging to the Indian Ocean (Fennessy, Roberts and Paterson 2016).

1.4.2 Mvoti River

The Mvoti River originates from the Natal Midlands, KZN province, South Africa, it meanders through South Easterly direction past Greytown and Stanger until pours into the Indian Ocean at a point that is close to Blythedale beach as shown in Figure 1.4 (Shaddock and Wepener 2015). The length of this river is approximately 197 km with a salt concentration of $0.704\ mol/m^3$ (Shaddock and Wepener 2015). The Hlimbitwa River is regarded as one of the main tributaries of the uMvoti River and they both join near Dhlakati (Sayer et al. 2013). The Department of Water Affairs and Forestry characterized the uMvoti River as a medium sized river with a total MAR of approximately $595 \times 10^6\ m^3/a$ (Tenza 2018) and (Gazette 23/08/2023).

Figure 1.4: Shows a picture of uMvoti river located at KwaZulu Natal (Rescue 25 December 2019).

1.4.3 Umgeni River

The Umgeni River is in KwaZulu Natal, South Africa. The river originates from Dargle, a small farming village on the outskirts of Howick in the KZN midlands, and its mouth is in the Indian Ocean, Durban as shown in Figure 1.5. The river is 232 kilometers long, with a catchment area of 4432 kilometers. The Umgeni River has a MAR of $334 \times 10^6\ m^3/a$, with a salt concentration ranging from 0-1.5 mg/l (Government Gazette 47133).

Figure 1.5: Shows Umgeni River discharging to the Indian Ocean (Stock 2022).

1.4.4 Mkhomazi River

The Mkhomazi River derives its source from the upper Drakensberg Mountains, with an altitude of 3300 m (Taylor 2001). The river is approximately 170 km in length and has a catchment area of 4387 km^2. The total natural mean annual runoff (MAR) of the catchment is $1078 \times 10^6\ m^3/a$ and salt concentration of $0.0269\ mol/m^3$ (Gazette 23/08/2023).

Figure 1.6: Shows a picture of uMkhomazi river (Noelmcdonogh 06 January 2017).

1.4.5 Mfolozi River

The Mfolozi river is a river located in KwaZulu-Natal, a province of South Africa. It is a combination of the Black uMfolozi and a White uMfolozi as shown in Figure 1.7. The total annual discharge of the river to the Indian Ocean is $146.6 \times 10^6\ m^3/a$, with a salt concentration of $0.0243\ mol/m^3$ (Gazette 23/08/2023).

Figure 1.7: picture of uMfolozi river which is the combination of Black and White uMfolozi rivers discharging in the Indian Ocean (NASA 14 March 2003).

1.4.6 Amanzimtoti River

The Amanzimtoti river is a river located in the Kwazulu-Natal province of South Africa, that originates northwest of Adams Mission, and flows through the town of Amanzimtoti, South Africa as shown in Figure 1.8. The Amanzimtoti river discharges to the Indian Ocean. The Amanzimtoti river has a discharge flowrate of $102 \times 10^6\ m^3/a$, and a salt concentration of $0.0240\ mol/m^3$ (Gazette 23/08/2023).

Figure 1.8: shows the Amanzimtoti river mouth that discharge to the Indian Ocean (Guastella and Smith 2014).

1.5 Problem Statement

The current increase of electricity demands has become a stressful topic in South Africa. The current method used to generate electricity by burning fossil fuels e.g., coals is not sustainable and a major contributor of greenhouse gases in the atmosphere. These problems have led to the sudden changes of weather and to acid rains.

The increase of electricity demands, and shortage of coals has led to loadshedding which is a method that is used in South Africa to reduce the high usage of electricity. The high demands of electricity are caused by the increase in population and the high usage of electricity by industries.

The search for energy source that would be environmentally friendly and meet the high demands of electricity is a very important matter, and it requires cost effective methods that would generate electricity. Renewable energies have gained an increasing focus in recent decades since they show a great potential over the years. The present study examined the renewable energy source called salinity gradient energy or blue energy in producing electricity for the future.

The outcomes would contribute to the building up of the pilot plant in the next five years, and the outcomes would also assist in providing answers, theoretically that is it possible to use this source of energy to generate electricity in KwaZulu Natal and in South Africa as a whole?

1.6 Aim and Objectives

The main aim of this study was to investigate the potential, existing in South Africa starting in KwaZulu Natal, of a renewable energy source called energy from salinity gradient (blue energy). This study established whether this energy is capable enough to meet and satisfy a notable fraction of the electricity demands in South Africa.

Based on the main aim, the project specific objectives were to:

1. Calculate the theoretical potential for blue energy production via RED of major KZN rivers discharging into the Indian Ocean.
2. Preliminary design RED-based power plant erected at the mouth of the river produced higher potential for energy.

3. Optimize operating parameters associated with RED-based power plants through simulations and considering all relevant parameters such as flow rates, stream salt concentration, temperature, membrane type.

1.7 Dissertation outline

This dissertation is presented in five chapters as described below:

Chapter 1: This chapter covers introduction, description of study areas, problem statement, aim and objectives of this study.

Chapter 2: This chapter outlines a literature review of the relevant reports that informs this study. This chapter gives the well detailed literature on the salinity gradient energy and its technologies, it's also giving details on the reverse electrodialysis which is the technology that this study focuses on. This chapter also include the background information of the different of techniques that are used to retrieve salinity gradient and it's also covering the background of previous work done on the research topic. This chapter also reflects on the results and findings done by other research related to this research topic.

Chapter 3: This section covers the research calculations methodology since it is theoretical research based on calculation findings and simulations. It gives a detailed description of methods followed in performing assumptions, calculations, and simulation for the report.

Chapter 4: This chapter outlines the results and discussion obtained from this study. It clearly shows the result about the theoretical potential energy of the major rivers, and it shows which river amongst the major rivers produces the highest theoretical potential energy. It provides the analysis in a form of tables, graphs, and plots.

Chapter 5: This chapter shows the conclusions and recommendations drawn from the study.

CHAPTER 2-LITERATURE REVIEW

2.1 Introduction

This study investigates the use of reverse electrodialysis to produce electricity, by mixing river water and sea water using their salinity concentration (salt concentration), where there is a distribution of salt ions from high to low concentrated solution (river water), this distribution of salt is caused by the chemical potential difference over each membrane. As a result, this chapter begins with a background on renewable energy source called salinity gradient energy or blue energy and a brief review of types of technologies used to produce blue energy.

Production or generation of electricity is based on fossil fuels, such as coals worldwide. On an international level, the use of coal is widespread, which is approximately 36% of the world's electricity production (Mitigation 2011). This electricity production method is characterized by vulnerability and imminent scarcity and by the contribution of continuous emission of greenhouse gases during the combustion of fuels (Mitigation 2011). This fossil fuel burning (burning of coals) is amongst the biggest contributors to climate changes, and the use of fossil fuel, such as coal to produce electricity is a non-renewable source of energy (Holloway *et al*. 2007). So, all these reasons illustrated above, motivated for the research of new methods that can be used to produce electricity. Methods that would be renewable source of energy and which would be environmentally friendly. The source of energy that would meet all the electricity demands in the world since the present method, which is burning of coals does not meet all the electricity demands due to the shortage of coals. Several types of renewable sources of energy have been developed to produce electricity and try to meet the need of electricity in the world, these renewable sources are solar energy, wind energy, and tidal energy, hydro energy, geothermal energy, biomass energy and salinity gradient energy. Then, salinity gradient energy is selected in this study as the source of energy.

Salinity gradient energy is the energy retrieved from mixing two solutions that have different salt concentration (high and low salt concertation) or is the energy available from the difference in the salt concentration between seawater and river water, and this energy is used to produce electricity (Post *et al.* 2007). To retrieve this energy, there are three technologies that are used to produce

salinity gradient energy, two of them uses the membrane process to produce salinity gradient energy. These two technologies are the most popular ones which are: reverse electrodialysis (RED), pressure-retarded osmosis (PRO) and the third one is the capacitive mixing (CAPMIX). The byproduct of these two processes that uses membranes to produce salinity gradient energy is brackish water (is water that has more salinity than fresh water), which results in mixing river water and sea water (Pattle 1954b). Salinity gradient technologies generate electricity from the chemical pressure differential created by difference in ionic concentration between fresh water and sea water. Seawater has a higher osmotic pressure than fresh water due to its high concentration of salt (Post 2009). Pilot plants in countries like Italy and the Netherlands have been built to further investigate about reverse electrodialysis. Salinity gradient energy shows promising results.

2.2 Environmental impacts

Revers electrodialysis technology is environmentally friendly because it does not produce any toxic gases that can harm the atmosphere. It is a clean and sustainable energy. However, the current energy source (burning of coals) in South Africa have been in the spotlight due to their negative effects on the environment and human health. The burning of coals (coal combustion) to generate electricity emits toxic substances such as Sulphur dioxide (SO_2), which contribute to smog and respiratory illness, carbon dioxide (CO_2), which is the primary greenhouse gas produced from burning coals (Dunmade *et al.* 2019).

2.3 Reverse electrodialysis

Salinity gradient energy (blue energy) is produced by mixing two constant flows of different salt concentration via ion-exchange membranes. In reverse electrodialysis, seawater and fresh water (river water) are let through a stack of alternating cation and anion exchange membranes where there is a transfer of ions, during that transfer of ions energy is produced (Chanda and Tsai 2019). The difference in concentration is the driving force for salinity gradient energy (Yip and Elimelech 2014). RED utilizes a flow system between electrodes and alternating cation and anion exchange membranes (Nam *et al.* 2021). The transport of dissolved salt ions through a stack of alternating membranes creates an electrical potential capable of generating electricity (Coleman Gilstrap 2013). The ions are forced to move in specific directions generating an electrical current (Altıok *et al.* 2021).

The chemical potential differences cause the transport of ions through the membranes from the high concentrated solution to the low concentrated solution (Hong *et al.* 2015). The process works through differences in ion concentration, when there is a transfer of ions through the membrane energy is produced. (Guimarães 2020) conducted research based on theoretical calculations to assess the potential of salinity gradient energy using five major rivers in Portugal. These five major rivers were: Douro, Mondego, Tejo, Sado and Guadiana, the aim was to find the annual potential in each of the rivers and to compare them in finding, which river produces higher potential between them. Assuming that the temperature of seawater and river water is 10℃, and using concentration of 0.48 M_{NaCl} for seawater in Portugal, the result concluded that Douro River had higher potential for electricity production than the other four rivers.

2.3.1 Ion Exchange

Ion exchange membranes are made of polymers that contain ionic groups or charged functional groups; these ionic groups are called polyelectrolytes (Guimarães 2020). These polymers contain ionic groups, which not only cause strong attraction between ions with opposing charges (counter-ions), but also strong repulsion between ions with the same charge (co-ions). According to the Donnan Exclusion principle, ions that have the same charge as the ionic groups fixed in the membrane structure are excluded and cannot penetrate the membrane when an ion exchange membrane is in contact with an ionic solution. Ion distribution would be established both in the solution and in the membrane because of ion exclusion and attraction.

Ion exchange membranes (IEMs) are most frequently categorized according to their charged functional groups or ionic groups: sulfonic acid ($-SO_3^-$), carboxylic acid (-COO^-), phosphoryl ($-PO_3^{2-}$), and phosphonic acid ($-PO_3H^-$) are a few examples of negatively charged groups found in CEMs (cation exchange membranes) that selectively let cations to pass but reject anions. While AEMs contain positively charged groups such as ammonium ($-NH_3^+$), secondary amine ($-NRH_2^+$), tertiary amine ($-NR_2H^+$), and quaternary amine ($-NR_3^+$), that preferentially transport anions while excluding cations (Xu 2005).

An IEM can be homogeneous or heterogeneous depending on the manufacture method as shown in Figure 2.1, and its physical makeup (Kariduraganavar *et al.* 2006). In a homogeneous membrane, the membrane matrix is uniformly charged, or it has fixed charges uniformly

distributed in the polymer matrix. In contrast, a heterogeneous membrane, often containing uncharged binding polymer separates charged domains of ion exchange resin, is characterized with non-uniform charge distribution (Xu 2005). According to the methods used in preparation of homogeneous membranes, homogeneous membranes can be further divided into two categories: (1) membranes prepared from copolymerization of monomers for example styrene and divinylbenzene, which can be functionalized (e.g., chloromethylation-amination for CEMs and sulfonation for AEMs), (2) membranes constructed of polymer, either polymer solution (e.g., polystyrene (PS), or polymer film (e.g., hydrocarbon polyethylene (PE), polypropylene (PP), and fluorocarbon, etc.), and then grafted with functional monomers or non-functional monomers that can be further functionalized (Xu 2005).

Contrarily, heterogeneous membranes are commonly created from blending powered or melted ion exchange resin with uncharged polymer (such as polyvinylchloride (PVC), acrylonitrile, etc.) and pressing or casting into membrane films (Nagarale, Gohil and Shahi 2006).

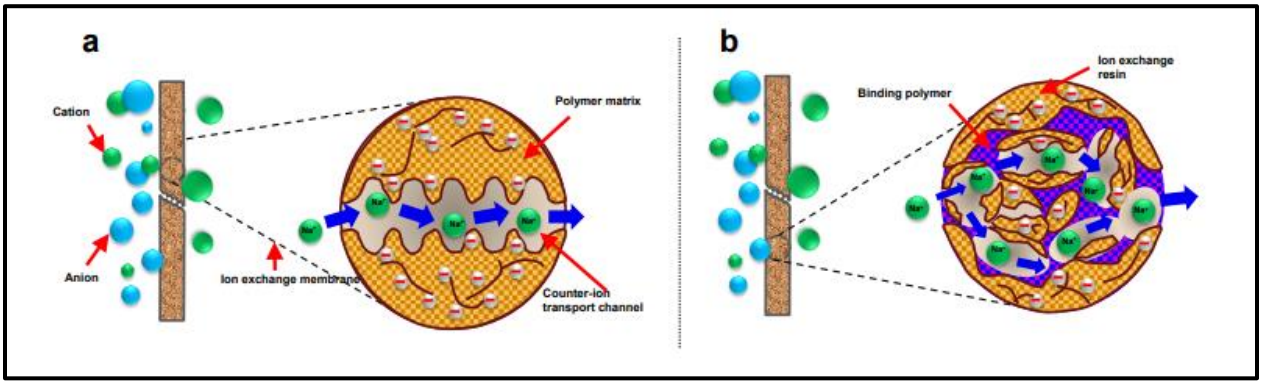

Figure 2.1: A schematic diagrams of the internal structure of (a) a homogeneous membrane in which fixed charges uniformly distribute in the polymer matrix and (b) a heterogeneous membrane in which charged domains of ion exchange resin mix with uncharged binding polymer. Source taking from (Mei and Tang 2018).

The type of ion exchange membranes utilized has a significant impact on how much energy is generated in a red stack or cell. The most significant ion exchange membranes characteristics are permselectivity and electrical resistance, which have a significant impact on the RED power output performance. Permselectivity describes an IEM's capacity to move specific counter-ions, such as cations in a CEM. The ideal IEM should have a permselectivity of 1, preventing co-ions from

passing through the membrane matrix in any way. Since co-ions movement is unavoidable in real life, membrane permselectivity is typically less than 1. According to electromotive force (EMF) equation, a larger permselectivity increases the voltage output.

Through their impact on permselectivity and electrical resistance, additional properties including water content on the membrane matrix, ion exchange capacity (IEC), and fixed charge density (FCD) might affect RED performance (Mei and Tang 2018). However, other factors, like concentrations of the solutions fed or the operating temperature, can also have an impact on selectivity and resistance (Mei and Tang 2018). Water content is critical to membrane dimensional stability and ionic transport capabilities, because most ion exchange membrane matrices are composed of hydrophobic polymers, the presence of ionic groups or fixed charges in their matrix means that they have a strong attraction for water.

Despite a positive impact water content have on membrane conductivity, excessive water content implies a loose mechanical structure and frequently leads to poor permselectivity (Hong *et al.* 2015). Water content is influenced by membrane material, ionic groups/fixed charged groups, cross-linking degree of membrane matrix and surrounding solution conditions (Nagarale, Gohil and Shahi 2006). For instance, some AEMs with relatively low cross-linking degrees tend to have higher water content than their more crosslinked CEMs counterparts. A given membrane's water content can be experimentally determined by measuring membrane swelling degree (SD) (Güler *et al.* 2013):

$$\mathbf{SD} = \frac{\mathbf{m_{wet} - m_{dry}}}{\mathbf{m_{dry}}} \times \mathbf{100} \qquad \textbf{Equation 2.1}$$

Where m_{dry} is weight of IEM in dry condition and m_{wet} is weight of IEM sample in its corresponding wet phase.

As a result, for a swelling, a membrane would have a high content of water in its structure when in contact with an aqueous solution. An increase in SD results in a higher ionic conductivity in the membrane, thereby decreasing the resistance to ionic transport, however, high amounts of water in the membrane cause a functional loss of the structure, thus leading to low selectivity values (Mei and Tang 2018). As a form of prevention, the polymer matrix of membranes is crosslinked, which is when two or more polymers are joined together. This strategy allows for a decrease in the membrane's affinity for water (Tedesco *et al.* 2015). As previously mentioned, ion exchange

capacity (IEC), plays an important role in the ion exchange membrane. This represents the number of fixed charges in its structure and is expressed in milliequivalents of fixed ionic groups per gram of dry membrane (Mei and Tang 2018). The Donnan exclusion principle states that as the number of ionic groups in a membrane structure increases, co-ions are excluded more effectively, enhancing the membrane's selectivity (Guimarães 2020). However, the increase in fixed charges in the polymer matrix leads to a greater affinity for water, which reduces the selectivity due to this effect (Mei and Tang 2018).

Thus, the idea of fixed charge density (FCD), appears in order to more accurately evaluate the effect of the rise in fixed ionic groups on the membrane structure. This property is the ratio of the ion exchange capacity to the degree of swelling and is expressed in milli-equivalents of fixed charges per gram of water contained in the membrane structure. When the fixed charge density value increases, co-ion exclusion is more effective. Therefore, the membrane selectivity also increases.

The co-ion exclusion becomes less and less effective as the solution's concentration rises. As a result, the co-ion concentration in the membrane will rise, resulting in a decrease in the membrane selectivity. Temperature is another environmental component that affects how well the membrane works. The membrane resistance decreases as ion mobility increases with temperature.

2.3.2 Spacers and Solution Compartments

In RED stacks, spacers are mostly used to support IEMs, by providing flow channels, and ensuring that there is space between them, in which the fed solutions can flow. Spacers also promote mixing, enhanced mixing caused by spacers tends to minimize concentration polarization and hence lower or reduce non-ohmic resistance (Mei and Tang 2018). By decreasing the concentration polarization at the membrane solution interface and decreasing the non-ohmic resistance results in the improvement of the RED battery's performance. The thickness of the spacers is crucial parameter, which strongly influence the energy produced by the stack, since spacers thickness affects the electrical resistance of the solution compartments.

When the thickness is low, the fed solutions' compartments experience greater pressure drops, which increases the energy required to pump the solutions (Guimarães 2020). However, for high values of thickness, the resistance of the compartments of the fed solutions increases. It is crucial

to note that the resistances increase as the thickness of the spacers increases, especially for the compartments that receive solutions with lower salt contents. Low salinity concentration solution compartments usually are the biggest contributors to the overall internal resistance, due to the low conductivity of these solutions (Mei and Tang 2018). To reduce the internal resistance of RED stack, thinner spacers are often recommended (Post, Hamelers and Buisman 2008).

Recent research showed that simply decreasing spacer thickness from 0.5 mm to 0.2 mm improved power density by a factor of 1.6 (correspondingly from $0.56\,W/m^2$ to $0.87\,W/m^2$) (Post, Hamelers and Buisman 2008). (Vermaas *et al.* 2013) reported a power density of as high as $2.2\,W/m^2$ utilising a 0.1mm thick spacer. Although, the use of excessively thin spacers can significantly increase energy consumption for pumping due to greater pressure drop in the flow channels, which reduced the available net power density. Therefore, ultrathin feed spacers (for example 0.06mm) are not practicable for RED application due to the high energy cost of pumping. In addition, thin or small spacers are more susceptible or vulnerable to fouling, which reduces stability of stack operation in practice (Mei and Tang 2018). To maximize net power density, spacer thickness needs to be carefully optimized. It is also important to keep in mind that the precise value of optimal spacer thickness varied with other parameters of an RED stack (Mei and Tang 2018). For instance, a spacer with greater open area favors a thinner spacer thickness since it is less likely to experience pressure loss.

The present of non-conductive spacers reduces active membrane area for ionic conduction (which is also known as the spacer shadow effect), and makes ionic transport to be partially blocked, resulting in higher ohmic resistance particularly in low salinity compartments (Weinstein and Leitz 1976). Using non-conductive spacers for a typical lab-scale RED stack, the shielding effect might increase internal resistance by a factor of 1.5 (Veerman *et al.* 2009), and possibly contribute to 30-40 % less energy generation compared to the theoretically available energy (Długołęcki *et al.* 2009). However, by using anionic and cationic conductive spacers, the shadowing effect of the spacers can be reduced. (Długołęcki *et al.* 2009), conducted research to explore the use of ion-conductive spacers to eliminate the spacer shadow effect, and their study showed 3-4 times increase in power density. To reduce the shielding effect, researchers have also created spacers with larger open areas. Additionally, these spacers have the tendency to greatly reduce the

hydraulic friction in the flow channels, enabling the use of thinner channel gaps (say ~ 100 μm or less) to obtain lower electrical resistance (Vermaas, Saakes and Nijmeijer 2011b).

Using profiled ion exchange membranes is another technique to reduce or perhaps get rid of the shadow effect of spacers. These membranes are embossed with well-defined geometric patterns on their surface, such as pillars or waves. These membranes are comparable to a conductive spacer (ionic and cationic conductive), as they guarantee a thickness for the compartments to which the solutions are fed and ensure a good mixing of the solutions (Guimarães 2020).

2.3.3 Electrodes and Electrolyte

Electrode systems is composed of electrodes (cathode, anode), and electrolytes filled in the electrode compartments, convert ionic current to electric current through redox reactions. As mentioned, these systems convert ionic fluxes or ionic current to electric current, due to the reduction reactions that take place in the cathode compartment and the oxidation reactions that takes place in the anode compartment (Mei and Tang 2018).

Electrode systems that are commonly used can be classified into two categories: with or without opposite electrode reactions (Mei and Tang 2018). Systems in which the reactions that take place in the anode compartment are not the opposite of those that occur in the cathode compartment, these are systems where there is production of gases. For this type of systems, water reduction reactions take place at the cathode, producing hydrogen, and at the anode electrode, oxidation reactions take place producing chlorine. Due to energy losses in the production of gases, these systems are not ideal from the perspective of producing electricity through a RED cell or stack. Additionally, huge RED batteries, those with numerous membranes and powered solution compartments, are required for these kinds of electrode systems to achieve a battery potential difference greater than its equilibrium potential. Due to the high activation overpotentials of the electrodes in these types of electrode systems, the equilibrium potential of the cell or stack is higher (Veerman *et al.* 2010). Additionally, these kinds of electrode systems require extra equipment for the collection of explosive gases (e.g., H_2), and dangerous gases (e.g., Cl_2) (Audinos 1992).

Electrodes systems in which the reduction reactions are opposite to the oxidation reactions are systems where there is no production of gases in the electrode compartments, as result, there are no energy losses related with the formation of gases (Guimarães 2020). These systems often have

substantially smaller overpotentials than the other type of system. As a result, RED cells with electrode systems of opposing reactions have very low equilibrium potentials, allowing for the creation of RED batteries with small number of stacks or cells (Veerman *et al.* 2010). Due to the mentioned above information, to improve power generation performance and to ensure safety, electrode systems with opposite reactions are more frequently used (Mei and Tang 2018). There are two subgroups within electrode systems with opposing reduction reactions to oxidation reactions, and they are distinguished by the fact that the electrodes have, or not, an active role in the reactions of reduction and oxidation.

The system built by Pattle, in which he used metallic copper electrodes and a copper II sulphate electrolyte, which is recirculated by means of a pump between the two electrode compartments, could serve as an illustration of how electrodes are involved in redox reactions. The cathode compartment undergoes the opposite reaction, the reduction of the copper II ion that is dissolved in the electrolyte, while the anode undergoes oxidation, converting metallic copper to copper II. As a result, the cathode would be formed in the reverse reaction while the anode is consumed in the oxidation reaction. Therefore, systems where the electrodes play an active role in redox reactions would not be appropriate at a salt gradient exploration level since after some time of operation, one would need to stop and change the electrodes, to address the formation issue. Theoretically, though, this issue might be resolved without having to stop the RED battery. When changing the feeds, that is, the compartments where a concentrated solution was fed, a diluted or low salt solution is fed and vice versa, the anode would be exchanged with the cathode (Guimarães 2020). However, the geometries of the compartments of a RED cell are optimized, for instance, the compartments containing diluted solutions are narrower than those of concentrated solutions. This indicates that the energy use is significantly reduced while changing the power supply (Mei and Tang 2018).

Finally, there is no need to change the anode with the cathode on a regular basis when using electrode systems with homogenous redox pairs and inert electrodes (Guimarães 2020). This type of system is the most desirable for a RED battery as it allows for continuous operation. Metal electrodes, which may even contain rare metals, have been replaced by graphite electrodes, in order to reduce the costs of RED batteries and increase profitability of the technology. The use of graphite as the electrode, either for the anode or for the cathode, with an aqueous solution of

potassium ferrocyanide as the electrolyte is one electrode system that appears to have received a lot of research. Equations (2.2) and (2.3) outline the redox reactions that take place in each of the compartments for this type of system (Veerman *et al.* 2010):

Oxidation reaction (anode compartment): $\mathbf{Fe(CN)_6^{4-} \rightarrow Fe(CN)_6^{3-} + e^-}$ **Equation 2.2**

Reduction reaction (cathode compartment): $\mathbf{Fe(CN)_6^{3-} + e^- \rightarrow Fe(CN)_6^{4-}}$ **Equation 2.3**

Cation exchange membranes that serve as a barrier for the anions present in the electrolyte are used to prevent the passage of ferrocyanide ion to concentrated and diluted solutions fed to the battery. Another example of an electrode system is the use of graphite electrodes with an iron chloride solution, for which anion exchange membranes are used to keep iron II/III ions in the electrode compartments (Veerman *et al.* 2010).

2.3.4 Flow configurations in a Reverse Electrodialysis stack

Reverse electrodialysis stack can be operated using three different flow configurations. These solutions of different salt concentrations can flow in co-current, counter-current, or cross flow (Guimarães 2020). However, if one keeps all other variables constant, the energy produced by the RED stack varies for the three types of configurations. (Vermaas, Saakes and Nijmeijer 2011b), examined, and compered, the energy generated and the energy efficiency in the three configurations for a RED cell using a theoretical model. Solution of 0.513 M of sodium chloride (sea water), and a solution of 0.017 M of sodium chloride (river water) where fed to the cell that was 0.1 m long and 0.1 wide, with 0.1 mm thickness of compartments. The river water flow rate was assumed to be constant at $3.33 \times 10^{-2} cm^3/s$, and a residence time of 30 seconds. The model assumes ideal membranes, with permselective equal to 1 for both membranes, and do not have ionic transport resistant. Additionally, it ignores non-ohmic resistances such as concentration polarization (Vermaas *et al.* 2013). Based on the above information of the RED stack that (Vermaas, Saakes and Nijmeijer 2011a), used, the results showed that a RED stack with counter-current configuration has a better energy utilization compared to the other two configurations for concentrated solution fractions between 0.1 and 0.5. The RED stack's maximum energy efficiency, reached in a counter-current configuration, was 95% and was attained for a fraction of 0.13.

However, operating a pile of stack with concentration solution fractions above the maximum efficiency point may be advantageous because the energy gain is substantial, and the efficiency

loss is minimal (Guimarães 2020). The energy lost through ohmic losses, and the energy not used, both increases as the flow rate of the concentrated solution increases (Guimarães 2020).

2.3.5 Ionic Transport in a Reverse Electrodialysis stack

Ions are transported through an ion exchange membrane from one solution to another due to the application of forces on them. The driving forces that act on the ions can be expressed by the potential gradient that is established along the membrane (Guimarães 2020). This potential gradient occurs because the membrane is in contact with two solutions of distinct potential gradients. Thus, because of the forces acting on the ions, ions would be forced to move from the solution with the highest potential (high salt concentration) to the one with the lowest potential (Guimarães 2020). As a result, the system naturally tends to move towards equilibrium, which is attained when the potential gradients of the two solutions are equal. In reverse electrodialysis, however, it is not preferred for the system to reach equilibrium since when it does, no energy is produced (Strathmann 2004). In this way solutions are fed continuously and then removed from the RED stack to ensure that the potential gradient remains constant (Mulder 1996).

There are two types of potential gradients for ion transport across ion exchange membranes in a RED cell. First potential gradient type is a chemical potential gradient, which is created along the membrane due to the feeding of two ionic solutions with different concentrations that are separated by an ion exchange membrane. The ionic solutes present in the solution with the highest chemical potential, in the solution with a higher concentration of salts would diffuse through the membrane to the most diluted solution (low salt concentration) as a result of the concentration difference (Guimarães 2020). The cations and anions present in the higher concentration solution would have to diffuse through the ion exchange membrane simultaneously and in the same direction since the phenomena of ion diffusion requires that electroneutrality be maintained in the system. Equation 2.4 uses Fick's Law to calculate the flux (J_i) of the simultaneous diffusion of cations and anions in the membrane (Mulder 1996):

$$\mathbf{J_i = -D_i \cdot \frac{dC}{dx}} \qquad \textbf{Equation 2.4}$$

Where D_i represent a diffusivity of the ionic solute (cation plus anion) in the membrane.

Phenomena of attraction and exclusion of ions present in ionic solutions (river, and sea water), is caused by ionic groups fixed in ion exchange membranes structure, thus this leads to a non-uniform distribution of ions. Non-uniform distribution leads to the formation of an electrical potential at the membrane-solution interface, which also called the Donnan potential (Guimarães 2020). The greater the concentration of an ion that would be exchanged through the membrane, the greater the potential established at the interface. This means that when two ionic solutions of different concentrations assuming that they would be ideal solutions, which would only apply to very dilute solutions. They are separated by an ion exchange membrane; an electric potential gradient would be established along the membrane. Because of this electrical potential gradient, the counter-ions (opposite charge ions) present in the high concentrated solution would migrate to the solution of less concentrated (diluted solution), crossing the ion exchange membrane (Mulder 1996).

Electrochemical potential gradient is the sum of the chemical potential gradient and the electrical potential gradient (Guimarães 2020). The following equation shows the flux of ions in a membrane due to the electrochemical potential gradient, which is given by the Nernst-Planck equation combining with the Fick diffusion process and ionic conduction:

$$\mathbf{J_i = -D_i \cdot \frac{dC}{dx} - \frac{z_i \cdot F \cdot C_i \cdot D_i}{R \cdot T} \frac{d\varphi}{dx}} \qquad \textbf{Equation 2.5}$$

Where F is the Faraday constant, R is the perfect gas constant, z_i represents the ion charge, T is the temperature of the solutions, C_i and D_i represents the concentrated solution and diluted solution.

The Nernst-Planck equation, however, does not account for possible synergistic phenomena between the driving forces, thus being able to give values of ionic fluxes different from the actual ones (Strathmann 2004). Because of the electrical potential gradient generated on the membrane, the ions that migrate from the more concentrated solution to the less concentrated solution are hydrated. In this way, each ion that migrates between the two solutions is taken with its molecules of water that are part of its hydration sphere. There is also an electro-osmotic transport, because of the migration of ionic species. However, there are also osmotic flows due to the difference in concentration between two solutions. This osmotic transport has an opposite direction to ionic transport and electro-osmotic transport, as water flows from a less concentrated solution to a more concentrated solution as shown in Figure 2.2 (Strathmann 2004).

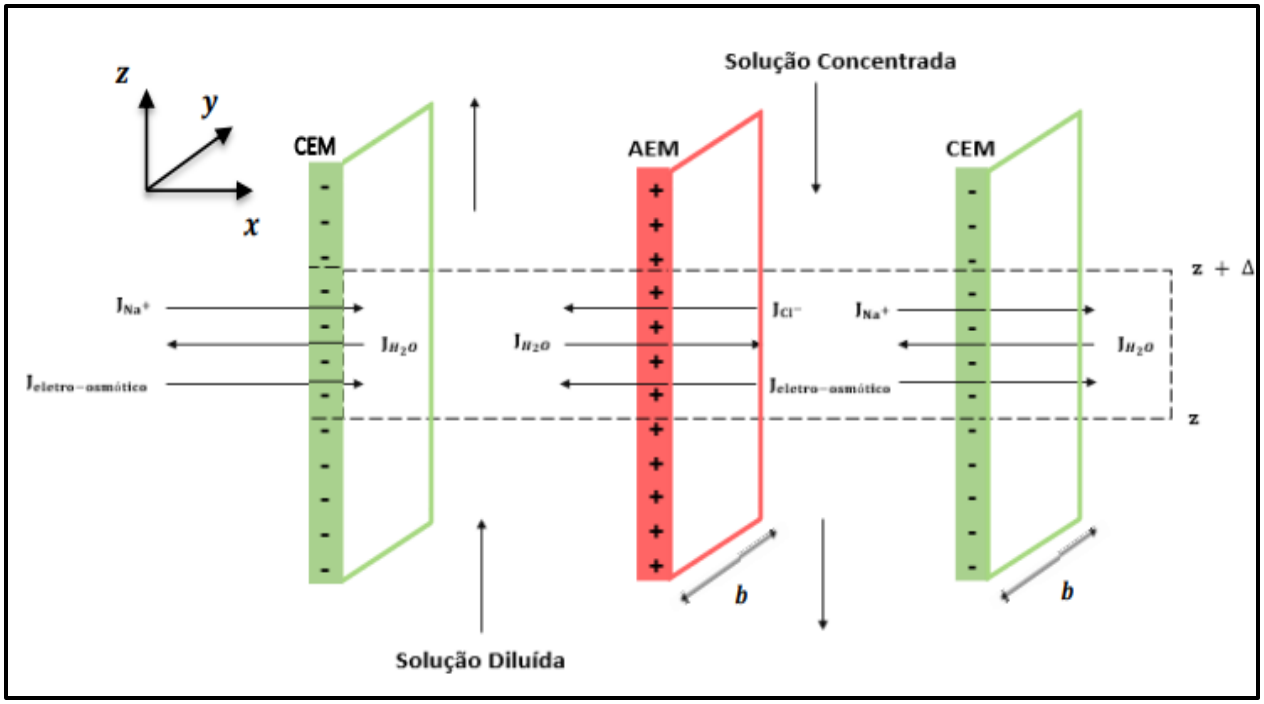

Figure 2.2: The ion transport and water across the RED stack in counter-current flow (Guimarães 2020).

This picture was taken from the literature written in Portuguese where: solucao diluida means diluted solution, solucao concentrada (concentrated solution), $J_{eletro-osmtica}$ means electro-osmotic.

2.4 Effects of operation conditions on RED performance

2.4.1 Feed solution properties

The feed solutions affect the internal resistance and electromotive force of the RED stack. In particular low salinity concentration compartment is a major contributor to the overall internal resistance since it has a low conductivity due to low salt concentration for example when sea water and river water were used, low salinity compartment may account for up to 45% of overall internal resistance (Daniilidis *et al.* 2014). Due to their easy accessibility, river water (usually 0.05-0.1%), and seawater (3%) are the most frequently reported feed solutions (Post, Hamelers and Buisman

2008) and (Vermaas *et al.* 2013). Alternative high salinity solution and low salinity solution sources have also been investigated. Most of the alternative high salinity solutions have higher salt concentration, often greater than 5% than ordinary seawater to achieve better RED power output performance. Hypersaline solutions, brine from seawater desalination plants, and synthetic high concentration solutions used in closed-loop osmotic heat engines are a few examples of high salinity solutions alternative (Luo *et al.* 2012). Brackish water and treated wastewater are few examples of alternative low salinity solutions (Logan and Elimelech 2012).

According to (Mei and Tang 2018), RED performance can be enhanced by higher high salinity concentration solution as well as greater salinity difference between high salinity and low salinity. For instance, by increasing the high salinity concentration solution from 0.5M to 5M, the power density can be enhanced by approximately 10 times (Post *et al.* 2007). (Daniilidis *et al.* 2014), performed an experiment using fresh water of 0.01 M NaCl and concentrated brine of 5 M NaCl at 60 ℃ and a power density of as high as 6.7 W/m^2. However, in concentrated brine, membrane permselectivity tends to decrease, which would limit further improvement of power generation (Daniilidis *et al.* 2014).

Higher low salinity concentrations for a given high salinity results in two opposing effects: decreased electromotive force that would reduce power output performance and reduce internal resistance that would promote greater power density (Tedesco *et al.* 2015). Higher low salinity concentration solution reduces concentration polarization and decreases non-ohmic resistance (Gurreri *et al.* 2014). Therefore, to achieve the maximum power density, precise optimization of the low salinity concentration is necessary. An optimal low salinity concentration in the range of 5-20 Mm was reported by (Mei and Tang 2017). Their research found that lower low salinity concentration caused excessive power loss due to the increased internal resistance, while higher low salinity concentration caused a significant drop in the available electromotive force. It is significant to remember that the optimal low salinity concentration depends on the properties and operation of the RED system. For instance, lower low salinity concentration can be better prevented in RED stacks by using thinner low salinity compartment thickness, for such conditions, the electrical resistance of the low salinity compartments would be less (Tedesco *et al.* 2015).

Numerous studies have also investigated the influence multivalent ions have on RED performance, these multivalent ions (such as SO_4^{2-}, Mg^{2+} , etc.) are common in natural water sources (Tufa *et*

al. 2014; Avci *et al.* 2016). The findings indicated that the presence of multivalent ions in feed solutions tends to increase the membrane resistance and as a result lowering power output performance (Post, Hamelers and Buisman 2009). Additionally, multivalent ions would move from low salinity to high salinity (also known as up-hill transport) at twice the number of monovalent ions moving from high salinity to low salinity, resulting in a decrease in voltage output (Vermaas *et al.* 2014b). This phenomenon occurs when multivalent ions are only present in low salinities and when multivalent ions are presented on both sides of solutions that electrochemical motive force of multivalent ions and monovalent ions are different (Lacey 1980) and (Jagur-Grodzinski and Kramer 1986).

The combined effects of higher resistance and lower voltage output when using natural water as feed solutions may result in a 50% reduction in power density when compared to that obtained using synthetic solutions (Vermaas *et al.* 2013). Monovalent ion selective membrane is preferred to prevent up-hill transport of divalent or multivalent ions against the overall concentration gradient (Post, Hamelers and Buisman 2009; Güler *et al.* 2014). By copolymerizing 2-acryloylamido-2-methylpropanesulfonic acid with N, N-methylenebis (acrylamide), (Güler *et al.* 2014), prepared a strongly negatively charged layer on a commercial AEM, and the resulting membrane demonstrated significantly reduced transport of multivalent ions. The enhanced hydrophilicity and anti-fouling ability were added as advantage of the membrane (Mei and Tang 2017). Additional strategies have also been studied, including softening pretreatment and combining higher flow rate of high salinity with thicker compartment channels (Tufa *et al.* 2014).

2.4.2 Feed flow velocity and temperature

Increasing feed solution flow velocity would enhance ionic mixing in water compartments (which reduces non-ohmic resistance), and boost electromotive force at the expense of more pumping energy (Mei and Tang 2018). Additionally, higher flow velocity can successfully reduce the effect of increased low salinity concentration due to the accumulation of ions transported from high salinity to low salinity (Zhu, He and Logan 2015). As a result, there is an optimal flow velocity that maximizes net power density (Długołęcki *et al.* 2009). Depending on the stack's design (for example compartment thickness and spacer geometry) and operational conditions (e.g., feed concentration of the solution), this optional value may change (Gurreri *et al.* 2014). A flow velocity on the order of 1 cm/s is often recommended for lab scale RED tests (Tedesco *et al.* 2015). It is

important to keep in mind that the optimal flow velocity of low salinity may differ from that of high salinity. A lower flow velocity can be used for high salinity solution to reduce its pumping energy, since its contribution to the total electrical resistance is typically less significant (Gurreria *et al.* 2013).

The optimal flow velocity for low salinity (such as river water) was determined by the competing effects of increasing concentration polarization and decreasing electrical resistance, as well as pumping energy usage (Tedesco *et al.* 2015). Low salinity optimal flow velocity would be higher than that of high salinity since the electrical resistance of the low salinity is many orders of magnitude larger than that of high salinity as shown in Figure 2.3.

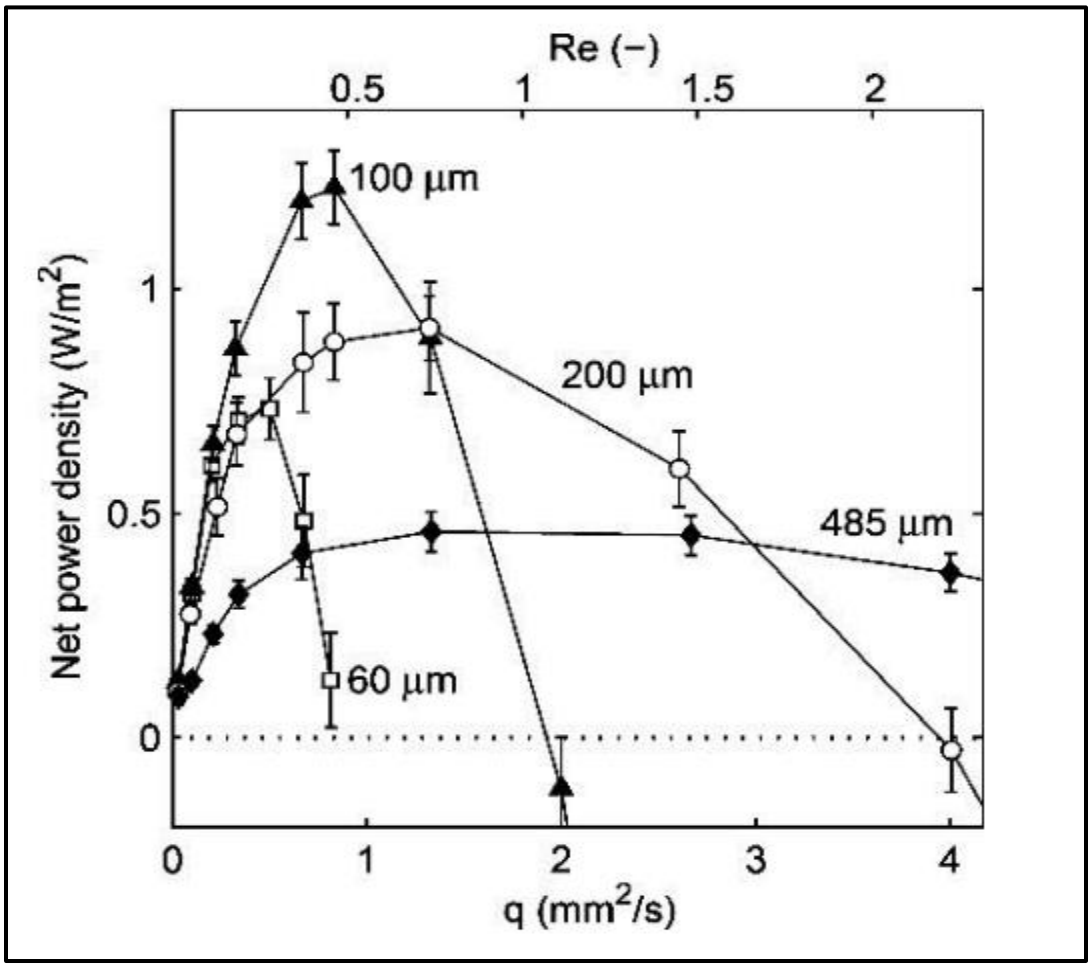

Figure 2.3: The correlation between maximum net power density and flow velocity. The flow velocity is reported per cell per unit width i.e., flow rate per cell divided by the cell width. (Vermaas, Saakes and Nijmeijer 2011a)

Temperature of feed solutions is another factor that needs to be considered because of its importance influence on electromotive force and conductivity of both solutions and ion exchange membranes (Długołęcki *et al.* 2009). RED performance can be influenced by the temperature of natural water sources since it can have significant seasonable and diurnal variations (Brauns 2009; Daniilidis *et al.* 2014). RED power production benefits from water sources with high temperatures, such as membrane distillation effluents, heated synthetic thermolytic solutions, and solar heated desalination brines (Luo *et al.* 2012; Tufa *et al.* 2015). However, membrane permselectivity may be affected by excessive high temperature of feed solutions (Mei and Tang 2018). At 60 ℃, (Daniilidis *et al.* 2014), reported a reduced permselectivity of 60%. On the other hand, (Mei and Tang 2017), demonstrated much improved power performance at the temperature of 60 ℃.

2.4.3. RED membrane fouling

One of the main obstacles to the practical application of RED is membrane fouling. The usage of natural water sources may cause membranes and spacers in a RED stack to get fouled. Fouling, which increases resistance and decreases apparent permselectivity of membrane, can drastically lower power density (by as much as 60% when utilizing natural seawater and natural river water) (Vermaas *et al.* 2013; Kingsbury *et al.* 2017). The fixed charges on the membrane surface significantly affect the type and rate of fouling. For instance, negatively charged CEMs tend to be sensitive to scaling (Vermaas *et al.* 2013). Positively charged AEMs, on the other hand, are more vulnerable to organic fouling and biofouling (Vermaas *et al.* 2013; Vaselbehagh *et al.* 2017). Additionally, spacers can also play a crucial role in fouling formation in solution compartments. According to (Vermaas, Saakes and Nijmeijer 2011b), reported that spacers were more vulnerable to biofouling than membranes. (Vermaas *et al.* 2013), found a 40% decrease in power density for profiled membranes compared to a 60% decrease for standard membranes (membranes with spacers), demonstrating how spacer less RED stacks (using profiled membranes) can achieve reduced fouling.

Additionally, the foulant location according to (Kingsbury *et al.* 2017) would also determine its impact on RED performance. According to research done by (Kingsbury *et al.* 2017), RED stacks containing naturally occurring organic matter presented in low salinity tends to be more sensitive to fouling. For fouling control in the context of reverse electrodialysis, numerous strategies have been investigated. Operational conditions optimization, improved spacer design, and membrane

surface modification are some of the examples of the strategies (Vermaas *et al.* 2014a; He *et al.* 2016; Vaselbehagh *et al.* 2017). Periodic air sparging and periodic feed solutions interchange, which involves switching the flow compartments of the high salinity and low salinity, proves to be an effective method to prevent both organic fouling and colloidal fouling (Vermaas *et al.* 2014a). However, (Moreno *et al.* 2017), recently applied carbon dioxide saturated feed solutions for fouling mitigation and demonstrated better result than air sparging due to bubble nucleation. Spacers providing more uniform flow distribution is less sensitive to fouling (He *et al.* 2016). Another promising and effective method for controlling fouling is membrane surface modification. According to several experiments, AEMs coated with a hydrophilic positively charged layer shown a clear improvement in fouling resistance (Vaselbehagh *et al.* 2017).

2.5. Other factors affecting RED performance in salinity gradient energy production.

2.5.1. Water quantity

The majority of rivers exhibit non-linear low and high water flow periods that are influenced by precipitation, the greater the river, the larger the fluctuations (Livina *et al.* 2003; Kuleszo 2008). The minimal monthly discharge can be as little as a few percent of the monthly average (Haines, Finlayson and McMahon 1988). Since energy systems are designed to provide a constant guaranteed power supply and constant power generation can only be ensured for constant discharge levels. River discharge variability may not be an issue in two situations: reservoirs are constructed to ensure a stable river water supply, or excess energy is stored until it is needed (or alternatively, it is traded at peak output and purchased at lower outputs), as may be the case with hydropower or wind power (Kuleszo 2008).

2.5.2. Salinity and temperature variability

Due to changing atmospheric conditions, sea water salinity and temperature varies during the year, just like river discharges, which also varies during the year. As a result, same to water quantity issue, the seasonal variations in salinity and temperature would have an impact on the availability of electricity generated by reverse electrodialysis (Kuleszo 2008).

2.5.3. Sea salt composition

Each of the seas has a different salt composition. Sodium (Na^+), magnesium (Mg^{2+}), calcium (Ca^{2+}), chlorides (Cl^-), sulphates ($SO_4{}^{2-}$), and bicarbonates ($HCO_3{}^-$) (Van der Leeden 1990; Stewart and Howell 2003). Together, sodium and chloride make up 84% of all salt ions in sea composition (Kuleszo 2008). The following, are the salt concentrations in ppt, for the common salt find in sea water (Van der Leeden 1990):

- 10.56 for sodium
- 18.98 for Chloride
- 2.56 for sulphate
- 1.27 for magnesium
- 0.40 for calcium
- 0.38 for potassium
- 0.14 for bicarbonate

According to (Kuleszo 2008), the energy dissipation in the mixing solution can be modelled, however, with sodium chloride only. This means that this parameter does not affect theoretical potential, when doing calculations, one can assume to neglect all other ions and work with sodium chloride only, since sodium and chloride together constitute majority of the salts. But it can matter in the technical potential though. Because using natural water and sea water may contain other ions except sodium chloride and one cannot ignore these ions in practical.

2.6. Developed models, to estimate power density production in RED stacks.

(Simões 2023), developed models to estimate reverse electrodialysis power density. To simplify, and develop models, Catarina Simoes, made few assumptions:

1. Fouling phenomena was negligible.
2. Only sodium chloride ions were present in the two solutions.
3. Membranes works the same way.

These assumptions created a path in developing equations or models to calculate and estimate power density of RED stack ($^{W}/_{m^2}$).

Theoretical potential difference E_{IEM} (V) generated across an ion exchange membrane pair by the salinity gradient can be calculated using the Nernst Equation 2.6 (Simões 2023).

$$\mathbf{E_{IEM} = \alpha_{IEM} \cdot \frac{RT}{zF} \cdot \ln\left(\frac{C_{sw} \cdot \gamma_{sw}}{C_{rw} \cdot C_{rw}}\right)} \qquad \textbf{Equation 2.6}$$

where C_{sw} and C_{rw} are the salt concentration of sea water and river water (mol/m^3), α_{IEM} is the ion exchange membrane permselectivity (-), R is the gas constant ($J/mol.K$), T is the absolute temperature (K), z is the ion valency (-), F is the Faraday constant (C/mol), and γ is the molar activity coefficient (-).

To calculate the voltage of the membrane pile at zero current, the overall electromotive force (EMF), calculated in volts (V) is the sum of individual membrane voltages and it can be also measured experimentally and is named open circuit voltage (OCV), which might differ slightly from the theoretical value (Simões 2023):

$$\mathbf{EMF = N \cdot (E_{AEM} + E_{CEM})} \qquad \textbf{Equation 2.7}$$

where N is the number of cell pairs in a stack (-).

The internal stack resistance (R_i, Ω), can be calculated using the following equation (Simões 2023):

$$\mathbf{R_i = N \cdot (R_{AEM} + R_{CEM} + R_{sw} + R_{rw}) + R_{elect}} \qquad \textbf{Equation 2.8}$$

Where R_{AEM} and R_{CEM} are the membranes' resistances (Ω), R_{sw} and R_{rw} are the sea and river water compartment resistances (Ω), and R_{elect} is the electrode compartment resistance (Ω).

The stack gross power (P_{gross}, V) is given as the current (A) times the terminal voltage in the following equation (Simões 2023):

$$\mathbf{P_{gross} = I \cdot U} \qquad \textbf{Equation 2.9}$$

Where U is the terminal voltage (V), and I is the current (A). Also, the electrical current can be deducted from the electrical circuit from the EMF, internal stack resistance R_i and external load resistance R_{load} (Simões 2023):

$$\mathbf{I} = \frac{\mathbf{EMF}}{\mathbf{R_i + R_{load}}} \qquad \textbf{Equation 2.10}$$

The terminal voltage is a function of the EMF, the current and the stack's internal resistance.

$$\mathbf{U = EMF - I \cdot R_i} \qquad \textbf{Equation 2.11}$$

Therefore, the power (W) produced by the stack depends on the value of the EMF and the internal stack resistance. Using the following equation power can be calculated (Simões 2023).

$$\mathbf{P_{gross} = I^2 \cdot R_{load} = \left(\frac{EMF}{R_i + R_{load}}\right)^2 \cdot R_{load}} \qquad \textbf{Equation 2.12}$$

where: EMF is the electromotive force, is the voltage of the membrane pile at zero current, and R_{load} is the external resistance, R_i is the stack internal resistance, and I is the current produced by the movement of ions through the membrane.

If one can assume no dependency on the location in the stack, the maximum power (P_{max}, W) is achieved when the terminal voltage is equal to half of the EMF and if the resistances are equal $(R_i = R_{load})$ and Equation 2.12 becomes (Simões 2023):

$$\mathbf{P_{max,gross} = \frac{(EMF)^2}{4 \cdot R_i}} \qquad \textbf{Equation 2.13}$$

The energy efficiency $(\eta_{energy}, \%)$ is calculated as the gross power produced over the Gibbs free energy per second $(\Delta G_{in}, W)$ (Simões 2023):

$$\mathbf{\eta_{energy} = \frac{P_{gross}}{\Delta G_{in}}} \qquad \textbf{Equation 2.14}$$

Therefore, for calculating power density (W/m^2), the gross power (P_{gross}, W) is divided by the total active ion exchange membrane area installed (A_{mem}, m^2) (Simões 2023):

$$\mathbf{P_d = \frac{P_{gross}}{A_{mem}}} \qquad \textbf{Equation 2.15}$$

(Lanjewar *et al.* 2020) developed another set of models to estimate the power density produced in a stack of membrane. To simplify and develop the model, the following assumptions were considered:

1. The impedance between the stack and load is equal.
2. The flow between the channels is taken as laminar flow between two infinite parallel plates.
3. Electro osmotic flux is considered negligible.

4. Effects of parasitic currents are negligible.
5. Effects of membrane fouling is negligible.
6. A salinity gradient from the surface to the depth of the system is assumed linear.

These assumptions created a path in developing, an equation used to calculate the net power density ($^{W}/_{m^2}$) produced by RED when two solutions with different salt concentrations mixed (Simões 2023):

$$\mathbf{P_{net} = P_{stack} - P_{pump} - P_{buoyant}} \qquad \textbf{Equation 2.16}$$

where P_{stack} andP_{pump}, $P_{buoyant}$ is the power applied to the load and pumping loss for the entire stack, consequent power loss respectively. Theoretical voltage $(V_{stack},), (volts)$ from Nernst Equation 2.17, which is generated due to the ion flux across the reverse electrodialysis stack (Lanjewar *et al.* 2020):

$$\mathbf{V_{stack} = n_{cell}\left(\frac{\alpha_{AEM}}{z} + \frac{\alpha_{CEM}}{z}\right)\frac{R_{gas}T}{F}\ln\left(\frac{C_H}{C_L}\right)} \qquad \textbf{Equation 2.17}$$

where C_H and C_L are the high salt concentration solution (sea water), and low salt concentration solution (river water). n_{cell} number of cell pairs in the stack. α_{AEM} and α_{CEM} are the membrane permselectivities. Power applied to the load (Lanjewar *et al.* 2020):

$$\mathbf{P_{stack} = I^2_{stack}R_{load}} \qquad \textbf{Equation 2.18}$$

$$\mathbf{P_{stack} = \frac{V^2_{stack}R_{load}}{(R_{stack}+R_{load})^2}} \qquad \textbf{Equation 2.19}$$

$$\mathbf{P_{stack} = \frac{V^2_{stack}R_{load}}{[n_{cell}(R_{ohmic}+R_{BL}+R_{\Delta C})+R_{load}]^2}} \qquad \textbf{Equation 2.20}$$

Where I_{stack} is the current and R_{load} is the resistance due to the load, R_{ohmic} ohmic losses, R_{BL} boundary layer losses, and losses along the channel's length due to decrease in the difference of concentration between the flows (Lanjewar *et al.* 2020).

Pumping loss for the entire stack is.

$$\mathbf{P_{pump} = 2 \cdot n_{cell} \cdot Q \cdot K_p \cdot \Delta p} \qquad \textbf{Equation 2.21}$$

where Q is volumetric flow rate (m^3/s), K_p is the correction factor for the pressure drop, and Δp is the pressure drop.

Where pressure drop (Pa) can be calculated by the following Darcy-Weisbach Equation 2.22 for laminar flow between two infinite parallel plates (Lanjewar *et al.* 2020):

$$\Delta \mathbf{p} = \mathbf{f}\frac{\mathbf{L}\rho \mathbf{v}^2}{\mathbf{d_H}2} = \frac{\mathbf{48}\mu \mathbf{Lv}}{\mathbf{d^2}_\mathbf{H}} \qquad \textbf{Equation 2.22}$$

where d_H is the hydraulic diameter, μ is the dynamic viscosity, L is the length of the compartment. v is the velocity.

The hydraulic diameter (m) (Lanjewar *et al.* 2020):

$$\mathbf{d_H} = \frac{\mathbf{4}\varepsilon}{{}^{2}/_{\mathbf{w}} + (\mathbf{1}-\varepsilon)\cdot \mathbf{S_{vsp}}} \qquad \textbf{Equation 2.23}$$

where ε is the porosity of membrane. S_{vsp} spacer surface area, and w is the width.

Since (Lanjewar *et al.* 2020) assumed a linear salinity profile, energy (E) required to transport a volume (V) of water can be estimated using the following Equation 2.24

$$\frac{\mathbf{E}}{\mathbf{V}} = \frac{\mathbf{1}}{\mathbf{2}}\left(\boldsymbol{\rho}_{\mathbf{top}} - \boldsymbol{\rho}_{\mathbf{bot}}\right)\cdot \mathbf{g}\cdot \mathbf{y} \qquad \textbf{Equation 2.24}$$

where ρ is the density of the water at the top and bottom, g is the gravitational acceleration, and y is the vertical distance traversed from top to bottom.

Then the consequent power (W) loss is estimated by the following Equation 2.25 (Lanjewar *et al.* 2020):

$$\mathbf{P_{buoyant}} = \mathbf{0.75n_{cell}}\cdot\frac{\mathbf{E}}{\mathbf{V}}\cdot \mathbf{Q} \qquad \textbf{Equation 2.25}$$

Equations modelled by (Simões 2023) where used in methodology chapter (chapter 3) to perform reverse electrodialysis membrane design calculations. Some of the assumptions done by (Simões 2023), and (Lanjewar *et al.* 2020) listed above were also utilized to simplify calculations.

CHAPTER 3-METHODOLOGY

This chapter is broken down into three sections. The first section defines the potential for energy production and describes how the information that was used to calculate the potential for energy production at the chosen rivers was discovered or gathered. The method or approach utilised by this study to calculate the potential for energy production is also shown in section 1, along with the assumptions made to carry out calculations and the potential for energy production equation that was employed in this dissertation. Section one also describes how the selected rivers were selected.

The second section demonstrates the approach used to design the reverse electrodialysis stack, and describes the steps required for design calculations (mass balance, power density), as well as the method used to design feed pumps. Section 2 shows the approach used to calculate the cost of the pilot plant. The third section explains more about the simulating and optimising software that was utilised in this study.

3.1 Theoretical potential for energy production

Potential for energy production is the potential that the river possesses for producing salinity gradient energy.

Few steps were taken in order to perform theoretical potential for energy production calculations. In the first step, relevant data such as the volumetric flowrates of the major rivers' discharges and the volumetric flowrate of the sea's discharge, as well as their salt concentrations were required in order to calculate the theoretical potential for energy production. The second step was to calculate the theoretical potential for energy production using Equation 1.2 found in Chapter 1.

3.1.2 Data collection

The Department of Water Affairs and other relevant and reliable sources, such (Tenza 2018) found in google scholar were used to research the discharge volumetric flowrates of the major rivers found in KwaZulu Natal as well as the salt content of these rivers. World Data Base for the Oceans was used to find the information on the Indian Ocean.

3.1.3 Site selection (river selection)

Rivers were selected based on their length, volumetric discharge, and availability of historical and current data. Pertinent sources such as Department of Water Affairs and (Tenza 2018) were used to find this information. This study is a component of an ongoing effort to identify acceptable energy sources that may both meet society's fundamental energy needs and be environmentally friendly. The current information was gathered in 2004-2022. The current data was gathered by Department of Water Affairs using a variety of techniques, including the use of velocity-area approaches and flow-gauging weirs. The theoretical potential for energy production was calculated using typical annual discharge flowrates.

3.1.4 Theoretical potential for energy production approach

The salinity potential for energy production may be influenced by a wide range of factors. Some of the factors can be divided into theoretical, technical, economical, and exploitable potential parameters. Only those factors pertinent to theoretical potential were considered for this study.

Theoretical potential parameters:

- River discharges
- Salinity
- Temperature

3.2 Basic assumptions

To calculate the theoretical potential for energy production, the following assumptions were made:

1. Salinity of sea water was assumed to be in terms of sodium chloride (NaCl) only.
2. The river water and sea water have the same temperatures.
3. The discharged river water mixes with equal amount of sea water.
4. To utilize all the river and sea water flow discharge to estimate the potential.

Regarding point number one, the composition of salt in the seas varies, but sodium chloride is typically the dominant component contributing to salinity. Additionally, this method or approach has also been adopted or used in all calculations by authors cited in this study. In point number two the sea temperature data was used as substitute for river water temperature as there is no

database available with such data. Due to a unique river regime or thermal pollution, for example, the equality of temperatures may not be true in practise. Different authors took different approaches to the issue of the volume's ratio of concentrated (sea water) and diluted (river water) streams (point 3): either as 1:1 or as an endless supply of salty water (sea water). Due to the unknown rate of real recirculation of unutilised salt water into the river mouth area, a 1:1 ratio was used for this thesis. It is safer to suppose or assume that only a little amount of mixing takes place right at the river's mouth and that further mixing occurs farther out to sea, where it cannot be controlled.

3.3 Calculating the theoretical potential for energy.

The following equation was used to calculate the potential for energy production after taking into consideration all the aforementioned information. The reason using the following equation it is because it easy to understand and straight forward. To get the power output (U, energy over time), the volume was replaced by discharge (Q, volume over time) (Forgacs 1982).

$$\mathbf{U = 2RT\left[C_D Q_D \ln \frac{C_D(Q_C+Q_D)}{C_D Q_D + C_C Q_C} + C_C Q_C \ln \frac{C_C(Q_C+Q_D)}{C_D Q_D + C_C Q_C}\right]} \qquad \textbf{Equation 3.1}$$

Where:

R- Universal gas constant (8.31 J/mol K)

T- Temperature (K)

C- Concentration (mol/ m^3)

Q- discharge volumetric flowrate (m^3/time)

Subscripts:

C- concentrated solution (sea water)

D- diluted solution (river water)

3.4 Potential for energy production power plant design

3.4.1 Reverse Electrodialysis membrane and stack design

To design the reverse electrodialysis in detail, the following parameters were determined using appropriate design models which were found in literatures: reverse electrodialysis membrane area, number of cell pairs required to form a stack, mass balance of the salt ion permeating the membrane, internal resistance, power produced by each cell pair in the RED stack, and pressure drops of concentrated and diluted solutions.

There were assumptions made to use all the design equations:

- The cells that make up the reverse electrodialysis stack work in the same way
- Solutions fed to the reverse electrodialysis cell were assumed to be aqueous sodium chloride solutions and the feed rate is almost the same.
- Non-ohmic resistances were neglected.
- Fouling phenomena were ignored in the membranes.
- The flow in the cells is counter- current.
- Ionic short-circuit currents were neglected.
- Electrode resistance neglected.

According to the second assumption, using the following models it would not be possible to assess the impact of different chemical compositions found in the solutions used in the production of salinity gradient energy in RED system. Therefore, it would not be possible to evaluate the impact of these chemical compositions (multivalent ions) have in the functioning or in the behaviour of the RED system. However, several studies have concluded that the presence of these ions in powered solutions can lead to an increase in membrane resistance, decreasing the power produced in a RED cell. The passing of divalent ions (oxygen, magnesium, etc) in the opposite direction of the concentration gradient, exchanging with two monovalent ions from the higher concentration solution. This phenomenon leads to a decrease in the potential difference of the battery, reducing its performance (Guimarães 2020).

The use of river water and sea water which are natural saline solutions, without any kind of previous treatment, can result in a sharp decrease in the power of a battery, due to the hard coating

that may occur on the surface of both membranes caused by other chemicals compositions found in these solutions. (Vermaas *et al.* 2013) concluded that without the use of pre-treatments, the battery power would be reduced to 40% of the theoretical power on the first day of the experiment. The type of fouling on an ion exchange membrane depends on the fixed charges present on its surface (Vermaas *et al.* 2013). An anion exchange membrane is normally more affected by organic fouling such as algae, but also by clay minerals (Vermaas *et al.* 2013). A cation exchange membrane would be more affected by inorganic scale (scaling). In this study, fouling phenomena in the membranes were not considered. This phenomenon can result in an increase in the membrane resistance and a possible decrease in their selectivity. So, it is of great importance to understand the impact that this phenomenon can have on a reverse electrodialysis membranes.

According to assumption six the ionic short-circuit currents associated with concentrated solutions represent a problem of greater importance, since the conductivity of these solutions is higher and, as such, they occur on a larger scale in concentrated solutions. To mitigate these parasitic currents, several strategies can be used, including reducing the number of cells in a stack or performing a supply/discharge in series instead of a supply/discharge in parallel. Finally, the ionic short-circuit currents related to electrolyte recirculation can be neglected using relatively long recirculation pipes (Guimarães 2020). According to last assumption the resistance of the electrodes system was neglected because the operability of RED was considered to be on a large scale (Vermaas, Saakes and Nijmeijer 2011a).

3.4.2 Mole balance and membrane design equations

The mole balance (mol/s) leads to the differential equations that describe the change in salt concentration within the compartments (Veerman *et al.* 2010).

$$\frac{dC_C}{dx} = -\frac{b}{Q_C} J_{NaCl} - C_c \frac{b}{Q_C} J'_{water} \qquad \textbf{Equation 3.2}$$

$$\frac{dC_d}{dx} = \frac{b}{Q_d} J_{NaCl} + C_d \frac{b}{Q_d} J'_{water} \qquad \textbf{Equation 3.3}$$

where J_{NaCl} is ionic flux across the membranes ($mol/m^2\ s$), b is the width of the membrane and J'_{water} is volumetric water flux across the membranes (m/s) and it is calculated by the following Equation 3.4 (Veerman *et al.* 2010):

$$\mathbf{J'_{water} = -\frac{2D_{water}}{\delta_m}(C_C - C_d)\frac{M_{water}}{\rho_{water}}} \qquad \textbf{Equation 3.4}$$

where D_{water} is the water diffusion coefficient (m^2/s), which is 2.299×10^{-9}, δ_m is the membrane thickness (m), M_{water} is water's molecular mass and ρ_{water} is the water density.

Two main factors influence the movement of sodium chloride ions through membranes: diffusion of co-ions (same charge) due to imperfections in membrane selectivity and migration of counter-ions (opposite charge) due to electrochemical potential difference (Veerman *et al.* 2010).

$$\mathbf{J_{NaCl}(x) = J_{dl} + J_{ml}} \qquad \textbf{Equation 3.5}$$

where J_{dl} is the diffusion of ions and J_{ml} is the migration of ions.

Diffusion transport was described by Fick's model (Veerman *et al.* 2010):

$$\mathbf{J_{dl} = \frac{2D_{NaCl}}{\delta_m}(C_C - C_d)} \qquad \textbf{Equation 3.6}$$

where D_{NaCl} is the diffusion constant of sodium chloride through membranes. Which was assumed to be $1.00 \times 10^{-12}\, m^2/s$ based on the literature (Guimarães 2020).

Ohm's concept was applied to describe migration (Veerman *et al.* 2010).

$$\mathbf{J_{ml} = \frac{1}{F}\frac{E_T}{R_{cell}}} \qquad \textbf{Equation 3.7}$$

where E_T is the electrical potential, it is the membrane potential (V) for a cell pair with no losses considered. R_{cell} is the cell resistance and F being the faraday constant (96485 C/mol). Electrical potential was calculated using Nernst Equation 3.8 (Simões 2023):

$$\mathbf{E_T = (\alpha_{CEM} + \alpha_{AEM}) \cdot \frac{RT}{F} \cdot \ln\left(\frac{\gamma_{sw} \cdot C_{sw}}{\gamma_{rw} \cdot C_{rw}}\right)} \qquad \textbf{Equation 3.8}$$

where α is the permselectivity of the membranes and γ is the activity coefficient of each of the ions in the different solutions. R is the universal gas constant (8.314 J/mol. K), T is the room temperature (298.15 K).

The activity coefficient of river and sea water (γ): the activity coefficient (-) depend on molar salt concentration, and it was estimated using the following equation (Raka *et al.* 2020).

$$\mathbf{\gamma = g_1 \cdot C_i + g_2} \qquad \textbf{Equation 3.9}$$

where C_i is the concentration of solution in mol/l, $g_1 = 0.1366\ l/mol$ and $g_2 = 1.0007$.

Area specific membrane resistance $(R_{CEM/AEM})$, which is expressed in (Ω) and it was calculated using the following Equation 3.10 (Raka *et al.* 2020).

$$\mathbf{R_{CEM} = R_{AEM} = r_1 \cdot (C_{rw})^{-0.236}} \qquad \textbf{Equation 3.10}$$

R_{CEM} and R_{AEM} are area specific membrane resistances for cation and anion exchange membrane, C_{rw} is inlet concentration of river water or low concentration solution. r_1 is fitting parameter $(\Omega m^2/M)$. It is estimated to be 0.0002 $(\Omega m^2/M)$ for present and market scenario and 0.00004 $(\Omega m^2/M)$ for future scenario (Bevacqua *et al.* 2017). When concentration is lower than 0.1 M, the contribution to resistance from low concentration solution is high.

The cell resistance (R_{cell}) calculated in ohms: is the cumulative sum of resistance of membranes and compartment or channels in a cell (Ω) (Raka *et al.* 2020).

$$\mathbf{R_{cell} = R_{CEM} + R_{AEM} + R_{rw} + R_{sw}} \qquad \textbf{Equation 3.11}$$

Channel ohmic resistance or compartment resistance (R_{rw}, R_{sw}): the resistance (Ω) due to the solution in the channel and spacer geometry, it was calculated using the following equation (Vallejo-Castaño and Sánchez-Sáenz 2017).

$$\mathbf{R_{rw} = f_{rw} \cdot \frac{\delta_{rw}}{\Lambda_{rw} C_{rw}}} \quad \mathbf{R_{sw} = f_{sw} \cdot \frac{\delta_{sw}}{\Lambda_{sw} \cdot C_{sw}}} \qquad \textbf{Equation 3.12}$$

where δ_{sw} and δ_{rw} is the intermembrane distance or compartment distance in (μm), Λ_{sw} and Λ_{rw} are the conductivities of the sea water and river water and the equation of estimating the conductivities is presented in appendix B. f_v is the correction factor.

Current density at peak power (I_{PP}): The peak power current density occurs at potential half the open circuit potential. As the resistance remains constant the current density (A/m^2) at peak power is calculated using the following equation (Raka *et al.* 2020).

$$\mathbf{I_{PP} = \frac{E_T}{2 \cdot R_{cell}}} \qquad \textbf{Equation 3.13}$$

Actual unit cell potential (E_{uc}): The unit cell potential (V) is calculated using the following Equation 3.14 (Raka *et al.* 2020).

$$\mathbf{E_{uc} = E_T - R_{cell} \cdot I_{PP}} \qquad \textbf{Equation 3.14}$$

Number of unit cell (N_m), the minimum number of cell pairs to be stacked in series was calculated using the following equation 3.15 (Raka *et al.* 2020).

$$\mathbf{N_m = \frac{1.5}{E_{uc}}} \qquad \textbf{Equation 3.15}$$

The overall electromotive force (EMF) in volts, which is the voltage of the membrane pile at zero current, is calculated using the following Equation 3.16 (Simões 2023):

$$\mathbf{EMF = NE_{uc}} \qquad \textbf{Equation 3.16}$$

The internal stack resistance (R_{stack}, Ω) is defined as.

$$\mathbf{R_{stack} = N \cdot (R_{cell}) + R_{electrode}} \qquad \textbf{Equation 3.17}$$

where $R_{electrode}$ is the electrode resistance (Ω) is the resistance from electrodes in electrode rinse solution. This resistance value is assumed to be $0.01(\ \Omega)$ but its contribution for large stacks is neglected since its contribution is very low (Bevacqua *et al.* 2017) . Hence the resistance of the electrodes system can be neglected here considering the operability of reverse electrodialysis on a large scale.

The stack gross power (P_{gross}, W) is given as the current times the terminal voltage in the following Equation 3.18 (Simões 2023).

$$\mathbf{P_{gross} = I \cdot U} \qquad \textbf{Equation 3.18}$$

where I is the current (A) and U is the terminal voltage (V). The electrical current I can be deduced from the electrical circuit from the EMF, internal stack resistance R_{stack} and external load resistance R_{load}. The terminal voltage is a function of the EMF, the current and the stack's internal resistance (Simões 2023).

$$\mathbf{I = \frac{EMF}{R_{stack}+R_{load}}} \qquad \textbf{Equation 3.19}$$

$$\mathbf{U = EMF - I \cdot R_{stack}} \qquad \textbf{Equation 3.20}$$

Therefore, the power (Watts) produced by the stack depends on the value of the EMF and the internal stack resistance. By using Ohm's law and Equations 3.18, 3.19, and equation 3.20 becomes 3.21 (Simões 2023).

$$\mathbf{P_{gross} = I^2 \cdot R_{load} = \left(\frac{EMF}{R_{stack}+R_{load}}\right)^2 \cdot R_{load}} \qquad \textbf{Equation 3.21}$$

The maximum power (P_{max}, W) is achieved when the terminal voltage is equal to half of the EMF and if the resistances are equal ($R_{stack} = R_{load}$) and the Equation 3.21 becomes (Simões 2023):

$$\mathbf{P_{max}} = \frac{\mathbf{EMF^2}}{\mathbf{4 \cdot R_{stack}}} \qquad \textbf{Equation 3.22}$$

The max power was divided by the total stack area installed (A_{stack}, m^2), this is called power density ($P_d,\ W/m^2$) and for this thesis power density was assumed to be 3 W/m^2 in order to obtained stack area using the following Equation 3.23 (Simões 2023).

$$\mathbf{P_d} = \frac{\mathbf{P_{max}}}{\mathbf{A_{stack}}} \qquad \textbf{Equation 3.23}$$

3.4.3 Pressure Drop

After calculating the efficiency of the reverse electrodialysis stack, the pressure drop of the stack was calculated using Equations 3.26 and 3.27 but first the Reynolds number (-) was needed to know flow regime of streams inside the compartments (Raka *et al.* 2020).

$$\mathbf{Re} = \frac{\mathbf{vD\rho}}{\mathbf{visc}} \qquad \textbf{Equation 3.24}$$

In this case v represents mean velocity (m/s), D is the hydraulic diameter (m), ρ is the liquid density and $visc$ is the dynamic viscosity which is $0.9 \times 10^{-3}\ Pas$ for water (Raka *et al.* 2020).

$$\mathbf{d_h} = \frac{\mathbf{4\varepsilon}}{\frac{\mathbf{2}}{\mathbf{\delta_{ch}}} + \left((\mathbf{1-\varepsilon}) \cdot \frac{\mathbf{8}}{\mathbf{\delta_{ch}}}\right)} \qquad \textbf{Equation 3.25}$$

where d_h is the hydraulic diameter in meters, δ_{ch} is the compartment distance (m) and ε is the porosity (-) of the spacer.

For laminar flow, pressure drop (Pascal) over the compartments was calculated using the following Equations 3.26 and 3.27 (Vallejo-Castaño and Sánchez-Sáenz 2017):

$$\Delta\mathbf{P_{sw}} = \frac{\mathbf{2viscLQ_{sw}}}{\mathbf{b\delta_{sw}^{\ 3}}} \qquad \textbf{Equation 3.26}$$

$$\Delta\mathbf{P_{RW}} = \frac{\mathbf{2viscLQ_{RW}}}{\mathbf{b\delta_{RW}^{\ 3}}} \qquad \textbf{Equation 3.27}$$

3.5 Feed water pump design.

After reverse electrodialysis design calculations, the next step was to design feed pumps for the plant. Pumps that pump the two solutions (river and sea water) were designed using the appropriate methods of equipment design, which are found in Chemical Engineering Equipment Design textbook, and the design equation used to design feed pumps. Centrifugal pumps were selected for this study since centrifugal pumps are highly versatile and they are available in many different shapes and sizes to handle a wide variety of installations and requirements. This type of pump can be driven electrically or magnetically, to self-prime, to be able to handle sanitary fluids, or big enough for large industrial applications, idealy centrifugal pumps designed for high-flow applications, with a very high efficiency. The assumptions taken to perform calculations are as follows:

3.5.1 Pump Assumptions

- Static suction head (h_s) = 3 m
- Length of suction pipe (L_s) = 5 m
- Static delivery head (h_d) = 15 m
- Length of delivery pipe (L_d) = 20 m

These assumptions were taken to perform pump design calculations since it was not possible to go to the site and measure all these parameters practically due to time constraints. To design feed pumps there were steps to follow.

It is not possible to utilise the whole river and sea water volumetric flow rate when designing pumps, so the ideal was to be as realistic as possible, so the assumption made was to channel the specific amount of volumetric flow discharge that can be used to design reasonable pipe discharge and pipe suction diameters and pumps.

Another important concept was the pump selection criteria for reverse electrocialysis stacks operating in higher salinity environments, pumps were selected based on the following criteria:

1. Corrosion resistance: pumps constructed from materials that are resistant to corrosion from the high salinity of the operating environment were chosen. Commonly used materials are stainless steels.

2. Chemical compatibility: pumps that are compatible with the chemicals present in the saline solution to prevent degradation or contamination of the solution were chosen.
3. Efficiency: the pumps with high efficiency were chosen to minimize energy consumption.
4. Durability: pumps that are capable of continuous operation in harsh environments were chosen to minimize downtime and maintenance.

The assumed volumetric flow rate for the high potential for energy producing river (uThukela river), from the original volumetric flow rate ($3865 \times 10^6\ m^3/y$) was $0.0613\ m^3/s$

Step number 1: design discharge

To account for leakage losses, taking 5% extra discharge.

Design discharge (Q) =$\mathbf{1.05 \cdot Q_1}$ **Equation 3.28**

where Q_1 is the given flow rate in m^3/s.

Step number 2: design of suction and delivery pipe.

For suction pipe and delivery pipe the continuity equation was used.

$\mathbf{Q = A \cdot v}$ **Equation 3.29**

where A is the area (m^2) of the pipe and v is the velocity in m/s.

Step number 3: calculation of manometric head (H_m) calculated in meters (m) which is the head that the pump must overcome.

$\mathbf{H_m = H_s + H_d}$ **Equation 3.30**

where H_s and H_d are the total suction and delivery heads in (m) and are found using following Equations 3.31:

$\mathbf{H_s = h_s + h_{f_s} + h_{fittings}}$ and $\mathbf{H_d = h_d + h_{f_d} + h_{fittings} + \frac{V_d^2}{2g}}$ **Equation 3.31**

where h_{f_s} and h_{f_d} are the head losses due to friction (m) in the suction pipe and delivery pipe. $h_{fittings}$ is the head loss due to fittings (valves, non-returns). $\frac{V_d^2}{2g}$ is the delivery velocity head.

Step number 4: motor selection and motor power calculation

$$\textbf{motor power} = \frac{\mathbf{wQH_m}}{\boldsymbol{\eta_{overall}}} \qquad \textbf{Equation 3.32}$$

where w is the weight density calculated by this equation $w = \rho \cdot g$. $\eta_{overall}$ is the overall efficiency of the pump and motor. After finding the motor power (W) the speed of motor was found in design textbook using the motor power calculated.

Pump power (W) was calculated using the following Equation 3.33:

$$\mathbf{P_P = Q \cdot H_m \cdot g \cdot \rho} \qquad \textbf{Equation 3.33}$$

where ρ (kg/m^3) is the density and g gravitational acceleration.

Step number 5: impeller design

First one need to find the specific speed (-) using the following Equation 3.34:

$$\mathbf{N_s} = \frac{\mathbf{N\sqrt{Q}}}{(\mathbf{H_m})^{3/4}} \qquad \textbf{Equation 3.34}$$

where N (RPM) is the motor speed found in step number four.

3.6 Simulation and optimization of Reverse Electrodialysis power plant

The simulation and optimization of reverse electrodialysis power plant was done using the software called COMSOL Multiphysics, which is a good tool for simulating electromagnetics, acoustic, fluid flow, heat transfer, chemical phenomena, and structural mechanics in one environment. This software is used for various physics and engineering applications, especially coupled phenomena and Multiphysics. The COMSOL Multiphysics software was also used as a decision-making tool in this thesis as it provided optimum point were the reverse electrodialysis plant can perform at its optimum level.

3.6.1 Assumption made.

When simulating the reverse electrodialysis plant it was assumed that the Reynolds number is small enough to consider laminar flow, and the two solutions are incompressible. Laminar flow is typically preferred in reverse electrodialysis systems to ensure optimal performance and to increase the lifespan of the membranes, turbulent flow are not considered in reverse electrodialysis

since turbulence can disrupt the efficient operation of the system. Turbulence can lead to inceased energy consumption, decreased ion selectivity, and reduced efficiency in generating electrical power. It can also cause mechanical wear and tear on the system components, potentially leading to maintenance issues and shorter lifespan (Vallejo-Castaño and Sánchez-Sáenz 2017). Additionally, water transport through RED membranes was not considered. Water transport through the membranes occurs because of the water molecules consumed in the splitting of water. It was also assumed that the concentration at the inlet were the same for the two simulations. At the outlet of the channels, flow convection drives the movement of fluid.

3.6.2 Geometry

To simulate the RED process plant, 2-D models were developed using COMSOL Multiphysics. These two models were differing in such way that one shows the transportation of ions from higher concentration solution to lower concentration solution, so it shows how ions moves and permeate on the surface of the membrane. The second simulation shows the fluid flow along the channels or the compartments and how velocity affects the transportation of ions. Both simulations use same membrane length and width and same channels.

3.6.3 Boundary conditions

The following boundary conditions have been considered:

1. The flow was considered to be laminar and fully developed. This boundary condition allowed for a time averaged laminar velocity profile to be used. It was assumed that at the outlet of the compartments the relative pressure was zero, so that there would be no return of the fluid. For the membranes it was assumed no slip boundary conditions.

Laminar flow is considered a boundary condition because, laminar flow is more stable and predictable compared to turbulent flow. This stability simplifies the modeling process and can lead to more reliable simulation results. Laminar flow allows for the assumption of ideal fluid behavior, which simplifies the mathematical modeling of fluid flow within the reverse electrodialysis system. Many analytical models and theoretical frameworks for reverse electrodialysis systems

are based on the assumptions of laminar flow. By using laminar flow as a boundary condition, simulations can be aligned with these theoretical foundations.

2. Temperature boundary condition: inlet temperature is 25℃ for both seawater and river water streams. Membrane temperature at 25℃ (assuming uniform temperature distribution across the membranes). Electrode temperature set at 25℃ (assuming uniform temperature distribution across the electrodes). Outlet temperature set at 25℃ for both outlet streams (assuming no heat exchange with the surroundings).

These boundary conditions specify the temperatures at various points within the RED system. The assumption of uniform temperature distribution across membranes and electrodes simplifies the modeling process.

3. Ion exchange membrane boundary conditions: ion selectivity (cation exchange membrane Na^+ ions permeate and anion exchange membrane Cl^-permeate). Diffusion coefficient of $1.00 \times 10^{-12}\ m^2/s$ for NaCl. Continuity of ion flux across the membrane interface.

These boundary conditions specify the properties and behaviour of the ion exchange membranes used in the RED system. The ion selectivity indicates which ions can pass through the membrane. These conditions are essential for accurately modeling the ion transport processes across the membranes and their role in generating electrical power from the salinity gradient between the seawater and river water streams.

4. Inlet boundary conditions: for the seawater the inlet salt concentration was $600\ mol/m^3$. Inlet seawater temperature was set at 25℃. For river water the inlet salt concentration was $0.814\ mol/m^3$. Inlet riverwater temperature set at 25℃.

These boundary conditions specify the properties of the incoming seawater and river water streams entering the RED system. These conditions are essential for accurately modeling the behaviour of the RED system and its performance in generating electrical power.

3.7 Model Validation

This study presents a validation of a COMSOL Multiphysics model for reverse electrodialysis using experimental data reported in the literature. The model accurately predicts the performance of a RED system under specific operating conditions, demonstrating its reliability and applicability for system optimization and design.

Reverse electrodialysis is a promising renewable energy technology that utilizes the salinity gradient between seawater and river water to generate electricity. The development of accurate computational models is crucial for understanding and optimizing RED system performance. This study validates a theoretical model using COMSOL Multiphysics against experimental data from previous literature studies.

3.7.1 Model Description

The COMSOL model simulates the transport of ions and fluid flow in a RED stack consisting of alternating ion exchange membranes and spacers. The model incorporates the Nernst-Planck equation for ion transport, the Navier-Stokes equation for fluid flow, and Butler-Volmer kinetics for electrochemical reactions. The geometry, material properties, and operating conditions were based on experimental parameters reported in the literature.

3.7.2 Validation Methodology

Experimental data from previous literature studies were used to validate the COMSOL model. Key parameters such as ion concentration, velocity, power density, current densities, residence time, compartment thickness, and power output were compared between the model predictions and experimental measurements. The validation process assesses the agreement between the simulated and observed reverse electrodialysis system performance under similar operating conditions.

3.7.3 Simulation Setup

The COMSOL model was configured to replicate the experimental setup described in the literature. The geometry of the RED stack, membrane properties, flow rates, concentrations, and applied potentials were specified based on the reported experimental parameters. The model was solved using appropriate physics interfaces and boundary conditions consistent with the experimental setup.

3.7.4 Validation Results

The simulation results obtained from COMSOL Multiphysics closely match the experimental data reported by Veerman *et al* (2009). (Veerman *et al.* 2009) used a stack with 50 cell pairs, $10 \times 10\ cm$ in size, equipped with Fumasep FAD/FKD membranes, and the standard river water and seawater concentrations of 17 $mol/m^3$and 500 mol/m^3 respectively. The simulation result obtained also correspond with the result obtained by Choi *et al* (2016). (Choi *et al.* 2016) used a small stack with only 1 cell pair, $5 \times 5\ cm$ in size, equipped with Selemion AMV/ CMV membranes and Ti-wire woven spacers. Ion concentration profiles, power density, membrane area, and velocity are in good agreement between the model predictions and experimental results.

The validation study demonstrates the accuracy and reliability of the COMSOL model for simulating RED systems using experimental data from the literature. The agreement between the model predictions and experimental results validates the underlying assumptions and numerical methodology employed in the model. The validated model provides a valuable tool for further research and development in the field of renewable energy technologies.

In conclusion, this study validates a COMSOL Multiphysics model for reverse electrodialysis using experimental data reported in the literature. The model accurately predicts the performance of RED systems under specified operating conditions, providing valuable insights for system optimization and design.

3.8 Mesh Independent Analysis

The mesh independent analysis was performed to determine the optimal mesh resolution for simulating a RED system.

3.8.1 Geometry and Physics Setup

A 2D model of a RED cell pair consisting of ion exchange membrane with two compartments (compartment of river water and seawater) was created in COMSOL. Fluid flow, mass tranfer (ion transport), and electrochemical reactions were modeled using appropriate physics interfaces.

3.8.2 Boundary Conditions and Material properties

Inlet/outlet conditions were specified for the river water and seawater streams. Material properties such as conductivity, diffusivity, and permittivity are assigned to the membrane.

3.8.3 Initial Mesh and Mesh Refinement

An initial coarse mesh with 6500 elements was generated to represent the geometry of the RED cell pair. The mesh was refined figure 3.1 for better mesh geometry since the initial meshing needed some optimization. The mesh refining was done by doubling the number of elements resulting in mesh with 6500 to 13000, 26000, 52000 elements making it more accurate, figure 3.1 illustrates the results. Mesh refinement focused on critical regions near membrane interfaces with two compartments.

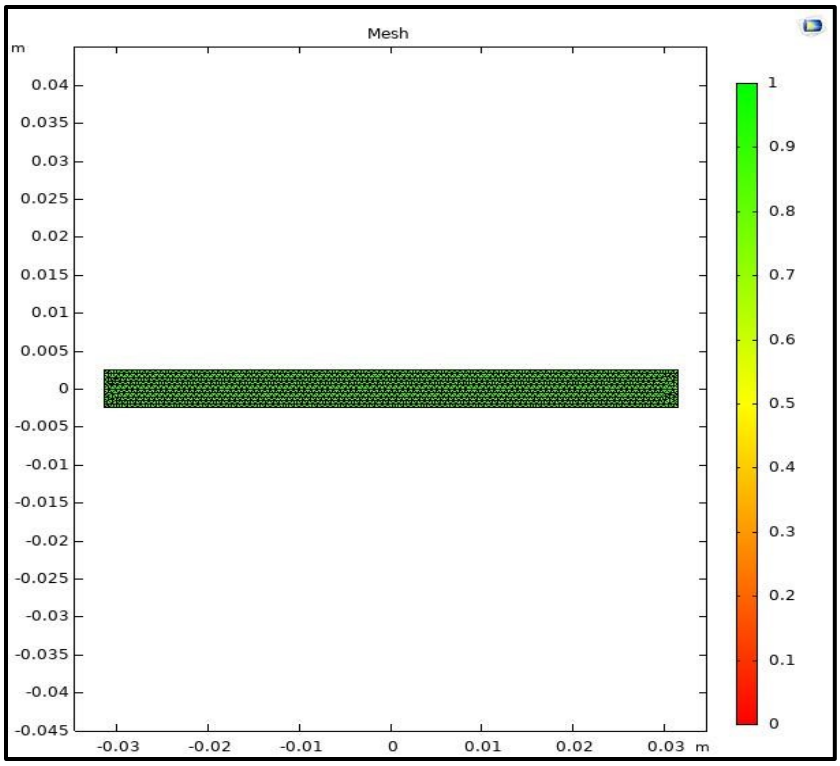

Figure 3.1: Shows the refined mesh for reverse electrodialysis cell pair.

3.8.4 Simualtion Runs

Simulations were performed for each mesh resolution, with the same solver settings and convergence criteria. Key solution variables such as ion concentrations, flow rates, velocity, and power density were monitored during the simulations.

3.8.5 Convergence Analysis

The convergence of the solution was assessed by comparing the results obtained with different mesh resolutions. Convergence was determined based on the stability of solution variables and the agreement between successive mesh refinements.

3.8.6 Optimal Mesh Resolution

The optimal mesh resolution was identified based on the convergence behavior of the solution. This was determined by analyzing the trend of solution variables as a function of mesh resolution and identifying the point of diminishing returns in solution accuracy.

Mesh refining shows improvement in solution accuracy, particularly in regions of high gradient such as near membrane interfaces. However, the rate of improvement diminishes with increasing mesh resolution, indicating diminishing returns in solution accuracy beyond a certain point. Based on the convergence behavior observed, the optimal mesh resolution was determined to be 52000 elements, where further refinement did not significantly improve solution accuracy.

3.9 Equipment Costing

All economic assumptions were based on values taken from literature for European market and converted to South African currency, since most of the reverse electrodialysis are manufactured in Europe and China.

Main economic parameters adopted as inputs for the engineering economic analysis are reported in Table 3.1.

Table 3.1: Shows the economic parameters.

Plant lifetime (t)	20	Years
Discount rate (r)	3	%
Working hour	8000	h/year
RED membrane lifetime (t_m)	4	Years

Capital cost (CAPEX)

The capital cost (R) of the pant is the sum of all cost as follows (Daniilidis, Herber and Vermaas 2014):

$$\mathbf{CAPEX} = \mathbf{C_m} + \mathbf{C_{electrode}} + \mathbf{C_{casing}} + \mathbf{C_{spacer}} + \mathbf{C_{pump}} + \mathbf{C_{piping}} + \mathbf{C_{labour}} \qquad \textbf{Equation 3.35}$$

where C_m is the cost of the membranes and different values has been proposed so far. A value of 15€· $m_{IEMs}{}^{-2}$ (R307.53 /$m_{IEMs}{}^{2}$) is generally considered a more than reasonable value, while a value of 4 €· $m_{IEMs}{}^{-2}$ is often adopted as a future cost (Daniilidis, Herber and Vermaas 2014; Giacalone *et al.* 2023). For this thesis an intermediate value of 10 €· $m_{IEMs}{}^{-2}$ is considered. $C_{electrode}$ is the cost of electrodes, C_{casing} is the casing cost, C_{spacer} is the cost of spacers, C_{pump} cost of pumps, C_{piping} is the piping cost and C_{labour} is the labour cost and it is 20% of equipment cost. The membrane cost, electrode cost, casing cost, spacers cost, and labour cost values can be found in Table 3.2.

Table 3.2: Shows the main cost items for the economic analysis adopted under Europe current market price of RED system.

Membrane cost C_m	10 (R205/m^2)	€· $m_{IEMs}{}^{-2}$	(Giacalone *et al.* 2023)
Electrode cost $C_{electrode}$	500 (R10245.29/m^2)	€· $m_{IEMs}{}^{-2}$	(Giacalone *et al.* 2023)
Casing cost C_{casing}	2 (R41/m^2)	€· $m_{IEMs}{}^{-2}$	(Giacalone *et al.* 2023)
Spacers cost C_{spacer}	5 (R102.51/m^2)	€· $m_{IEMs}{}^{-2}$	(Giacalone *et al.* 2023)
Labour C_{labour}	20% of equipment cost	€	(Raka *et al.* 2020)

The pump cost was determined using the following Equation 3.36 (€) (Quoilin *et al.* 2011):

$$\mathbf{C_{pump} = 900\left(\frac{P_{pump}}{300}\right)^{0.25}} \qquad \textbf{Equation 3.36}$$

where P_{pump} is the pump power in watts.

Piping cost (€) was determined using the following Equation 3.37 (Quoilin *et al.* 2011):

$$\mathbf{C_{piping} = (0.087 + 0.21D_{pipe})L_{pipe}} \qquad \textbf{Equation 3.37}$$

For labour cost the following Equation 3.38 was used to find the equipment cost first to use it to find labour cost (Quoilin *et al.* 2011):

$$\mathbf{equipment = C_m + C_{electrode} + C_{casing} + C_{spacer} + C_{pump} + C_{piping}} \qquad \textbf{Equation 3.38}$$

Operational and maintenance cost (OPEX)

OPEX (€) includes labour maintenance, service and repairs expenses and it was assumed to be 2% of CAPEX. Indirect and direct operational cost such as emissions, chemical, supply of water, taxes, administration, and insurance are not included (Raka *et al.* 2020).

$$\mathbf{OPEX = 0.02 \cdot CAPEX} \qquad \textbf{Equation 3.39}$$

The cost of electricity production was calculated based on the LCOE index (Khatib 2010).

$$\mathbf{LCOE = \frac{CAPEX \times \left(1 + \frac{discount\ rate\ (r)}{100}\right)^{plant\ lifetime\ (n)} + OPEX \times plant\ lifetime}{Total\ energy\ generation\ over\ plant\ lifetime}} \qquad \textbf{Equation 3.40}$$

The total energy generation over plant lifetime is in kWh, r is the discount rate and n the system life in years.

The equations listed above were used to obtain results that are presented in chapter 4 (thoeretical potential for energy production, membrane design, cost analysis of the plant).

CHAPTER 4-RESULTS AND DISCUSSION

4.1 Introduction

This chapter present the results of the annual potential for energy production assessment in the following estuaries: uThukela, Umgeni, uMvoti, uMfolozi, Amanzimtoti, and uMkhomazi. The annual potentials were calculated using Equation 3.1 in Chapter 3, assuming that the temperature of sea and river water is 25℃. To calculate the potential for energy production, the flow rates and salinity concentrations of the major rivers were required and were found in sources such as (Gazette 23/08/2023) and (Tenza 2018). The value adopted for the concentration of sea water was 600 mol/m^3. However, the flow rate found in the Department of Water Affairs and Sanitations for the rivers were not constant due to the raining season, which is not constant due to the climate issues. The annual average volumetric flow rate was used to perfume calculations. It is important to highlight that the salinity data for the various estuaries under study are scarce.

The issue illustrated in the above paragraph made the analysis of the potential for energy production of each of the sites less accurate. For a better comparison of the theoretical potential in each of the estuaries, the ideal would be to have salinity and flow rate data from the different rivers, all in the same time frame or period. However, due to the lack of salinity or salt concentration data and possible lack of flow rates values for a river in a specific period, it was not possible to compare the estuaries in the same time frame. This chapter also shows the membrane design calculated results, this result includes the membrane area, total stack membrane area, number of cells pairs.

4.2 Theoretical potential for energy production assessment

The river that produces high power was uThukela which can produce up to 360.50 MW yearly with well maintained ion exchange membranes, this high value is due to high volumetric and higher salt concentration compared to the other five major rivers as shown in Table 4.1. However, when mixing the whole uThukela annual volumetric flow rate and the whole Indian ocean annual volumetric flow rate the estimated power is high (360.50 MW), which is also due to high salt concentration of the sea and high volumetric flow rate. Figure 4.1 represents graphical power that can be found in each of the five major rivers and these power values were converted from the

theoretical potential of energy production values that were found through calculations. Sample of calculations were done in Appendix A.

Table 4.1: Showing the results obtained for the theoretical power production of rivers and energy produced in a year.

RIVER	POWER (MW)	ENERGY PRODUCED (GWh)
Uthukela	360.5	3158.33
Umkhomazi	101.47	888.88
Umvoti	55.59	486.97
Umgeni	31.46	275.59
Umfolozi	13.83	121.15
Amanzimtoti	9.61	84.180

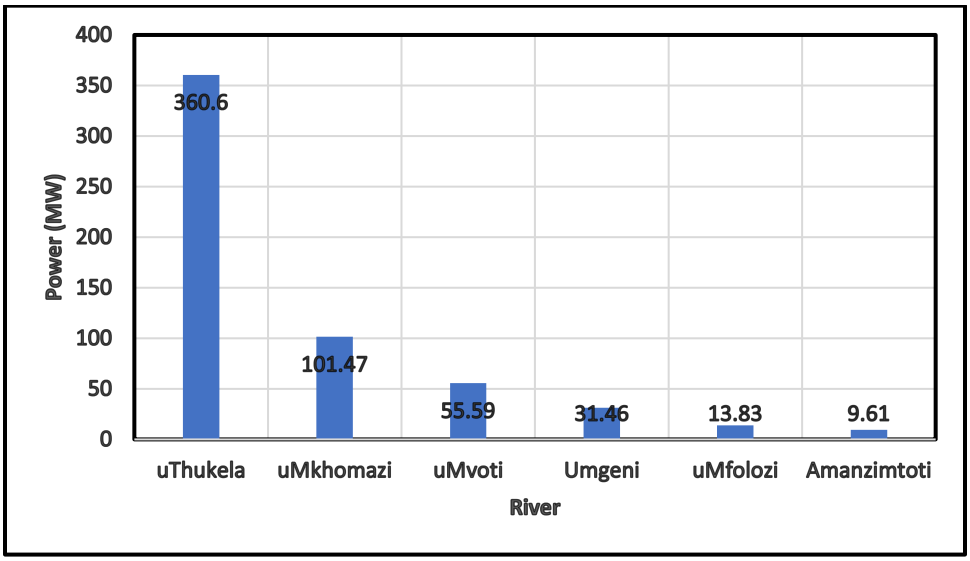

Figure 4.1: Shows the results of power output produced by the rivers mentioned above.

Table 4.2 shows the theoretical potential for energy production results found from the studied estuaries. The uThukela estuary was found to have the highest theoretical potential for energy production when assuming to utilize all its volumetric discharge flow rate, this makes this estuary to have the highest potential in the production of salinity gradient energy (blue energy). However, practically this high potential of energy production may not be possible due to rains, which affect

flow rates, this means that there are some cases where there will be no flow rates at all due to rains and this potential for energy production may decrease practically. Climate and weather conditions affects the flow rates of the rivers, and this can make the energy production to be different at some times. Rivers such as Umgeni and Amanzimtoti they have a salt concentration which fluctuates during different seasons, at some other times the salinity concentration may be equal to zero and this may affect the production of salinity gradient energy, which this may result in low electricity production. South African energy demands sit at 30306 GWh (Ferreira and Pierce 2022), and KwaZulu Natal province sits at 3504 GWh. It can be observed that uThukela alone can meet just a notable fraction of energy demands in South Africa since uThukela alone can provide 3158.33 GWh of energy per year utilising the whole annual volumetric discharge.

It was observed that the power produced by uThukela may decrease or fluctuate due to rains since rains affect the volumetric flow rate and salt concentration. There are seasons where there is a low percentage of rains, and it was observed that during those seasons (winter) power decreases from 360.5 MW in the uThukela estuary to 90.13 MW, and on raining seasons the power increases and it was observed that the power can increase and reach approximately 721 MW of power. To prevent this fluctuation of power it was concluded that energy can be produced and be stored during the low raining seasons.

Table 4.2: Shows the obtained theoretical potential for energy production values for the studied esturies.

ESTUARY	**THEORETICAL POTENTIAL FOR ENERGY** (J/y)
uThukela	1.137×10^{16}
Umkhomazi	3.20×10^{15}
Umvoti	1.753×10^{15}
Umgeni	9.992×10^{14}
Umfolozi	4.36×10^{14}
Amanzimtoti	3.031×10^{14}

4.3 Pilot Design of Reverse Electrodialysis plant on uThukela Estuary

Since uThukela estuary produced higher theoretical potential for energy production than the other rivers. Therefore, it was considered that the pilot plant should be located there. This subchapter discusses the design values found when performing RED pilot plant design calculations. Table 4.3 presents the results of the values of reverse electrodialysis stack parameters that are needed in order to be possible to develop the RED stack pilot plant.

Table 4.3: Shows design results for RED's stack and membranes.

PARAMETER	VALUE	SYMBOL
Resistance of cation exchange membrane (R_{CEM})	2.0995×10^{-4}	Ω
Resistance of anion exchange membrane (R_{AEM})	2.0995×10^{-4}	Ω
Cell resistance (R_{cell})	2.96×10^{-2}	Ω
Stack resistance (R_{stack})	2.664×10^{-1}	Ω
Maximum power (P_{max})	2.0	W
Area of RED stack (A_s)	0.67	m^2
Membrane area (A_{mem})	0.037	m^2
Number of cell pairs in a stack (N_m)	9	–

According to the findings listed in Table 4.3, the cation and anion exchange membranes resistances, cell resistance and stack resistance correspond with the result found by (Vallejo-Castaño and Sánchez-Sáenz 2017). According to (Vallejo-Castaño and Sánchez-Sáenz 2017) the resistances of cation, anion, stack, and cell must be very low because that implies that the power density produced would be higher if your membrane resistances are low. The resistance values obtained for both ion exchange membranes were the same due to the assumption made. In chapter 3, it was assumed that the cell works the same way, which means that membranes have the same properties, such as membrane thickness, and same surface area. In practical or experimental conditions, it is possible to have the same resistance for both anion and cation exchange membranes. This could occur if the membranes have similar properties, such as thickness, surface area, and ion conductivity, and if the experimental setup and conditions are controlled carefully to minimise any differences in resistance (Vallejo-Castaño and Sánchez-Sáenz 2017). In terms of the

membrane area and stack area the value obtained are small because of the sea water salt concentration is high, which means that to produce high power, one needs to reduce the membrane area and membrane thickness because of the high salt concentration solutions used.

In terms of power, the value obtained (table 4.3) is low and this can be due to low ion selectivity of the ion exchange membranes. Other factors such as membrane spacers, fouling or scaling on the membranes, temperature variations, and the concentration difference between the two solutions can also affect power production. The number of cell pairs found in this study (9 cell pairs), was found to be in the same range as the number of cell pairs found by (Guimarães 2020) which was 10 cell pairs. The number of cell pairs used in the RED stack should be small enough to able to eliminate the phenomena of ionic short-circuit currents.

4.4 Economic Study

Table 4.4 presents the result obtained for the equipment cost and the cost of electricity production, all these results are based on current market price. Cost of pumps were estimated using the pump power for both seawater suction pump and river water suction pump. The value of pump cost was increased by the amount of water that the pump needs to suck and deliver, and this made the pumps to require more power since the volume flow rate are bit higher, and this means more power the bigger the pumps required and the cost increases automatically with the size of pumps. Cost of piping was estimated using the diameter of suction and discharge pipes of both solutions.

The cost of piping value that was found which is R27835.74 as shown in table 4.4 includes the cost of suction pipes for both solutions and include the cost of discharge pipes for both solutions. The equipment cost includes all the plant equipment such as cost of pumps, cost of piping and cost of electrodes etc. Sample of calculations are presented in Appendix A.

Table 4.4: Shows the results for cost analysis obtained for the RED plant including the pump cost, piping cost, equipment cost, capital cost, operational cost, and levelized cost of electricity (LCOE) produced.

PARAMETER	VALUE (R)
C_{pump}	R20260.26
C_{piping}	R27835.74
$Equipment\ cost$	R58689.82
$CAPEX$	R70427.78
$OPEX$	R1408.56
$LCOE$	R221953.67 kWh

Table 4.5 shows the result obtained when the capital expenses increased by R1000, the cost of electricity produced also increases with the increase in CAPEX. This means that when the capital expenses increase, it can impact the cost of electricity production. Since the capital expenses are directly related to the production capacity of the plant so when the capital expenses rise, the cost per unit of electricity production may rise. Higher capital expenses often lead to increased fixed costs, which are spread across the electricity production, potentially making each unit of electricity more expensive to produce. It's crucial to carefully manage and optimize capital expenses in order to have less cost of electricity production. The calculations were done and presented in Appendix A.

Table 4.5: Shows the relationship between capital expenses (CAPEX) and the cost of electricity production (LCOE) when the CAPEX is increased by R1000.

CAPITAL EXPENSES (CAPEX)	COST Of ELECTRICITY PRODUCTION (LCOE)
R70427.78	R221953.67 kWh
R71427.78	R224539.59 kWh
R72427.78	R227119.75 kWh
R73427.78	R229699.91 kWh
R74427.78	R232280.07 kWh

Figure 4.2 shows a relationship between LCOE and plant lifetime, the relationship is in the descending order, this means that when plant lifetime increases the LCOE decreases due to equipment aging. Generally, extending the plant lifetime leads to a decrease in the cost of electricity production (LCOE), primarily due to spreading of capital cost over a longer period reducing the annual amortization expense, leading to lower fixed costs per unit of electricity produced. Increasing plant lifetime by well maintaining of the plant may help the plant to continue operating efficiently, potentially reducing operational costs per unit of electricity leading to the reduced cost of electricity production.

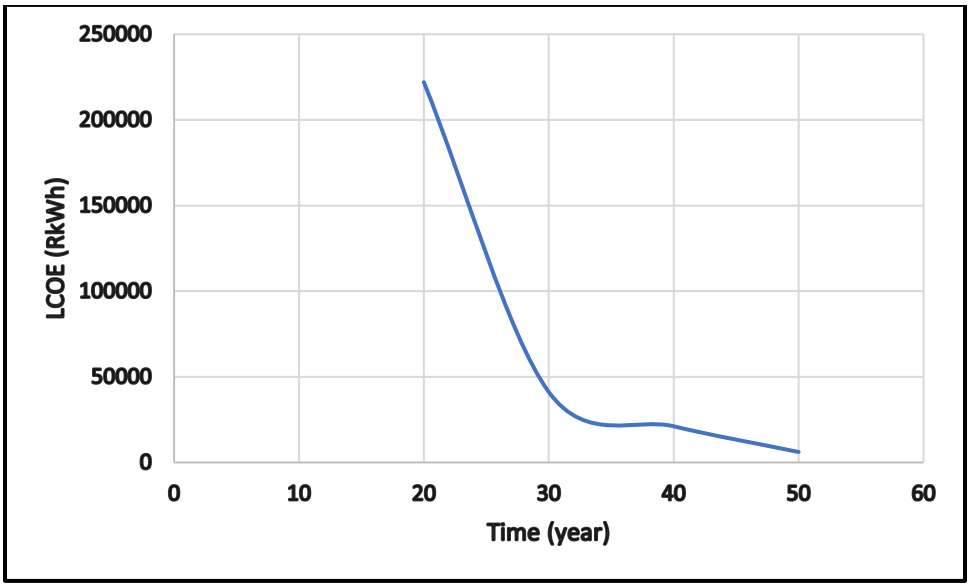

Figure 4.2: Shows the relationship between the cost of electricity produced and the plant lifetime.

4.5 Simulation results

4.5.1 Ion transportation along the membrane simulation.

Figure 4.3 shows the transportation of salt ions from seawater channel across the membrane. The salt is highly concentrated at the surface of the membrane. It shows that using thin membranes can help in the better transportation of salt and also in lowering hydrodynamic resistance but it also shows that using a low salt solution with a very low salt content can affect the production of power since the value obtained was 2 W and this value is too small and also if the membranes used have

a low ion selectivity that can also reduce the power even if the thickness is very thin, so this means that in terms of salt content and ion selectivity there is still some improvement needed . Figure 4.3 also shows that the electrochemical energy is produced at the surface of the membranes as it is shown on the diagram the salt ions are more concentrated on the surface of the membrane.

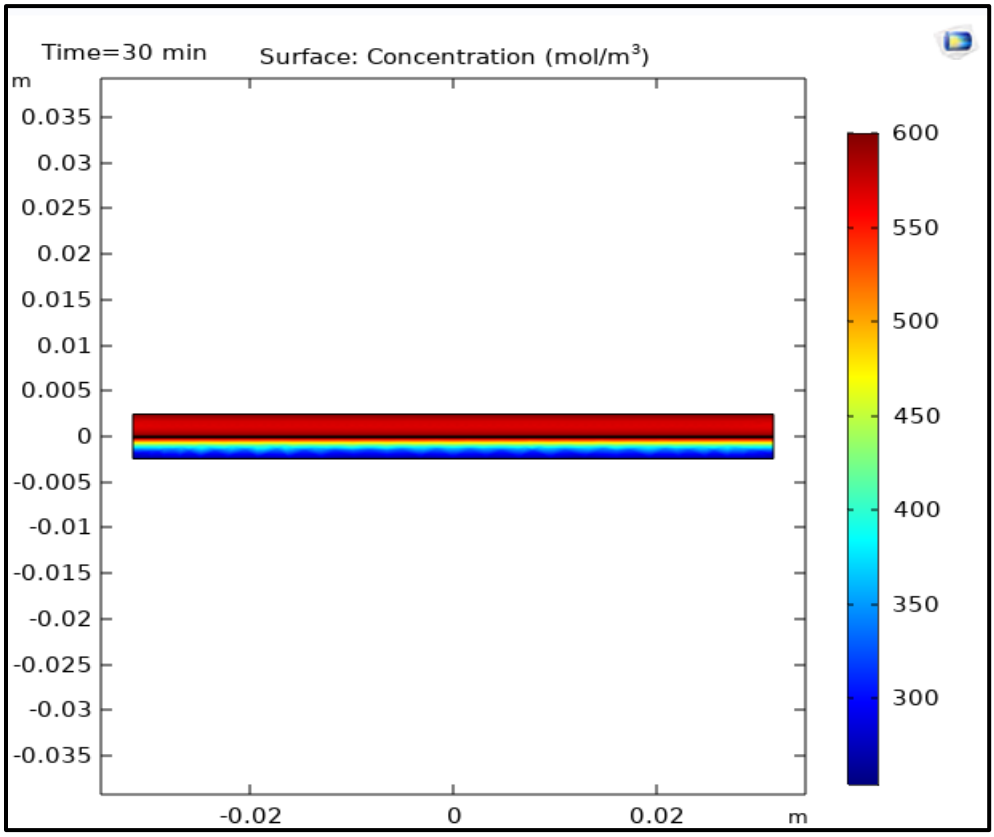

Figure 4.3: Shows a simulation RED cell consist of a river water and seawater channels and a membrane in between these channels.

Figure 4.4 shows the relationship between time and salt concentration transportation. Time is a crucial parameter in the diffusion and migration of salt along the membrane cell pairs because time defines how well is the transportation of ions is going to be. For example, if the residence time is too small the transportation rate of ions would be limited to time because the time that the solutions spend on the membranes is too small, so this means that there is not enough time for the ions to permeate well enough across the membranes. The transportation of ions from seawater channel to river water channel takes about 30 minutes as figure 4.4 illastrate and as you increase the distant that ions need to travel going down the river water channel, ion concentration tends to decrease along the channel due to distance increased.

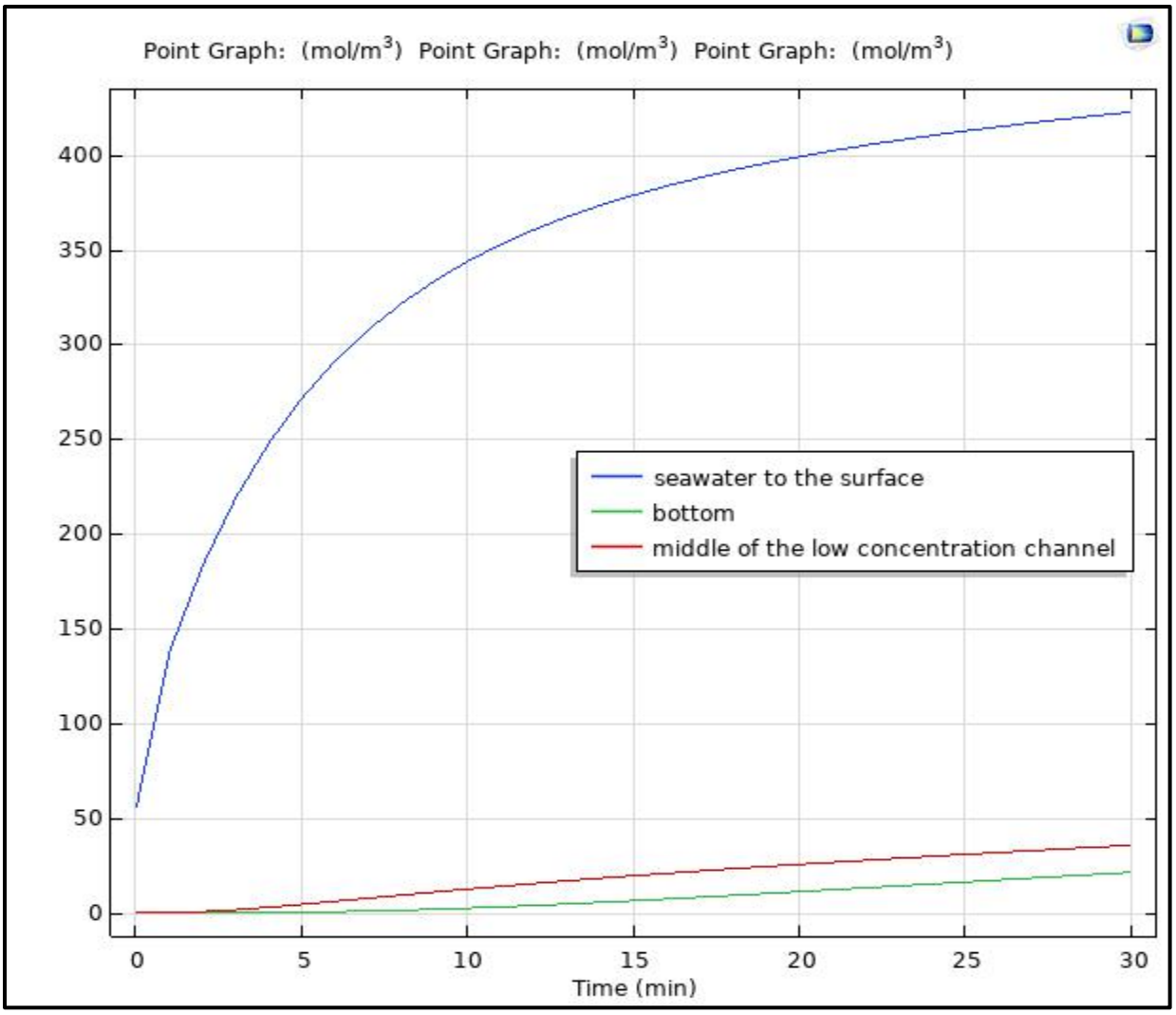

Figure 4.4: Shows the graph of concentration against time along the RED cell.

Figure 4.5 represents the effect of arc length on salt ion transportation. Figure 4.5 also illustrates that as the ions move away from the membrane after passing through going down across the river channel the concentration of salt decreases with increase of arc length. Figure 4.5 shows that when ions pass through the ion-selective membranes towards the low salt concentration solution compartment or channel, the salt concentration generally decreases along the arc length. This is due to the selective permeability of the ion-selective membranes, which allow specific ions to pass through based on their charge and this also illustrate that ions will be more concentrated at the surface of the permeated membrane, so as you go down the low solution compartment the concentration decreases. The graphs that are illustrated in figure 4.5 shows a descending order this

means that ions are being transported to the low concentrated solution this implies that the potential difference is established across the stack. Potential difference is the driving force for ion movement, which encourages cations to move towards the cathode and anions towards the anode.

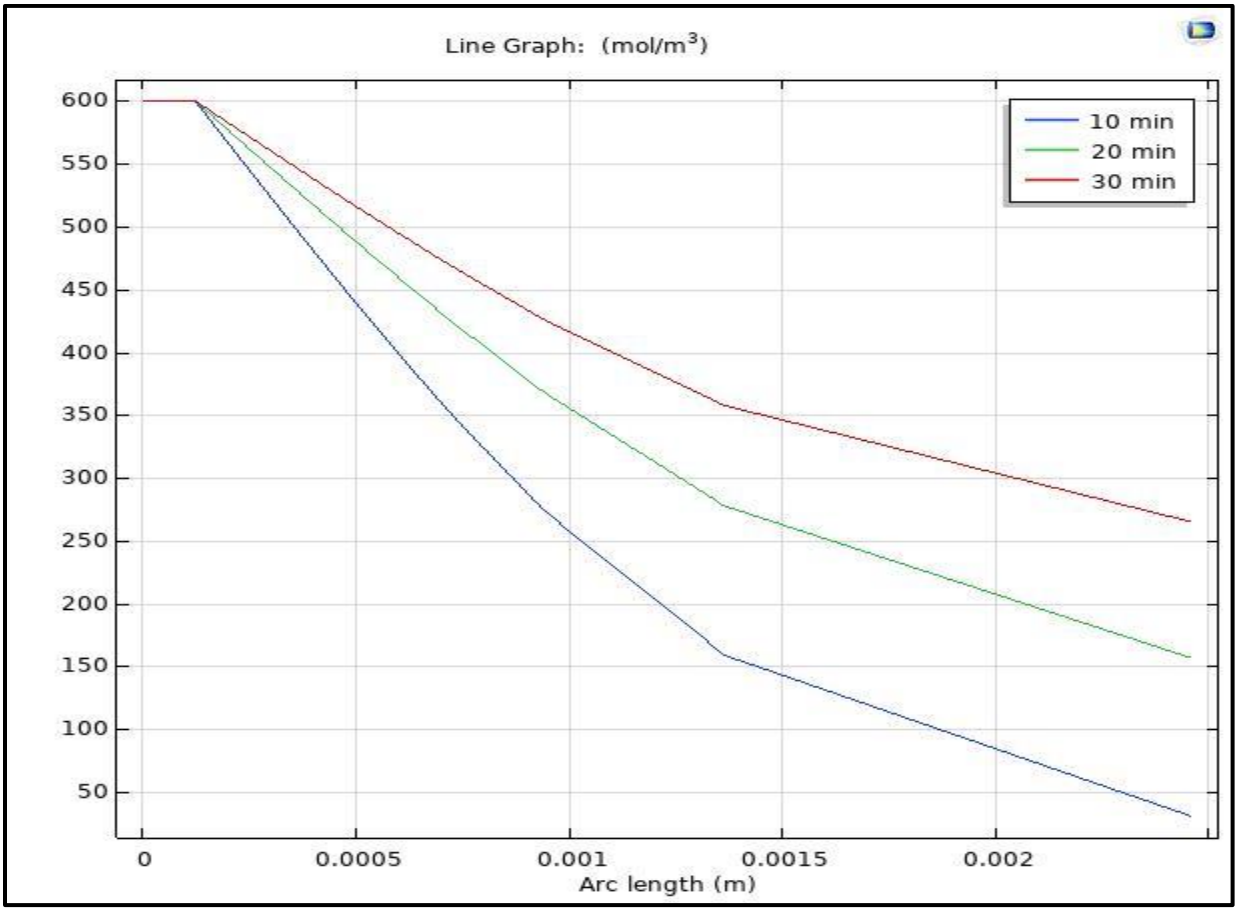

Figure 4.5: Shows the distribution of salt in different arc length from the membrane to river water channel.

4.5.2 Fluid flow along the seawater and river water channels

Figure 4.6 shows the flow of the two solutions in their channels. Sea water is represented by red color and river water by a blue color. Figure 4.6 shows that laminar flow can be recommended for the reverse electrodialysis cell pairs since laminar flow gives good results in terms of ion distribution and provides orderly movement of fluids through the stack. Laminar flow provides a perfect and smooth flow that allows ions to pass through the membrane easily and laminar flow ensures uniform flow patterns result in consistent ion movement through ion-selective membranes,

promoting more efficient energy conversion. Laminar flow allows for better mass transfer of ions between the high and low salt concentrations and the ordered flow patterns provided by laminar flow facilitate a more controlled exchange of ions, maximizing concentration gradients and improving the overall RED efficiency. The design was carried out using a counter-current since this configuration provides good results in theoretical analysis because it maximizes the utilization of concentration gradients along the entire length of the stack this setup creates a continuous and increasing potential difference, allowing for better extraction of energy from the salt concentration gradient, but for practical co-current is recommended due to practical engineering considerations. Co-current flow is more straightforward to implement and manage in terms of system design, and it can be more forgiving regarding potential issues such as membrane fouling and scaling. It simplifies the fluid flow dynamics and can be more robust in real-world operating conditions.

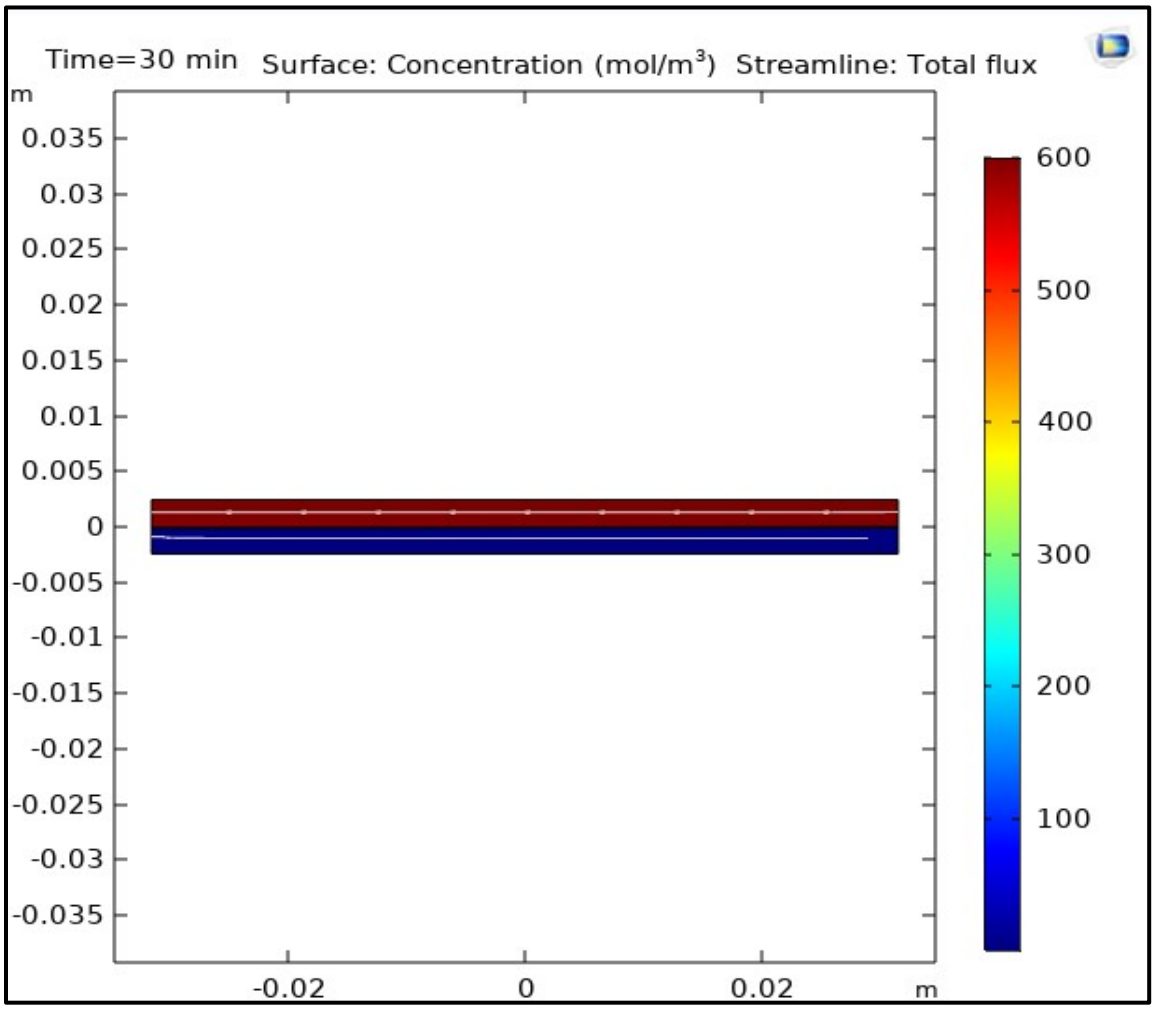

Figure 4.6: Represents flow of river water and seawater in the channels.

Figure 4.7 shows the behavior of velocity in the channels. The velocity decrease at the channel walls and on the membrane surface due to friction as figure 4.7 illustrate. The velocity profile in laminar flow across the channel is typically parabolic, with higher velocities at the center and lower velocities near the walls. Reduced velocity near the walls can lead to lower mass transfer rates, potentially limiting the movement of ions through ion-selective membranes. Mass transfer limitations caused by velocity decrease near the walls can result in concentration polarization (a stagnant boundary layer formed near the membrane due to reduced mass transfer) near the membrane surface, reducing the overall efficiency of ion exchange. Concentration polarization decreases the effective driving force for ion movement, impacting the RED system's efficiency. Lower velocity near the walls may result in increased ohmic losses due to higher electrical resistance in these regions. Ohmic losses contribute to a decrease in power density and overall system efficiency. Figure 4.7 also shows that stagnant regions with lower velocity are more prone to fouling and scaling, especially near the walls and this can further reduce mass transfer efficiency, increase electrical resistance, and diminish overall RED performance.

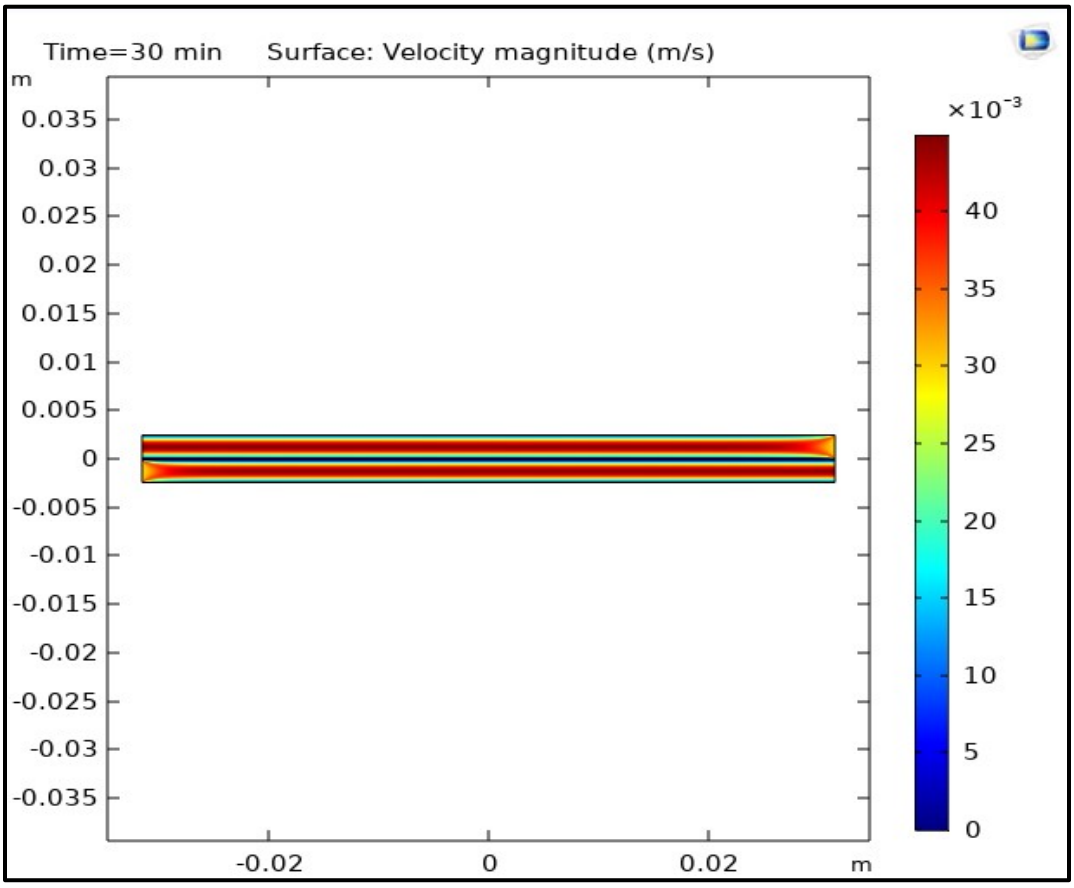

Figure 4.7: Shows the velocity profile along the channels.

Figure 4.8 illustrates how pressure behave along the channels. It shows that in the inlet the pressure is high but moving toward the outlet the pressure decreases until it reaches zero. It is common for the pressure to decrease from the inlet to the outlet. As the feed solution flow through the channel or compartment, there is a natural hydrodynamic pressure drop along the length of the channel. This drop is influenced by factors such as flow rates, channel dimensions, and fluid properties. Ion-selective membranes in the RED stack contribute to the overall resistance to fluid flow. As solutions passes through these membranes, there is resistance, leading to the decrease in pressure. As the electrical resistance contributed by ion-selective membranes increases the ohmic losses occurs and these losses contribute to pressure drops.

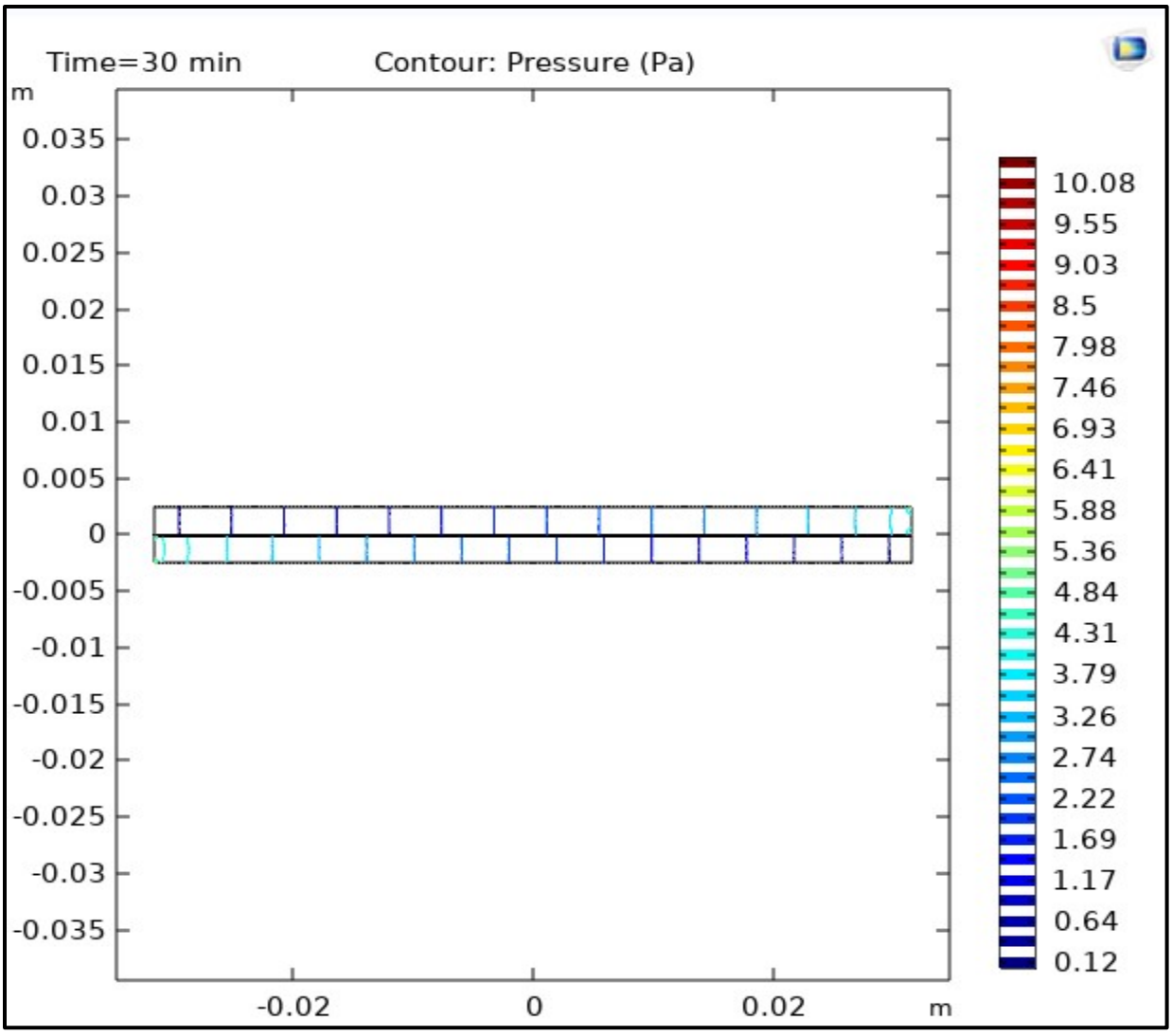

Figure 4.8: Represent the pressure behavior on the solution channels.

4.6 Optimized Parameters

The values obtained from optimization they correspond with the values recommended (Vallejo-Castaño and Sánchez-Sáenz 2017), in order for the RED membranes to perform at its maximum capacity. In terms of the membrane thickness the value obtained from optimization shows that the membrane should be very thin so that ions can permeate faster and easier the value is shown in table 4.6. The velocity near the ion-selective membrane should be low but not very low than the value given on the table 4.6, using low velocity help by minimizing concentration polarization. Low velocity promotes more uniform ion exchange through the ion-selective membranes. This can result in improved efficiency in utilizing the concentration gradients between the high and low salt concentration solutions. Low velocity can reduce the likelihood of fouling and scaling on the membrane surface, and this is important for maintaining the long-term performance of the RED system and minimizing the need for frequent cleaning or maintenance. Smaller velocities generally lead to lower hydrodynamic pressure drops and prevent channel erosion, low velocity also simplify the design of the RED system by reducing the impact of turbulent flow and minimizing the need for complex flow control mechanisms, which this leads to a more straightforward and cost-effective system. So, it is very important to use low velocity in the RED system due to the reasons mentioned above.

The resident time should be 30 minutes in order to give the transportation process of ions enough time. longer residence time allows for more extended contact between the feed solutions and the ion-selective membranes. This can promote improved mass transfer, allowing ions to diffuse more effectively through the membrane. Longer residence time helps in increasing utilization of the concentration gradients between the high and low salt concentration solutions. Longer residence time help mitigate concentration polarization (buildup of ions near the membrane surface). By providing more time for diffusion, concentration polarization can be minimized. Higher residence time contribute to improved ion exchange efficiency, which can result in higher power density in RED stacks. Prolonged residence time allows for more efficient energy conversion by maintaining consistent ion movement through the ion-selective membranes.

(Vallejo-Castaño and Sánchez-Sáenz 2017) recommended a thinner membrane thickness for better RED performance. This report found a thinner membrane through optimization, figure 4.6

represents the results. The use of a thinner membrane typically results in lower electrical resistance, reducing ohmic losses. This contributes to a more efficient ion movement and improves overall system performance. Smaller membrane thickness allows for quicker ion transport across the membrane. This is beneficial for maintaining higher mass transfer rates, resulting in improved ion exchange efficiency. Thinner membranes lead to reduced electrical resistance, this means the energy required to drive ion movement is lower, this can contribute to energy savings and increased overall energy efficiency of the RED system. Thinner membrane can also contribute to higher power density in the RED stack, and thinner membranes may help mitigate concentration polarization by facilitating more efficient ion movement.

Table 4.6 shows the value (0.00246) for channel or compartment thickness which is small. Using of small compartment thickness leads to lower electrical resistance, which can enhance ion movement through the membrane, thinner compartment facilitates quicker mass transfer across the ion-selective membranes. Smaller compartment thickness allows for a more rapid exchange of ions between the high and low salt concentration solutions. Smaller compartment thickness can lead to higher power density.

Table 4.6: Shows the optimized parameters results for the proposed RED membrane design.

Velocity (m/s)	Time (minutes)	Length (m)	Membrane thickness (m)	Compartment thickness (m)
0.03	30	0.063	0.00012	0.00246

The result obtained and presented in this chapter indicates that the design of reverse electrodialysis can be possible in KwaZulu-Natal region in terms of design and theoretical potential of energy production, but there are some improvements that are needed to improve the RED performance and some recommendations are mentioned in chapter 5. In terms of the economic analysis, it can be observed from the result that the plant will be economical viable, the recommendations are presented in chapter five to improve the economic status of the plant. The ion exchange membranes cost was $R205/m^2$ and with well maintained and regular cleaning of membranes to prevent fouling can help in prolonging the lifespan of membranes for normally six to twelve months. Design calculations and economic calculations are presented in Appendix A.

CHAPTER 5-CONCLUSIONS AND RECOMMENDATIONS

5.1 Conclusion

The objectives of this study were as follows:

1. To calculate the theoretical potential for blue energy production via RED of major KZN rivers discharging into the Indian Ocean.

2. To preliminary design RED-based power plant erected at the mouth of the river produced higher potential energy.

3. To optimize operating parameters associated with RED-based power plant through simulation and considering all relevant parameter such as flow rate, stream salt concentration, temperature, membrane type.

From the analysis carried out on the uThukela, uMvoti, Umgeni, uMkhomazi, Amanzimtoti, and uMfolozi estuaries, it was concluded that uThukela estuary has a higher potential for electricity production than the others. Therefore, the feasibility of an installation that would make an energy use of a saline gradient in the uThukela estuary was evaluated. It was concluded that the location of the salinity gradient energy plant has a greater impact on the cost and power produced. It was concluded that the location of the plant where the energy produced is greater and the capital costs are lower is at the mouth of the uThukela river.

Based on the findings it is concluded that salinity gradient energy may have a chance to meet a notable amount of energy demands in KwaZulu-Natal, if all the flowrates can be utilized. Also, it is concluded that using the energy produced by reverse electrodialysis to power up pumps for pumping water to the reverse electrodialysis could be a suitable idea since, one is cutting cost by doing two things at once (treating water by desalinating and power production that can also be utilised at the same plant as source of energy). For water usage the energy production will not compete with it since water is collected at the discharge point of the river.

An economic study was carried out to determine the cost of electricity production and to find pump cost, piping cost of the plant, and to evaluate that the plant will make profit or not. Due to this finding, it was concluded that this technology is economically vaible but interms of profit generation it still needs some improvement, since the value obatined for profit/loss was R0 this means that the plant will not generate profit but at the same time no loss and at this stage the focus is to try to generate power first.

5.2 Recommendations

To increase the power density and power production in a RED system it is recommended to increase salt concentration difference to maximize the ion flow across the ion exchange membranes, this will automatically increase power output. Power production can be also improved by optimising membrane properties (using of membranes with high selectivity, control temperature, and using membranes with a thinner thickness). In terms of flowrate using proper flowrate can help to maintain concentration gradients and promote efficient ion exchange.

It is also recommended to use high concentrated solutions to decrease the internal resistance and membrane resistances. It is also recommended for practical to use co-current operation because co-current configuration causes smaller local pressure differences between the river and seawater compartments therefore leakages chances are very small, and to use very thin membranes with high fluxes and very open spacer structure with low resistance is also recommended.

To prevent decreasing of velocity near the walls of RED stack channels it recommended to design channels with proper dimensions and geometry to promote uniform velocity distribution. Consider features like tapering or shaping the channels to maintain laminar flow characteristics and reduce the likelihood of stagnant. Design the inlet and outlet sections of the channels to encourage smooth and well-distributed flow. Utilize Computational fluid Dynamics (CFD) simulations to model and analyse the flow patterns within the RED stack channels. Optimize operational parameters such as flow rates, temperature, and pressure to maintain the desired velocity profile. Implement regular maintenance practices to prevent fouling and scaling, which can disrupt the velocity profile near the channels and cleaning protocols to ensure consistent flow.

It is very hard to know the exact lifespan of the ion exchange membranes since it can be vary widely depending on factors such as the specific application, operating conditions, maintenance protocols, and the quality of the membranes themselves. In industrial applications, membranes may typically last anywhere from several months to several years before needing replacement. But with proper care and maintenance such as proper cleaning to remove fouling substances, such as scaling or organic deposits, optimising operating conditions by ensuring that the membranes operate within their specified parameters, such as temperature, pressure, and pre-treatment such as filtration or softening, to remove particulates substances that could foul the membranes can help maintain the membranes performance and prolong their lifespan. Regular monitoring of membrane perfomence and condition is essential to determine when replacement is necessary and this can have a positive affect on operational costs, because this will help by decreasing the frequently purchasing of new membranes.

There are other ions present in seawater other then sodium chloride and these ions may have a negative impact such as membrane fouling caused by ions such as magnesium, calcium, and sulfate which are present in seawater. Selective permeability may also be affected by the present of these ions since some ions present in seawater may have different selectivity or transport rates through ion exchange membranes compared to sodium and chloride ions. The presence of other ions in seawater may affect the energy requirements for electricity production through ion exchange membranes. Depending on the specific ions and their concentrations, additional energy may be needed to overcome the affects of fouling or to maitain optimal membrane performance. To mitigate the effects of other ions other than sodium and chloride in seawater strategies such as pre-treatment (filtration, softening, or chemical conditioning can remove or reduce the concentrations of fouling ions) before they reach the ion exchange membranes this can helps minimize membrane fouling and maintain performance. It is also recommended to choose or select membrane materials with higher resistance to fouling and better selectivity for target ions can improve performance in seawater applications. It is also recommended that chemical cleaning of membranes can remove fouling deposits and restore membrane performance and modifying of membrane surface using techniques, such as coatings can alter the surface properties of membranes to reduce fouling tendencies and improve selectivity for target ions.

REFERENCES

Altıok, E., Kaya, T. Z., Güler, E., Kabay, N. and Bryjak, M. 2021. Performance of reverse electrodialysis system for salinity gradient energy generation by using a commercial ion exchange membrane pair with homogeneous bulk structure. *Water*, 13 (6): 814.

Audinos, R. 1992. Electric power produced from two solutions of unequal salinity by reverse electrodialysis. Article ID.

Avci, A. H., Sarkar, P., Tufa, R. A., Messana, D., Argurio, P., Fontananova, E., Di Profio, G. and Curcio, E. 2016. Effect of Mg2+ ions on energy generation by Reverse Electrodialysis. *Journal of Membrane Science*, 520: 499-506.

Bevacqua, M., Tamburini, A., Papapetrou, M., Cipollina, A., Micale, G. and Piacentino, A. 2017. Reverse electrodialysis with NH4HCO3-water systems for heat-to-power conversion. *Energy*, 137: 1293-1307.

Brauns, E. 2009. Salinity gradient power by reverse electrodialysis: effect of model parameters on electrical power output. *Desalination*, 237 (1-3): 378-391.

Chanda, S. and Tsai, P. A. 2019. Numerical simulation of renewable power generation using reverse electrodialysis. *Energy*, 176: 531-543.

Choi, I., Han, J. Y., Yoo, S. J., Henkensmeier, D., Kim, J. Y., Lee, S. Y., Han, J., Nam, S. W., Kim, H. J. and Jang, J. H. 2016. Experimental Investigation of Operating Parameters in Power Generation by Lab-Scale Reverse Electro-Dialysis (RED). *Bulletin of the Korean Chemical Society*, 37 (7): 1010-1019.

Coleman Gilstrap, M. 2013. Renewable electricity generation from salinity gradients using reverse electrodialysis. Article IDMS Thesis, Georgia Institute of Technology.

Daniilidis, A., Herber, R. and Vermaas, D. A. 2014. Upscale potential and financial feasibility of a reverse electrodialysis power plant. *Applied energy*, 119: 257-265.

Daniilidis, A., Vermaas, D. A., Herber, R. and Nijmeijer, K. 2014. Experimentally obtainable energy from mixing river water, seawater or brines with reverse electrodialysis. *Renewable energy*, 64: 123-131.

Długołęcki, P., Gambier, A., Nijmeijer, K. and Wessling, M. 2009. Practical potential of reverse electrodialysis as process for sustainable energy generation. *Environmental science & technology*, 43 (17): 6888-6894.

Duke, S. 2016. *The Water Cycle*. Weigl Publishers.

Dunmade, I., Madushele, N., Adedeji, P. A. and Akinlabi, E. T. 2019. A streamlined life cycle assessment of a coal-fired power plant: the South African case study. *Environmental Science and Pollution Research*, 26: 18484-18492.

Fennessy, S., Roberts, M. and Paterson, A. 2016. A brief overview of the ACEP project: Ecosystem Processes in the KwaZulu-Natal Bight. *African Journal of Marine Science*, 38 (sup1): S1-S6.

Ferreira, B. A. and Pierce, W. T. 2022. Statistics of utility-scale power generation in South Africa in 2021. Article ID.

Forgacs, C. 1982. Recent developments in the utilization of salinity power. *Desalination*, 40 (1-2): 191-195.

Gazette, G. 23/08/2023. *National Water Resource Strategy third edition (NWRS-3).* Available: https://www.dws.gov.za/Documents/Gazettes/Approved%20National%20Water%20Resource%20Strategy%20Third%20Edition%20(NWRS3)%202023.pdf (Accessed

Ghiorso, M. S., Carmichael, I. S., Rivers, M. L. and Sack, R. O. 1983. The Gibbs free energy of mixing of natural silicate liquids; an expanded regular solution approximation for the calculation of magmatic intensive variables. *Contributions to Mineralogy and Petrology*, 84: 107-145.

Giacalone, F., Papapetrou, M., Kosmadakis, G., Tamburini, A., Micale, G. and Cipollina, A. 2023. Application of reverse electrodialysis to site-specific types of saline solutions: A techno-economic assessment. *Energy*, 181: 532-547.

Goldemberg, J. 2001. World energy assessment. Energy and the challenge of sustainability. Article ID.

Guastella, L. A. and Smith, A. M. 2014. Coastal dynamics on a soft coastline from serendipitous webcams: KwaZulu-Natal, South Africa. *Estuarine, Coastal and Shelf Science*, 150: 76-85.

Guimarães, J. N. 2020. Aproveitamento Energético de um Gradiente Salino. Article ID.

Güler, E., Elizen, R., Vermaas, D. A., Saakes, M. and Nijmeijer, K. 2013. Performance-determining membrane properties in reverse electrodialysis. *Journal of membrane science*, 446: 266-276.

Güler, E., van Baak, W., Saakes, M. and Nijmeijer, K. 2014. Monovalent-ion-selective membranes for reverse electrodialysis. *Journal of membrane science*, 455: 254-270.

Gurreri, L., Tamburini, A., Cipollina, A., Micale, G. and Ciofalo, M. 2014. CFD prediction of concentration polarization phenomena in spacer-filled channels for reverse electrodialysis. *Journal of membrane science*, 468: 133-148.

Gurreria, L., Tamburini, A., Cipollinaa, A., Micalea, G. and Ciofalob, M. 2013. CFD simulation of mass transfer phenomena in spacer filled channels for reverse electrodialysis applications. *CHEMICAL ENGINEERING*, 32.

Haines, A., Finlayson, B. and McMahon, T. 1988. A global classification of river regimes. *Applied Geography*, 8 (4): 255-272.

He, Z., Gao, X., Zhang, Y., Wang, Y. and Wang, J. 2016. Revised spacer design to improve hydrodynamics and anti-fouling behavior in reverse electrodialysis processes. *Desalination and Water Treatment*, 57 (58): 28176-28186.

Holloway, S., Pearce, J., Hards, V., Ohsumi, T. and Gale, J. 2007. Natural emissions of CO2 from the geosphere and their bearing on the geological storage of carbon dioxide. *Energy*, 32 (7): 1194-1201.

Hong, J. G., Zhang, B., Glabman, S., Uzal, N., Dou, X., Zhang, H., Wei, X. and Chen, Y. 2015. Potential ion exchange membranes and system performance in reverse electrodialysis for power generation: A review. *Journal of Membrane Science*, 486: 71-88.

Ibrahim, I. A., Ötvös, T., Gilmanova, A., Rocca, E., Ghanem, C. and Wanat, M. 2021. *International energy agency*. Kluwer Law International BV.

Isaacs, J. D. and Schmitt, W. R. 1980. Ocean energy: forms and prospects. *Science*, 207 (4428): 265-273.

Jagur-Grodzinski, J. and Kramer, R. 1986. Novel process for direct conversion of free energy of mixing into electric power. *Industrial & Engineering Chemistry Process Design and Development*, 25 (2): 443-449.

Kariduraganavar, M., Nagarale, R., Kittur, A. and Kulkarni, S. 2006. Ion-exchange membranes: preparative methods for electrodialysis and fuel cell applications. *Desalination*, 197 (1-3): 225-246.

Khatib, H. 2010. Review of OECD study into "Projected costs of generating electricity—2010 Edition". *Energy Policy*, 38 (10): 5403-5408.

Kingsbury, R., Liu, F., Zhu, S., Boggs, C., Armstrong, M., Call, D. and Coronell, O. 2017. Impact of natural organic matter and inorganic solutes on energy recovery from five real salinity gradients using reverse electrodialysis. *Journal of Membrane Science*, 541: 621-632.

Kuleszo, J. 2008. The global and regional potential of salinity-gradient power. *Dept. Environmental Sciences, Environmental Systems Analysis Group, Wageningen University and Research Centre*, Article ID.

Kweku, D. W., Bismark, O., Maxwell, A., Desmond, K. A., Danso, K. B., Oti-Mensah, E. A., Quachie, A. T. and Adormaa, B. B. 2018. Greenhouse effect: greenhouse gases and their impact on global warming. *Journal of Scientific research and reports*, 17 (6): 1-9.

Lacey, R. 1980. Energy by reverse electrodialysis. *Ocean engineering*, 7 (1): 1-47.

Lanjewar, S., Mukherjee, A., Rehman, L. M. and Roy, A. 2020. Blue energy and its potential: the membrane based energy harvesting. *Advances in Membrane Technologies*, Article ID: 171.

Livina, V., Ashkenazy, Y., Kizner, Z., Strygin, V., Bunde, A. and Havlin, S. 2003. A stochastic model of river discharge fluctuations. *Physica A: Statistical Mechanics and its Applications*, 330 (1-2): 283-290.

Logan, B. E. and Elimelech, M. 2012. Membrane-based processes for sustainable power generation using water. *Nature*, 488 (7411): 313-319.

Luo, X., Cao, X., Mo, Y., Xiao, K., Zhang, X., Liang, P. and Huang, X. 2012. Power generation by coupling reverse electrodialysis and ammonium bicarbonate: Implication for recovery of waste heat. *Electrochemistry communications*, 19: 25-28.

Malanima, P. 2022. World Energy Consumption A Database 1820-2020. Article ID.

Mei, Y. and Tang, C. Y. 2017. Co-locating reverse electrodialysis with reverse osmosis desalination: Synergies and implications. *Journal of Membrane Science*, 539: 305-312.

Mei, Y. and Tang, C. Y. 2018. Recent developments and future perspectives of reverse electrodialysis technology: A review. *Desalination*, 425: 156-174.

Mitigation, C. C. 2011. IPCC special report on renewable energy sources and climate change mitigation. *Renewable Energy*, 20 (11).

Moreno, J., De Hart, N., Saakes, M. and Nijmeijer, K. 2017. CO2 saturated water as two-phase flow for fouling control in reverse electrodialysis. *Water research*, 125: 23-31.

Mulder, M. 1996. *Basic principles of membrane technology*. Springer science & business media.

Nagarale, R., Gohil, G. and Shahi, V. K. 2006. Recent developments on ion-exchange membranes and electro-membrane processes. *Advances in colloid and interface science*, 119 (2-3): 97-130.

Nam, J.-Y., Jwa, E., Eom, H., Kim, H., Hwang, K. and Jeong, N. 2021. Enhanced energy recovery using a cascaded reverse electrodialysis stack for salinity gradient power generation. *Water Research*, 200: 117255.

NASA. 14 March 2003. *Umfolozi river*. Available: https://mapcarta.com › Africa › Southern Africa › South Africa › KwaZulu-Natal (Accessed

Noelmcdonogh. 06 January 2017. *Umkomazi by air*. Available: https://en.wikipedia.org/wiki/Umkomaas (Accessed

Pattle, R. 1954a. Production of electric power by mixing fresh and salt water in the hydroelectric pile. *Nature*, 174: 660-660.

Pattle, R. E. 1954b. production of electro power by mixing fresh water and sea water. Article ID.

Post, J. W. 2009. electricity production from salinity gradients by reverse electrodialysis. *blue energy*, 1: 224.

Post, J. W., Hamelers, H. V. and Buisman, C. J. 2008. Energy recovery from controlled mixing salt and fresh water with a reverse electrodialysis system. *Environmental science & technology*, 42 (15): 5785-5790.

Post, J. W., Hamelers, H. V. and Buisman, C. J. 2009. Influence of multivalent ions on power production from mixing salt and fresh water with a reverse electrodialysis system. *Journal of Membrane Science*, 330 (1-2): 65-72.

Post, J. W., Veerman, J., Hamelers, H. V., Euverink, G. J., Metz, S. J., Nymeijer, K. and Buisman, C. J. 2007. Salinity-gradient power: Evaluation of pressure-retarded osmosis and reverse electrodialysis. *Journal of membrane science*, 288 (1-2): 218-230.

Price, T. and Probert, D. 1997. Harnessing hydropower: A practical guide. *Applied energy*, 57 (2-3): 175-251.

Quoilin, S., Declaye, S., Tchanche, B. F. and Lemort, V. 2011. Thermo-economic optimization of waste heat recovery Organic Rankine Cycles. *Applied thermal engineering*, 31 (14-15): 2885-2893.

Raka, Y. D., Karoliussen, H., Lien, K. M. and Burheim, O. S. 2020. Opportunities and challenges for thermally driven hydrogen production using reverse electrodialysis system. *International Journal of Hydrogen Energy*, 45 (2): 1212-1225.

Rescue, I. M. 25 December 2019. *uMvoti river*. Available:

https://www.citizen.co.za/north-coast-courier/news-headlines/local-news/2019/12/25/childs-body-found-five-day-se (Accessed

Simões, C. 2023. Advances in reverse electrodialysis for renewable energy generation. Article ID.

Stewart, B. A. and Howell, T. 2003. *Encyclopedia of Water Science (Print)*. CRC press.

Stock, S. 2022. *Umgeni river*. Available: https://www.shutterstock.com/search/umgeni-river (Accessed

Strathmann, H. 2004. *Ion-exchange membrane separation processes*. Elsevier.

Tedesco, M., Brauns, E., Cipollina, A., Micale, G., Modica, P., Russo, G. and Helsen, J. 2015. Reverse electrodialysis with saline waters and concentrated brines: A laboratory investigation towards technology scale-up. *Journal of Membrane Science*, 492: 9-20.

Tenza, N. P. 2018. Macroinvertebrates as ecological indicators of the wellbeing of the lower uMvoti and Thukela Rivers, KwaZulu-Natal, South Africa. Article ID.

Tshibangu, M. M. 2017. Investigation of perfluorocarbons as potential physical solvents for flue gas cleaning. Article ID.

Tufa, R. A., Curcio, E., Brauns, E., van Baak, W., Fontananova, E. and Di Profio, G. 2015. Membrane distillation and reverse electrodialysis for near-zero liquid discharge and low energy seawater desalination. *Journal of Membrane Science*, 496: 325-333.

Tufa, R. A., Curcio, E., van Baak, W., Veerman, J., Grasman, S., Fontananova, E. and Di Profio, G. 2014. Potential of brackish water and brine for energy generation by salinity gradient power-reverse electrodialysis (SGP-RE). *RSC Advances*, 4 (80): 42617-42623.

Vallejo-Castaño, S. and Sánchez-Sáenz, C. I. 2017. Design and optimization of a reverse electrodialysis stack for energy generation through salinity gradients. *Dyna*, 84 (202): 84-91.

Van der Leeden, F. 1990. *The water encyclopedia*. CRC Press.

Vaselbehagh, M., Karkhanechi, H., Takagi, R. and Matsuyama, H. 2017. Biofouling phenomena on anion exchange membranes under the reverse electrodialysis process. *Journal of Membrane Science*, 530: 232-239.

Veerman, J., Saakes, M., Metz, S. and Harmsen, G. 2009. Reverse electrodialysis: Performance of a stack with 50 cells on the mixing of sea and river water. *Journal of Membrane Science*, 327 (1-2): 136-144.

Veerman, J., Saakes, M., Metz, S. J. and Harmsen, G. 2010. Reverse electrodialysis: evaluation of suitable electrode systems. *Journal of Applied Electrochemistry*, 40: 1461-1474.

Vermaas, D. A., Kunteng, D., Saakes, M. and Nijmeijer, K. 2013. Fouling in reverse electrodialysis under natural conditions. *Water research*, 47 (3): 1289-1298.

Vermaas, D. A., Kunteng, D., Veerman, J., Saakes, M. and Nijmeijer, K. 2014a. Periodic feedwater reversal and air sparging as antifouling strategies in reverse electrodialysis. *Environmental science & technology*, 48 (5): 3065-3073.

Vermaas, D. A., Saakes, M. and Nijmeijer, K. 2011a. Doubled power density from salinity gradients at reduced intermembrane distance. *Environmental science & technology*, 45 (16): 7089-7095.

Vermaas, D. A., Saakes, M. and Nijmeijer, K. 2011b. Power generation using profiled membranes in reverse electrodialysis. *Journal of membrane science*, 385: 234-242.

Vermaas, D. A., Veerman, J., Saakes, M. and Nijmeijer, K. 2014b. Influence of multivalent ions on renewable energy generation in reverse electrodialysis. *Energy & environmental science*, 7 (4): 1434-1445.

Weinstein, J. N. and Leitz, F. B. 1976. Electric power from differences in salinity: the dialytic battery. *Science*, 191 (4227): 557-559.

Xu, T. 2005. Ion exchange membranes: State of their development and perspective. *Journal of membrane science*, 263 (1-2): 1-29.

Yip, N. Y. and Elimelech, M. 2014. Comparison of energy efficiency and power density in pressure retarded osmosis and reverse electrodialysis. *Environmental science & technology*, 48 (18): 11002-11012.

Zhu, X., He, W. and Logan, B. E. 2015. Reducing pumping energy by using different flow rates of high and low concentration solutions in reverse electrodialysis cells. *Journal of Membrane Science*, 486: 215-221.

APPENDIX A

Sample of Calculations

Salinity gradient power can be produced by mixing two solutions with different salt concentrations which are commonly seawater and river water pumped to the reverse electrodialysis system. These two solutions can be pre-treated before entering the reverse electrodialysis system, which consists of alternating ion exchange membranes to harness the energy from the salinity gradient between the two input streams as it is illustrated on Figure A1.1. The membranes selectively allow the passage of either positive or negative ions, creating a potential difference that can be converted into electrical energy. The generated electrical energy by salinity gradient is then captured and converted into power through electrodes at the end of the ion exchange membranes.

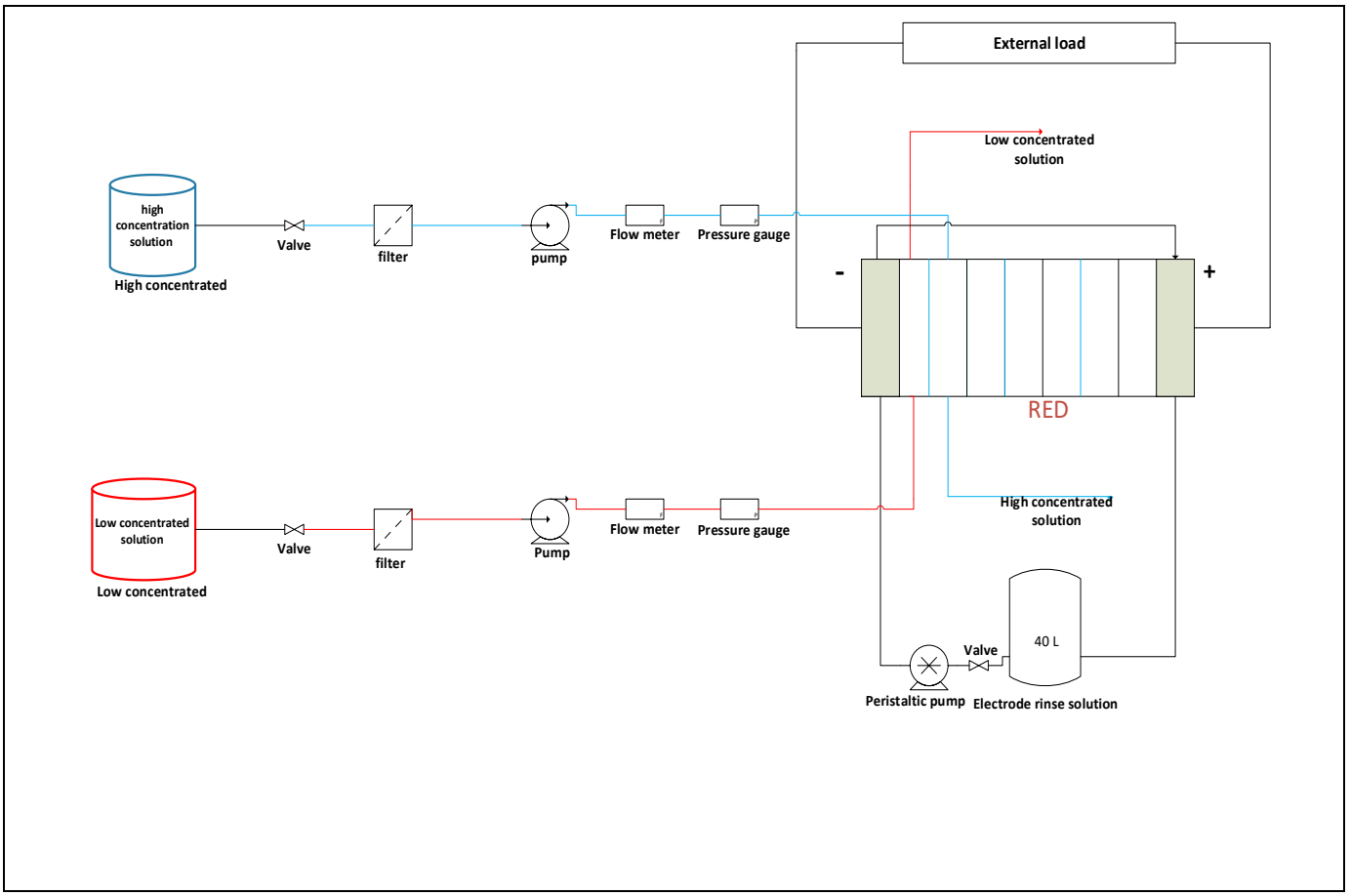

Figure A1.1: Shows RED pilot plant schematic diagram.

Theoretical potential of energy production calculations

uThukela river theoretical potential of energy production calculations assuming to utilize the whole volumetric flow rate of the river and sea water.

uThukela data:

Volumetric flow rate of uThukela river $(Q_D) = 3865 \times 10^6\ m^3/a$

Salt concentration was expressed in (mol/m^3)

uThukela river salt concentration $(C_D)\ = 0.814\ mol/m^3$

Indian Ocean data:

Volumetric flow rate of Indian Ocean $(Q_C) = 1338 \times 10^{12}\ m^3/a$

Indian Ocean salt concentration $(C_C) = 600\ mol/m^3$

The operational temperature was assumed to be 25℃

$R = 8.31\ J/molK$

$T = 298.15\ K$

$$U = 2RT\left[C_D Q_D\, ln\frac{C_D(Q_C+Q_D)}{C_D Q_D + C_C Q_C} + C_C Q_C\, ln\frac{C_C(Q_C+Q_D)}{C_D Q_D + C_C Q_C}\right]$$

$$= \mathbf{2}\cdot(\mathbf{8.31})\cdot\mathbf{298}\left[(\mathbf{0.814})(\mathbf{3865}\times\mathbf{10^6})\cdot\ln\frac{0.814\cdot(1338\times10^{12}+3865\times10^6)}{(0.814)(3865\times10^6)+(600)(1338\times10^{12})} + (\mathbf{600})(\mathbf{1338}\times\mathbf{10^{12}})\cdot\ln\frac{600(1338\times10^{12}+3865\times10^6)}{(0.814)(3865\times10^6)+(600)(1338\times10^{12})}\right]$$

$$U = 4955.253\times(-2.077288871\times10^{10} + 2.315850535\times10^{12})$$

$$U = 4955.253\times(2.295077646\times10^{12})$$

$$U = 1.137\times10^{16}\ J/y$$

$$\frac{1.137\times10^{16}J}{y}\times\frac{(1\times10^0)kJ}{(1\times10^3)\,J}\times\frac{1y}{365days}\times\frac{1day}{24hrs}\times\frac{1hr}{3600s} = 360540.33\ kJ/s$$

Conversion of theoretical potential for energy production to power calculation

$$\frac{1.137\times10^{16}J}{y}\times\frac{1y}{365days}\times\frac{1day}{24hrs}\times\frac{1\,hr}{3600s} = 3.60540335\times10^8 J/s$$

$1J/s = 1W$

$\frac{3.60540335\times10^{8}W}{1} \times \frac{1\times10^{-6}\ MW}{1W} = 360.54\ MW$

Converting megawatts to gigawatts

$\frac{360.6\ MW}{1} \times \frac{0.001GW}{1MW} = 0.3606\ GW$

Design calculations of reverse electrodialysis in uThukela estuary.

Assumptions

The temperature of the solutions was assumed to be 25℃

The volumetric flow rate of two solutions were assumed to be slightly equal to each other.

It was assumed not to utilize the whole annual volumetric flow rate of the two solutions, because ideal it is not possible to use the whole annual volumetric flow rate of the river or sea, one can channel and use only small amount of water or maybe build a reservoir to channel it.

The assumed value to be used for uThukela river was $0.0613\ m^3/s$ from $3865 \times 10^6\ m^3/a$ and it was converted from cubic meters per year to cubic meters per second, for calculation purpose. It was assumed that the volumetric flow rates of the solutions should be equal to ensure proper operation and maximize power production. Also, equal flow rates help to sustain a cosistent difference in salt concentration between the two solutions as they pass through the ion exchange membranes.

For the Indian Ocean the value was $0.0613\ m^3/s$

To design the RED membrane the power density was required, and it was assumed to $3\ W/m^2$ same value found in literatures.

Mole balance

Ion masses passing the membrane going toward low solution compartment was found using the following equation:

$\frac{dC_d}{dx} = \frac{b}{Q_d}J_{NaCl} + C_d\frac{b}{Q_d}J'_{water}$

Ion masses moving from the high concentrated solution to low concentrated solution was found using the following equation:

$$\frac{dC_C}{dx} = -\frac{b}{Q_C} J_{NaCl} - C_c \frac{b}{Q_C} J'_{water}$$

Volumetric water flux (J'_{water})

$D_{water} = 2.299 \times 10^{-9} (m^2/s)$ and $M_{water} = 1.80152800 \times 10^{-2}\ kg/mol$ is the molar mass of water.

$$J'_{water} = -\frac{2D_{water}}{\delta_m} \left(C_C(x) - C_d(x)\right) \frac{M_{water}}{\rho_{water}}$$

$$J'_{water} = -\frac{2 \cdot \left(2.299 \times 10^{-9}\right)}{0.00012} (600 - 0.814) \cdot \left(\frac{1.80152800 \times 10^{-2}}{997}\right)$$

$$J'_{water} = -4.15 \times 10^{-7} m/s$$

Ion Flux

$$J_{NaCl}(x) = J_{dl}(x) + J_{ml}(x)$$

$$J_{dl} = \frac{2D_{NaCl}}{\delta_m} \left(C_C(x) - C_d(x)\right)$$

Assume to use $D_{Nacl} = 1.00 \times 10^{-12}\ m^2/s$

$$J_{dl} = \frac{2\left(1 \times 10^{-12}\right)}{0.00012} (600 - 0.814)$$

$$J_{dl} = 9.986 \times 10^{-6}$$

$$J_{ml} = \frac{1}{F} \frac{E_T}{R_{stack}}$$

$$J_{ml} = \frac{1}{96485} \cdot \frac{0.3257}{2.96 \times 10^{-2}}$$

$$J_{ml} = 1.14 \times 10^{-4}$$

$$J_{Nacl} = 9.986 \times 10^{-6} + 1.14 \times 10^{-4}$$

$$J_{Nacl} = 1.24 \times 10^{-4}\ mol/m^2 s$$

Mole balance for low concentrated solution (uThukela river)

$$\frac{dC_d}{dx} = \frac{b}{Q_d} J_{NaCl} + C_d \frac{b}{Q_d} J'_{water}$$

$$\frac{dC_d}{dx} = \frac{0.063}{0.0613} \cdot (1.24 \times 10^{-4}) + (0.814) \cdot \left(\frac{0.063}{0.0613}\right) \cdot (-4.15 \times 10^{-7})$$

$$\frac{dC_d}{dx} = 1.274 \times 10^{-4}\ mol/s$$

Mole balance for high concentrated solution (Indian Ocean)

$$\frac{dC_C}{dx} = -\frac{b}{Q_C} J_{NaCl} - C_c \frac{b}{Q_C} J'_{water}$$

$$\frac{dC_c}{dx} = -\frac{0.063}{0.0613} \cdot (1.24 \times 10^{-4}) - (600) \cdot \left(\frac{0.063}{0.0613}\right) \cdot (-4.15 \times 10^{-7})$$

$$\frac{dC_c}{dx} = 1.285 \times 10^{-4}\ mol/s$$

Theoretical potential of energy production that can be obtained using the channeled flow rates.

$$U = 2RT \left[C_D Q_D\, ln \frac{C_D(Q_C+Q_D)}{C_D Q_D + C_C Q_C} + C_C Q_C\, ln \frac{C_C(Q_C+Q_D)}{C_D Q_D + C_C Q_C}\right]$$

$$U = 2(8.31)(298.15)\left[(0.814)(0.0613)\ln\frac{0.814(0.0613+0.0613)}{(0.814)(0.0613)+(600)(0.0613)} + (600)(0.0613)\ln\frac{600(0.0613+0.0613)}{(0.814)(0.0613)+(600)(0.0613)}\right]$$

$$U = 4955.253 \times (25.14914398)$$

$$U = 124620.37\ J/y$$

$$\frac{124620.37\ J}{y} \times \frac{1y}{365\ day} \times \frac{1day}{24hrs} = 14.22606963\ J/h$$

$$\frac{14.22606963\ J}{h} \times \frac{1h}{3600\ s} = 3.95168601 \times 10^{-3}\ J/s$$

$3.95168601 \times 10^{-3}\ J/s$ = $3.95168601 \times 10^{-3}\ W$

$$\frac{3.95168601 \times 10^{-3}\ W}{1} \times \frac{0.001\ kW}{1\ W} = 3.95168601 \times 10^{-6}\ kW$$

Energy production per year =$(3.95168601 \times 10^{-6}) \times (365 \times 24) = 3.5 \times 10^{-2}\ kWh$

RED membrane design calculations.

Step 1: Electrical potential (V)

Assumed to use permselectivity of 0.96 for each membrane (CEM and AEM).

Activity coefficient equation (γ):

$$\gamma = g_1 \cdot C_i + g_2$$

$$\gamma = 0.1366 \times (8.14 \times 10^{-4}) + 1.0007$$

$$\gamma = 1$$

$$E_T = (\alpha_{CEM} + \alpha_{AEM}) \cdot \frac{RT}{F} \cdot ln\left(\frac{\gamma_{sw} \cdot C_{sw}}{\gamma_{rw} \cdot C_{rw}}\right)$$

$$E_T = (0.96 + 0.96) \cdot \frac{(8.314)(298.15)}{96485} \ln\left(\frac{1 \times 600}{1 \times 0.814}\right)$$

$$E_T = 0.3257\ V$$

Step 2: Ion exchange membranes resistance (R_{CEM} and R_{AEM}).

$$R_{CEM} = R_{AEM} = r_1 \cdot (C_{rw})^{-0.236}$$

$$= (0.0002)(0.814)^{-0.236}$$

$$= 2.0995 \times 10^{-4}\ \Omega$$

Step 3: cell resistance.

$$R_{cell} = R_{CEM} + R_{AEM} + R_{rw} + R_{sw}$$

First need to find compartments resistances.

Low salinity water compartment resistance, and the values for Λ_0, A_A, B_A, and C_A can be found in appendix C.

$$R_{rw} = \frac{\delta_{rw}}{\Lambda_{rw} \cdot C_{rw}}$$

$$\Lambda_{rw} = \Lambda_0 - \frac{A_A C^{1/2}}{1 + B_A C^{1/2}} - C_A C$$

$$\Lambda_{rw} = 126.5 - \frac{91.0239(8.14\times10^{-7})^{1/2}}{1+(1.6591)(8.14\times10^{-7})^{1/2}} - (6.8041)(8.14\times10^{-7})$$

$$\Lambda_{rw} = 126.42\ Scm^2/mol$$

$$\frac{126.42\ Scm^2}{mol} \times \frac{(1\times10^{-2})^2\ Sm^2}{(1\times10^{0})^2\ Scm^2} = 0.012642\ Sm^2/mol$$

$$R_{rw} = f_c \frac{\delta_{rw}}{\Lambda_{rw}.C_{rw}}$$

$$R_{rw} = (1)\frac{0.0003}{(0.012642)(0.814)}$$

$$R_{rw} = 2.915\times10^{-2}\ \Omega$$

High salinity water compartment (sea water)

$$\Lambda_{sw} = \Lambda_0 - \frac{A_A C^{1/2}}{1+B_A C^{1/2}} - C_A C$$

$$\Lambda_{sw} = 126.5 - \frac{91.0239(0.0006)^{1/2}}{1+(1.6591)(0.0006)^{1/2}} - (6.8041)(0.0006)$$

$$\Lambda_{sw} = 124.35\ Scm^2/mol$$

$$\frac{124.35\ Scm^2}{mol} \times \frac{(1\times10^{-2})^2\ Sm^2}{(1\times10^{0})^2\ Scm^2} = 0.012435\ Sm^2/mol$$

$$R_{sw} = f_c \frac{\delta_{sw}}{\Lambda_{sw}.C_{sw}}$$

$$R_{sw} = (1)\frac{0.0003}{(0.012435)(600)}$$

$$R_{sw} = 4.021\times10^{-5}\ \Omega$$

$$R_{cell} = R_{CEM} + R_{AEM} + R_{rw} + R_{sw}$$

$$R_{cell} = (2.0995\times10^{-4}) + (2.0995\times10^{-4}) + (2.915\times10^{-2}) + (4.021\times10^{-5})$$

$$R_{cell} = 2.96\times10^{-2}\Omega$$

Step 4: current density (A/m^2).

$$I_{PP} = \frac{\mathrm{E_T}}{2 \cdot R_{cell}}$$

$$\frac{0.3257}{2 \times (2.96 \times 10^{-2})}$$

$$I_{PP} = 5.5\ A/m^2$$

Step 5: actual unit cell potential (V).

$$E_{uc} = E_T - R_{cell} \cdot I_{PP}$$

$$E_{uc} = 0.3257 - (2.96 \times 10^{-2})(5.5)$$

$$E_{uc} = 0.1629\ V$$

Step 6: number of cell pairs in a stack.

$$N_m = \frac{1.5}{E_{uc}} = \frac{1.5}{0.1629} = 9.21 = 9$$

Step 7: stack open circuit potential or electromotive force (v).

$$EMF = NE_{\mathrm{uc}}$$

$$EMF = (9)(0.1629)$$

$$EMF = 1.466\ V$$

Step 8: RED stack resistance (ohms).

$$R_{stack} = N_m \cdot (R_{cell}) + R_{electrode}$$

It was assumed to neglect $R_{electrode}$ because electrode resistance contribution is very small so for pilot plant and large-scale plant it is neglected. The equation becomes:

$$R_{stack} = N_m \cdot (R_{cell})$$

$$R_{stack} = (9)(2.96 \times 10^{-2})$$

$$R_{stack} = 0.266\ \Omega$$

Step 9: Power output calculation.

$$P_{gross} = I \cdot U$$

$$I = \frac{EMF}{R_{stack}+R_{load}}$$

Assumed R_{stack} = R_{load}

$$I = \frac{1.466}{0.266+0.266} = 2.752\ A$$

Internal voltage:

$$U = EMF - I \cdot R_{stack}$$

$$U = 1.466 - 2.752(0.266) = 0.733\ V$$

$$P_{max} = I \cdot U$$

$$P_{max} = (2.752)(0.733) = 2.0\ W$$

Efficiency estimation:

$$Eff = \frac{I^2 \cdot R_{stack}}{I^2 \cdot R_{load}+I^2 \cdot R_{stack}} = \frac{(2.752)^2 \cdot (0.266)}{(2.752)^2 \cdot (0.266)+(2.752)^2 \cdot (0.266)}\ 0.5 = 50\%$$

Step 10: RED membrane area estimation.

Assumed a power density of 3 W/m^2 because in literature is the most obtained power density.

$$P_d = \frac{P_{max}}{A}$$

$$3 = \frac{2}{A}$$

$$A = 0.67\ m^2$$

The membrane area:

$$P_d = \frac{P}{2 \cdot A_m \cdot N}$$

$$3 = \frac{2}{2 \cdot A \cdot (9)}$$

$$A_{membrane} = 0.037\ m^2$$

Step 11: river water (uThukela) and sea water (Indian Ocean) pressure drops estimation.

$$R_e = \frac{vD\rho}{visc} = \frac{(5.5)(1.91\times10^{-4})(997)}{0.9\times10^{-3}} = 1163.72$$

This means it's a laminar flow.

$$\Delta P_{sw} = \frac{2viscLQ_{sw}}{b{\delta_{sw}}^3} = \frac{2(0.9\times10^{-3})(0.0613)(0.587)}{(0.063)(0.0003)} = 3.43\ Pa$$

$$\Delta P_{RW} = \frac{2viscLQ_{RW}}{b{\delta_{RW}}^3} = \frac{2(0.9\times10^{-3})(0.587)(0.0613)}{(0.063)(0.0003)} = 3.43\ Pa$$

A.3 **Water feed pumps design**.

Since there was not much information about the site of uThukela river mouth, there were assumptions taken. The assumed parameters were assumed to be the same for both pumps.

River water feed pump (uThukela)

Assumptions

(i) Static suction head $(h_s) = 3\ m$

(ii) Length of suction pipe $(L_s) = 5\ m$

(iii) Static delivery head $(h_d) = 15\ m$

(iv) Length of delivery pipe $(L_d) = 20\ m$

Step: No 1: Design discharge

Design discharge $(Q_D) = 1.05Q_{given}$

$Q_D = 1.05 \times (0.0613)$

$Q_D = 0.0644\ m^3/s$

Step: No 2: Design of suction and delivery pipe.

For suction pipe:

$Q_D = A_s v_s$

From the design data book, the design suction recommended velocities for suction pipe are:

$v_s = 1.25\ m/s$ to $5.5\ m/s$

For this thesis the average velocity was taken which equal to $3.375\ m/s$

$Q_D = A_s v_s$

$0.0644 = \frac{\pi}{4} \cdot {d_s}^2 \cdot 3.375$

$0.01907111111 = \frac{\pi}{4} \cdot {d_s}^2$

$d_s = 0.1558m$

$\frac{0.1558\ m}{1} \times \frac{1\times10^0\ mm}{1\times10^{-3}\ m} = 155.8\ mm$

$\frac{155.8\ mm}{1} \times \frac{1''}{25.44\ mm} = 6.12''$

For delivery pipe:

The velocities recommended for the discharge ranges from $3.5\ m/s$ to $7.5\ m/s$ the average of these velocities was taken which is equal to $5.5\ m/s$.

$Q_D = A_d v_d$

$0.0644 = \frac{\pi}{4} \cdot {d_d}^2 \cdot (5.5)$

$0.01170272727 = \frac{\pi}{4} \cdot {d_d}^2$

$d_d = 0.1221\ m \approx 122.1\ mm$

$122.1mm = 4.7995 \approx 5''$

Step: No 3: calculation of manometric head (H_m)

$H_m = H_s + H_d$

$H_s = h_s + h_{f_s} + h_{fittings}$

$h_{fittings} = h_{bend} + h_{f.v}$

Assumed to use one bend and one strainer, because on a suction pipe there is no need of too many bends.

$h_{fittings} = h_{bend} + h_{f.v}$

$h_{fittings} = 0.1 + 0.28$

$h_{fittings} = 0.38\ m$

$h_{f_s} = \frac{f_s L_s {v_s}^2}{2.g.d_s} = \frac{(0.0863)(5)(3.375)^2}{2\times9.81\times0.1558} = 1.608\ m$

$h_s = 3\ m$

$H_s = h_s + h_{f_s} + h_{fittings}$

$H_s = 3 + 1.608 + 0.38$

$H_s = 4.988\ m$

$\therefore H_s < 8\ m$ this mean there is no cavitation.

Delivery head and the recommended velocities for delivery:

$v_d = 3.5\ m/s$ to $v_d = 7.5\ m/s$ for this thesis the average velocity was taken $(v_d = 5.5\ m/s)$

$H_d = h_d + h_{f_d} + h_{fittings} + \frac{{V_d}^2}{2g}$

$h_{fittings} = h_{G.V} + h_{bend}$

$h_{fittings} = 0.2 + 0.1$

$h_{fittings} = 0.3\ m$

$h_{f_d} = \frac{f_d L_d {v_d}^2}{2.g.d_d} = \frac{(0.0863)(20)(5.5)^2}{2\times9.81\times0.1221} = 21.795\ m$

$velocity\ head = \frac{{v_d}^2}{2.g} = \frac{(5.5)^2}{2\cdot(9.81)} = 1.54\ m$

$h_d = 15\ m$

$H_d = 15 + 21.795 + 0.3 + 1.54$

$H_d = 38.64\ m$

$\therefore H_m = H_s + H_d$

$H_m = 4.988 + 38.64$

$H_m = 43.62\ m$ the value of head that the pump needs to overcome.

Step: No 4: motor selection

$$motor\ power = \frac{wQH_m}{\eta_{overall}}$$

$$w = \rho g = 997 \times 9.81 = 9780.57\ N/m^3$$

$$\eta_{overall} = 0.70 = 70\%$$

If the overall is not given assume 70%.

$$m.p = \frac{9780.57 \times 0.0644 \times 43.62}{0.70} = 3.92 \times 10^4\ W$$

$$\frac{3.92 \times 10^4 W}{1} \times \frac{1 \times 10^0\ kW}{1 \times 10^3\ W} = 39.2\ kW$$

For 39.2 kW$= 2960 \times 0.96 = 2842\ rpm$

$\therefore N = 2842\ rpm$

Step: No 5: Impeller design

$$N_s = \frac{N\sqrt{Q}}{(H_m)^{3/4}}$$

$$N_s = \frac{2842\sqrt{0.0644}}{(43.62)^{3/4}} = 42.48$$

Radial flow- medium runner impeller type.

Pump power:

$$P_P = Q \cdot H_m \cdot g \cdot \rho$$

$$P_P = (0.0644) \times (43.62) \times (9.81) \times (997)$$

$$P_P = 27459.94\ W$$

$$P_P = 27.46\ kW$$

Energy required to pump liquid.

$E = P_P \times t$

$E = 27.46 \times (365 \times 24) = 240549.6\ kWh$

The above obtained energy is the energy required yearly.

For Indian Ocean feed pumps

Assumed to use same suction pipe, static suction head, static delivery head, length of delivery pipe as uThukela river.

Step: No 1: Discharge flow rate

$design\ discharge\ (Q_D) = 1.05(Q_1)$

$Q_D = 1.05 \times (0.0613)$

$Q_D = 0.0644\ m^3/s$

Step: No 2: design of suction and discharge pipe

For suction pipe

$Q_D = A_s v_s$

For this thesis the average velocity was taken which equal to $3.375\ m/s$

$Q_D = A_s v_s$

$0.0644 = \frac{\pi}{4} \cdot {d_s}^2 \cdot 3.375$

$0.01907111111 = \frac{\pi}{4} \cdot {d_s}^2$

$d_s = 0.1558\ m$

$\frac{0.1558\ m}{1} \times \frac{1 \times 10^0\ mm}{1 \times 10^{-3}\ m} = 155.8\ mm$

$\frac{155.8 mm}{1} \times \frac{1''}{25.44\ mm} = 6.12''$

For deliver pipe

$Q_D = A_d v_d$

$0.0644 = \frac{\pi}{4} \cdot {d_d}^2 \cdot (5.5)$

$0.01170272727 = \frac{\pi}{4} \cdot {d_d}^2$

$d_d = 0.1221\, m \approx 122.1\, mm$

$122.1mm = 4.7995 \approx 5''$

Step: No 3: calculation of manometric head (H_m)

$H_m = H_s + H_d$

$H_s = h_s + h_{f_s} + h_{fittings}$

$h_{fittings} = h_{bend} + h_{f.v}$

Assumed to use one bend and one strainer, because on a suction pipe there is no need of too many bends.

$h_{fittings} = h_{bend} + h_{f.v}$

$h_{fittings} = 0.1 + 0.28$

$h_{fittings} = 0.38\, m$

$h_{f_s} = \frac{f_s L_s {v_s}^2}{2.g.d_s} = \frac{(0.0863)(5)(3.375)^2}{2\times 9.81\times 0.1558} = 1.608\, m$

$h_s = 3\, m$

$H_s = h_s + h_{f_s} + h_{fittings}$

$H_s = 3 + 1.608 + 0.38$

$H_s = 4.988\, m$

$\therefore H_s < 8\, m$ this mean there is no cavitation.

Delivery head and the recommended velocities for delivery:

$v_d = 3.5\ m/s$ to $v_d = 7.5\ m/s$ for this thesis the average velocity was taken ($v_d = 5.5\ m/s$)

$$H_d = h_d + h_{f_d} + h_{fittings} + \frac{{V_d}^2}{2g}$$

$$h_{fittings} = h_{G.V} + h_{bend}$$

$$h_{fittings} = 0.2 + 0.1$$

$$h_{fittings} = 0.3\ m$$

$$h_{f_d} = \frac{f_d L_d {v_d}^2}{2.g.d_d} = \frac{(0.0863)(20)(5.5)^2}{2\times 9.81\times 0.1221} = 21.795\ m$$

$$velocity\ head = \frac{{v_d}^2}{2.g} = \frac{(5.5)^2}{2\cdot(9.81)} = 1.54\ m$$

$$h_d = 15\ m$$

$$H_d = 15 + 21.795 + 0.3 + 1.54$$

$$H_d = 38.64\ m$$

$$\therefore H_m = H_s + H_d$$

$$H_m = 4.988 + 38.64$$

$H_m = 43.62\ m$ the value of head that the pump needs to overcome.

Step: No 4: motor selection

$$motor\ power = \frac{wQH_m}{\eta_{overall}}$$

$$w = \rho g = 997 \times 9.81 = 9780.57\ N/m^3$$

$$\eta_{overall} = 0.70 = 70\%$$

If the overall is not given assume 70%.

$$m.p = \frac{9780.57\times 0.0644\times 43.62}{0.70} = 3.92 \times 10^4\ W$$

$\frac{3.92\times10^4 W}{1} \times \frac{1\times10^0\ kW}{1\times10^3\ W} = 39.2\ kW$

For 39.2 kW$= 2960 \times 0.96 = 2842\ rpm$

$\therefore N = 2842\ rpm$

Step: No 5: Impeller design

$N_S = \frac{N\sqrt{Q}}{(H_m)^{3/4}}$

$N_S = \frac{2842\sqrt{0.0644}}{(43.62)^{3/4}} = 42.48$

Radial flow- medium runner impeller type.

Pump power:

$P_P = Q \cdot H_m \cdot g \cdot \rho$

$P_P = (0.0644) \times (43.62) \times (9.81) \times (997)$

$P_P = 27459.94\ W$

$P_P = 27.46\ kW$

Energy required to pump liquid.

$E = P_P \times t$

$E = 27.46 \times (365 \times 24) = 240549.6\ kWh$

The above obtained energy is the energy required yearly.

Economical cost calculations.

$CAPEX = C_m + C_{electrode} + C_{casing} + C_{spacer} + C_{pump} + C_{piping} + C_{labour}$

$C_m = 10€ \cdot {m_{IEMs}}^{-2}$

$\frac{10€}{m^2} \times \frac{R1}{0.048776€} = R205/{m^2}_{IEM}$

Cost of pump for uThukela river

$$cost\ of\ pump = 900\left(\frac{P_P}{300}\right)^{0.25}$$

$$cost\ of\ pump = 900\left(\frac{27.46}{300}\right)^{0.25}$$

$$cost\ of\ pump = 495.04\ €$$

Cost of pump for Indian Ocean

$$cost\ of\ pump = 900\left(\frac{P_P}{300}\right)^{0.25}$$

$$cost\ of\ pump = 900\left(\frac{27.46}{300}\right)^{0.25}$$

$$cost\ of\ pump = 495.4\ €$$

$$total\ cost\ of\ pumps = 495.04 + 495.04 = 990.08\ €$$

$$990.08\ € = R20260.26$$

$$equipment\ cost = C_m + C_{electrode} + C_{casing} + C_{spacer} + C_{pump} + C_{piping}$$

$$= 205.0189 + 10245.29 + 41 + 102.51 + 20260.26 + 27835.74$$

$$= R58689.72$$

$$C_{labour} = 58689.82 \times 20\% = R11737.96$$

Other values found or used in the equation above can be found in table 3.2.

$$CAPEX = C_m + C_{electrode} + C_{casing} + C_{spacer} + C_{pump} + C_{piping} + C_{labour}$$

$$= 205.0189 + 10245.29 + 41 + 102.51 + 20260.26 + 27835.74 + 11737.96$$

$$= R70427.78\ kWh$$

$$OPEX = 0.02 \times CAPEX$$

$$OPEX = 0.02 \times (70427.78)$$

$$OPEX = R1408.56\ kWh$$

Levelized cost of electricity (cost of electricity production), the values for t and r can be found in table 3.1 chapter 3. The fuel and carbon values were negleted since they are not applicable to RED plant. The total energy generated was equal to $3.5 \times 10^{-2}\ kWh$

$$LCOE = \frac{CAPEX \times \left(1+\frac{discount\ rate}{100}\right)^{plant\ lifetime} + OPEX \times plant\ lifetime}{total\ energy\ generation\ over\ plant\ lifetime}$$

$$LCOE = \frac{70427.78 \times \left(1+\frac{3}{100}\right)^{20} + 1408.56 \times 20}{0.035 \times 20}$$

$$LCOE = \frac{127196.37 + 28171.2}{0.7}$$

$$LCOE = R221953.67\ kWh$$

To find whether the plant will be economically viable or profitable the revenue was compared to the cost of electricity production.

$$Total\ Quanty\ of\ electricity\ produced = cost\ of\ electricity\ production \div cost\ of\ electricity\ per\ kWh$$

$$TQ = 221953.67 \div 2.07/kWh$$

$$TQ = 107223.10\ kWh$$

Now calculating the revenue.

$$Revenue = Total\ Quality\ of\ electricity\ produced \times cost\ per\ kWh$$

$$Revenue = 107223.10 \times 2.07$$

$$Revenue = R221951.82$$

$$Revenue - cost\ of\ electricity\ production = profit/loss$$

$$221951.82 - 221951.82 = R0$$

Since the result was R0 (break-even point), the plant is not generating a profit, but it's also not incurring a loss. It is economically viable in the sense that it covers its costs, but it's not profitable in terms of generting surplus revenue. Therefore, the plant is economically viable but not profitable and since it is a pilot plant the focus is to try and generate electricity for now.

APPENDIX B

Calculated membrane parameters

Table B1.1: RED stack membrane calculated parameters.

PARAMETER	VALUE
Area of one membrane (m^2)	0.037
Width (m)	0.063
Length (m)	0.587
Membrane pairs	9
Resistance of cation exchange membrane (Ω)	2.0995×10^{-4}
Resistance of anion exchange membrane (Ω)	2.0995×10^{-4}
RED stack membrane area (m^2)	0.67

Assumed parameters used in the design calculations of reverse electrodialysis membrane.

Table B1.2: assumed values for membrane design.

PARAMETER	VALUE
AEM permselectivity	0.96
CEM permselectivity	0.96
Membrane thickness (μm)	120
Compartment or channel thickness (μm)	300
Velocity (m/s)	0.03

General photos of a reverse membrane.

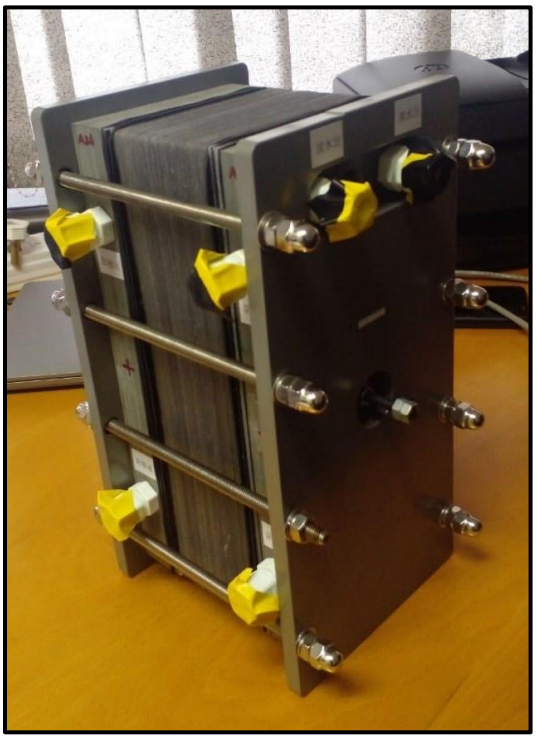

Figure B1.1: Reverse electrodialysis stack photo.

Figure B1.2: RED stack picture.

APPENDIX C

Thermodynamic Properties of Solutions

The activity coefficients of the solutions are determined by Equation (C.1)

$$\ln \gamma_{\pm} = -A_{DH} \cdot \left[\frac{\sqrt{m}}{1+b' \cdot \sqrt{m}} + \frac{2}{b'} \cdot \ln\left(1 + b' \cdot \sqrt{m}\right)\right] + m \cdot B_{\gamma} + m^2 \cdot C_{\gamma} \qquad \textbf{Equation (C.1)}$$

$$B_{\gamma} = 2 \cdot \beta^0 + 2 \cdot \beta^1 \cdot \left[1 - \left(1 + \alpha' \cdot \sqrt{m} - \alpha'^2 \cdot \frac{m}{2}\right) \cdot e^{\left(-\alpha \cdot \sqrt{m}\right)}\right] \cdot \frac{1}{\alpha'^2 \cdot m} \qquad \textbf{Equation (C.2)}$$

$$C_{\gamma} = \frac{3}{2} \cdot C_{\emptyset} \qquad \textbf{Equation (C.3)}$$

In equation (C.1) A_{DH} is the Debye-Huckel constant which at 25℃ is equal to 0.3915 and b' is a constant dependent on the valences of the ions that make up the ionic solute. For 1:1 $b'$is equal to 1.2. The coefficient C_{γ} and B_{γ} are determined using equation (C.3) and (C.2). The parameters α', β^0, β^1, $C_{\emptyset}$ that are used in equation (C.2) and (C.3) are shown in table C.1.

Table C1.1 – Parameters of thermodynamic functions for aqueous electrolytes of sodium chloride at 25℃.

α' $(kg^{0.5} \cdot mol^{-0.5})$	β^0	β^1	$C_{\emptyset}$
2.00	0.0767	0.26495	0.00122

Another equation for calculating the activity coefficient which is a shorter version follows:

$$\gamma = g_1 \cdot C_i + g_2 \qquad \textbf{Equation (C.4)}$$

Where g_1 and g_2 are equal to 0.1366 l/mol and 1.0007 and there were estimated at $T = 298.15\ K$.

The equivalent conductivity can be estimated using the Jones and Dole's equation:

$$\Lambda = \Lambda_0 - \frac{A_A C^{1/2}}{1+B_A C^{1/2}} - C_A C \qquad \textbf{Equation (C.5)}$$

Where Λ_0 is the equivalent conductivity of salt at infinite dilution, C is the molar salt concentration. The values of the following parameters A_A, B_A, and C_A are found in table C.2 for sodium chloride.

Table C 1.2: Parameters of Jones and Dole's correlation.

Salt	Λ_0	A_A	B_A	C_A
NaCl	126.5	91.0239	1.6591	6.8041

APPENDIX D-PUBLICATIONS

39th JOHANNESBURG International Conference on "Chemical, Biological and Environmental Engineering" (JCBEE-23) Nov. 16-17, 2023 Johannesburg (South Africa)

Reverse Electrodialysis Technology installation in KwaZulu-Natal coastal region: A modelling study using COMSOL Multiphysics.

Lungisani Ngcobo[1], Peterson T. Ngema[2], Tumba A. Kaniki[3], and Nkululeko Nkosi[4]

***Abstract*—Due to high export demand, Sub-Saharan Africa's South Africa is a rapidly developing nation. This has, however, led to a sharp increase in energy demand. Since most industries are experiencing increased production demand, Eskom, the state-owned entity, has been put in more stress. The Energy and Environmental Affairs Ministry has been receiving energy and environmental concerns from citizens. Since the COP21 deal was signed, renewable energy technologies have emerged as alternative energy mix technologies for substantiating Eskom's grid. This has alleviated environmental worries. Emerged renewable technologies include reverse electrodialysis. In South Africa, the technology's advantage of minimizing waste while producing electricity has drawn the interest of research groups in academia and engineers in the industry. KwaZulu-Natal has an untapped resource of blue ocean energy that could be used with this technology. A high salinity gradient can produce high energy due to the high salinity gradient found along the coast. A preliminary assessment of the location where the technology might be installed is the purpose of this paper. Based on the maximum power production, the selection was made. Different streams in coastal KZN, which feed the ocean, have salinity gradients that differ. Tugela, Mgeni,**

world's energy demand[1]. Due to global warming concerns caused by the burning of fossil fuels and the increasing demands of energy, environmentally friendly strategies and technologies are being developed to ensure sustainable and alternative energy sources. Utilizing renewable energy sources is one approach to the problem. Salinity gradient energy or blue energy may hold the solution among them. This renewable energy source generates energy from two aqueous natural solutions with different salt concentrations, utilizing an alternative set of anion exchange membranes (AEM), and cation exchange membranes (CEM), through reverse electrodialysis (RED), and this technology is recognized as an attractive membrane-based process[2], [3].

The membranes are packed to be a stack and each stack consists of cell pairs that consist of ion exchange membranes (AEM, and CEM). Salinity gradient energy or blue energy is a renewable energy source that has an estimated global theoretical potential of 1.4-2.6 TW[4], [5], and approximately 1 TW is considered technically retrievable from the theoretical potential[6], [7].

Figure 1 shows the diagram of a reverse electrodialysis stack for salinity gradient energy production, including the electrodes, at which redox reactions occur to change the ionic current into electron current. Pattle in 1954 was the first